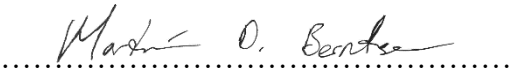




Universitetet
i Stavanger

FACULTY OF SCIENCE AND TECHNOLOGY

MASTER'S THESIS

Study programme/specialisation: Master of Science in Engineering Structures and Materials/Mechanical Systems	Spring semester, 2019 Open/ Confidential
Author: Martin Daleng Berntsen	 (signature of author)
Programme coordinator: Dimitros Pavlou Supervisor: Torfinn Havn	
Title of master's thesis: Investigation of Corrosion Resistance of Duplex, Lean Duplex and Austenitic Stainless Steels in Simulated Offshore Environment.	
Credits: 30	
Keywords: General Corrosion, Pitting Corrosion, Marine Atmosphere, Pitting potential, Corrosion resistance, Austenitic Stainless Steels, Duplex, Lean Duplex, Chemical composition	Number of pages: 53 + enclosure: 36 (Appendix) Stavanger, 14 June, 2019

Abstract

Some duplex grades are developed to replace the 300 series of austenitic stainless steels in harsh chloride applications due to superior mechanical and corrosive properties. Since the market price for nickel and molybdenum have surged, it has caused an increase in the cost of production of stainless steels and created a competitive market. Some of the duplex and lean duplex grades are now considered to be a cheaper choice in these applications. The purpose of this study is to investigate the corrosion resistance of different types of duplex and stainless steels, namely: 2205 (UNS S32205), 2304 (UNS S32304), 2003 (UNS S32003), 316L (UNS S31603) and 304 (UNS S30400). The grades of lean duplex, 2003 and 2304, are similar to each other in terms of corrosion resistance and are of focus in this thesis, while the other steels serve as reference samples for comparison.

Two main experiments were carried out to test the materials resistance in chloride environments, where one was performed as general- and localized corrosion testing in a simulated offshore environment, consisting of three test rounds with different temperatures. The other experiment was performed as an electrochemical test by cyclic polarization according to ASTM G61-86, with two different sodium chloride solutions. The samples were weight tested before and after exposure of the offshore environment and was evaluated after testing based on visual inspection. The interest of the ASTM G61-86 experiment was to test the materials susceptibility to pitting corrosion by finding and comparing the materials pitting-, repassivation- and corrosion potentials. The materials chemical compositions were found by a scanning electron microscope and compared to their corresponding material certificates. The materials pitting resistant equivalent numbers were also assessed and compared to the results of cyclic polarization.

None of the samples showed initiation of localized corrosion after being exposed for the simulated offshore environment. General corrosion was observed on many of the samples tested, but there was not registered any deviations in mass after the experiments. However, it was found by visual inspection of the samples after testing that the grades of duplex and lean duplex had less corroded areas on their surfaces. From the ASTM G61-86 experiment it was found that duplex 2205 had the best corrosion resistance against pitting corrosion. Also, lean duplex grade 2003 was found to be superior to 2304 in corrosion resistance against pitting corrosion. The order of the materials resistance to pitting corrosion fits their corresponding pitting resistance equivalent number and are in the following order, from best to worst: 2205, 2003, 2304, 316L and 304. Chemical analysis showed that the materials compositions match their certificates, with a few deviations on elements that were difficult to measure.

Acknowledgement

This thesis was provided by my faculty supervisor, Prof. Torfinn Havn, from the University of Stavanger. I want to thank him for providing me with good guidance, motivation and supervision throughout the project.

The test materials were provided by Gateway Stainless AS and the heating cabinet was provided by Multi Phase Meters. I want to give them my gratitude for their contribution with materials and equipment needed for testing.

I also want to thank the people working in the Machine hall at the University of Stavanger for their help and guidance on using different tools and equipment's needed for the experiments performed in this project.

I want to give a special thanks to Wakshun Mekonnen Tucho for helping me with the scanning electron microscopy analysis to find the chemical compositions of each material and for providing input to the thesis. Many thanks to Utsav Raj Dotel for giving me good advice, input and guidance with performing the ASTM G61-86 experiment.

Finally, I want to express how grateful I am to my friends and family for giving me great support and motivation throughout my whole study period. Without them, this thesis would never have been written. This thesis is dedicated to the memory of my grandfather Per Edgar Mikal Daleng and my grandmother Anny Elise Berntsen, whose role in my life was, and remains, immense.

Abbreviations

BCC	Body Centred Cubic
BHN	Brinell Hardness Number
CPS	Cyclic Polarization Scan
DSS	Duplex Stainless Steel
EDS	Energy Dispersive Spectroscopy
FCC	Face Centred Cubic
LDSS	Lean Duplex Stainless Steel
OCP	Open Circuit Potential
PRE	Pitting Resistance Equivalent
PTFE	Polytetrafluoroethylene
SS	Stainless Steel
WDS	Wave Dispersive Spectrometer

List of contents

Abstract	i
Acknowledgement.....	ii
Abbreviations	iii
Figure list.....	vii
Table list.....	ix
1 Introduction	1
1.1 Background of the thesis	1
1.2 Objective.....	1
1.3 Scope and limitations.....	2
2 Literature review	3
2.1 Introduction to corrosion	3
2.2 Classification of corrosion.....	4
2.2.1 General corrosion	4
2.2.2 Localized corrosion	4
2.3 Mechanisms of corrosion.....	5
2.4 Polarisation	6
2.5 Mixed potential theory.....	6
2.6 Passivation and passivity	7
2.7 Pitting corrosion	7
2.7.1 Principle of pitting corrosion.....	8
2.8 Crevice corrosion.....	9
2.8.1 Principle of crevice corrosion	10
2.9 Austenitic stainless steels	11
2.9.1 Properties of 304 and 316L	11
2.10 Duplex stainless steels	12
2.10.1 Properties of 2003, 2304 and 2205.....	12

2.11	The effect of alloying elements.....	13
2.11.1	Chromium.....	13
2.11.2	Nickel	13
2.11.3	Molybdenum	13
2.11.4	Nitrogen.....	13
2.11.5	Pitting resistance equivalent number.....	14
2.12	Atmospheric marine corrosion.....	14
2.13	Electrochemical testing	15
2.13.1	Method for Cyclic Potentiodynamic polarization	16
2.14	X-ray	17
2.14.1	Energy dispersive spectroscopy analysis	17
2.14.2	Characteristic X-rays.....	17
3	Materials and methods	18
3.1	Material certification	18
3.2	Preparing the test materials.....	19
3.3	Atmospheric marine corrosion test.....	20
3.4	Scanning electron microscope	21
3.5	ASTM G61-86 test	22
3.5.1	Preparation	22
3.5.2	Equipment	23
3.5.3	Test procedure	23
3.5.4	Interpretation of the polarization plots	26
3.5.5	Deviation from standard.....	27
4	Results	28
4.1	Evaluation of samples after atmospheric marine corrosion testing.....	28
4.1.1	Samples from test round 1	30
4.1.2	Samples from test round 2.....	31

4.1.3	Samples from test round 3.....	32
4.2	Analysis of materials using SEM	33
4.2.1	EDS scan of 304.....	34
4.2.2	EDS scan of 316L	35
4.2.3	EDS scan of 2003.....	35
4.2.4	EDS scan of 2304.....	36
4.2.5	EDS scan of 2205.....	36
4.3	Analysis of ASTM G61-86 test.....	37
4.3.1	Polarization scan of 304.....	39
4.3.2	Polarization scan of 316L.....	40
4.3.3	Polarization scan of 2003.....	41
4.3.4	Polarization scan of 2304.....	42
4.3.5	Polarization scan of 2205.....	43
4.3.6	Comparison of 2304 and 2003.....	44
5	Discussion.....	45
5.1	Atmospheric marine corrosion testing.....	45
5.2	Material compositions.....	47
5.3	Corrosion potentials.....	48
6	Conclusion and recommendations	50
7	References.....	51
	Appendix A: Material Certificates	I
	Appendix B: Pictures of The Samples Before and After Testing	VI
	Appendix C: Weight Test Results.....	XVI
	Appendix D: Composition Test Results.....	XVII
	Appendix E: Open Circuit Potentials.....	XXVII
	Appendix F: Surface Images of The Materials	XXXII

Figure list

Figure 1: Illustration of corrosion as metallurgy in reverse [4]	3
Figure 2: Illustration of the corrosion process of iron [9].....	5
Figure 3: Evans diagram for iron immersed in an acidic solution [12].....	6
Figure 4: Pitting shapes, ASTM-G46 [13]	8
Figure 5: Illustration of pitting corrosion on a metal in chloride solution [8]	9
Figure 6: Idealized geometry of crevice corrosion [14].....	10
Figure 7: Mechanism of crevice corrosion [16]	10
Figure 8: Standard polarization cell [4].....	15
Figure 9: General CPDP curve and corrosion parameters [29].....	16
Figure 10: Rusch horizontal metal cutting band saw	19
Figure 11: Pilous ARG 220 plus band saw	19
Figure 12: Stainless steel tubes	19
Figure 13: Metal file used on a sample	19
Figure 14: Sample ready for testing	19
Figure 15: Samples ready for general and localized corrosion testing	20
Figure 16: Heating cabinet	21
Figure 17: Samples inside the heating cabinet	21
Figure 18: Samples cut for SEM-analysis.....	22
Figure 19: SEM ZIESS SUPRA 35VP	22
Figure 20: Calibration of Gamry instrument.....	24
Figure 21: Polarization cell	24
Figure 22: Experimental Setup in Gamry software.....	25
Figure 23: Hardware Settings in Gamry software.....	25
Figure 24: Pitting- and repassivation potential of SS 304 plot	26
Figure 25: Pitting- and repassivation potential of DSS 2205.....	26
Figure 26: Salt layer on samples after testing of round 1.....	28

Figure 27: 20x20 grid illustrated on sample 3.AC 304	29
Figure 28: Percent corrosion of the sample surfaces.....	29
Figure 29: Frontside of the samples after test round 1	30
Figure 30: Backside of the samples after test round 1	30
Figure 31: Frontside of the samples after test round 2	31
Figure 32: Backside of the samples after test round 2	31
Figure 33: Frontside of the samples after test round 3	32
Figure 34: Backside of the samples after test round 3	32
Figure 35: EDS spectrum from one sample	34
Figure 36: Pitting potentials of the samples	38
Figure 37: Open circuit potentials of the samples.....	38
Figure 38: Repassivation potentials of the samples	38
Figure 39: CPS ordinary P304	39
Figure 40: CPS modified M304	39
Figure 41: CPS ordinary P316L.....	40
Figure 42: CPS modified M316L.....	40
Figure 43: CPS ordinary P2003	41
Figure 44: CPS modified M2003	41
Figure 45: CPS ordinary P2304	42
Figure 46: CPS modified M2304	42
Figure 47: CPS ordinary P2205	43
Figure 48: CPS modified M2205	43
Figure 49: CPS samples; 2P2304 vs. 2P2003	44
Figure 50: CPS samples; 2M2304 vs. 2M2003.....	44

Table list

Table 1: Corrosion forms in general and localized corrosion [5]	4
Table 2: Chemical composition of 304 and 316L [18, 19]	11
Table 3: Mechanical and physical properties of 304 and 316L [18, 19].....	11
Table 4: Chemical composition of 2003, 2304 and 2205 [21, 22, 23].....	12
Table 5: Mechanical and physical properties of 2003, 2304 and 2205 [21, 22, 23]	12
Table 6: Typical PRE numbers for stainless steels [18, 23].....	14
Table 7: Mechanical properties of the materials	18
Table 8: Composition and PRE-value of the materials	19
Table 9: Material types with sample names	21
Table 10: Ordinary and modified test samples with names	24
Table 11: Result of general- and localized corrosion on the samples	28
Table 12: Composition of sample 304	34
Table 13: Composition of sample 316L.....	35
Table 14: Composition of sample 2003	35
Table 15: Composition of sample 2304	36
Table 16: Composition of sample 2205	36
Table 17: Results of cyclic polarization scans	37
Table 18: Ranking of the materials based on cyclic polarization and PRE values	49

1 Introduction

1.1 Background of the thesis

Austenitic grades of stainless steel forms the largest portion of the global stainless steel market. They have a unique combination of high ductility, strengthening potential, weld ability, toughness at low temperatures and corrosion resistance. However, some of the duplex and new types of lean duplex stainless steels are developed for the replacement of the 300 series of austenitic stainless steels. This is due to the grades of DSS and LDSS having superior mechanical and corrosive properties in harsh chloride environment applications, whereas the 300 series of stainless steels could be limited. Also, the market price for nickel and molybdenum have surged, causing an increase in the cost of production of stainless steels. Some of the duplex grades are now considered to be a cheaper choice in these applications, particularly DSS 2205 has become very competitive to 316 [1, 2].

New types of LDSS are developed as economical alternatives to standard duplex and highly alloyed stainless steels grades, having lower additions of nickel and molybdenum which is compensated by higher nitrogen additions. As the prices of nickel and molybdenum are unstable, LDSS of type 2304 has become competitive to grades 304 and 316. It is expected that 2304 will replace them in volume markets. A newer version of LDSS 2304 has recently been developed, named 2003, with similar corrosive and mechanical properties. The market price for LDSS 2003 is less expensive in alloying elements than 2205, but more expensive than 2304 [1, 2].

1.2 Objective

In this thesis, an investigation of the resistance against localized and general corrosion in the marine environment will be performed on different types of stainless steels, namely: 304, 316L, 2205, 2304 and 2003. Since the lean duplex grades 2304 and 2003 are competitive and comparable to each other, they will be of focus in the experiments. The other steels will serve as reference samples for comparison. The two materials of lean duplex, 2304 and 2003, will be investigated and assessed to see if 2003 is superior in corrosive properties to 2304. The chemical compositions of all the materials will also be checked against their corresponding material certificates.

1.3 Scope and limitations

Two types of experiments will be carried out in this thesis. One experiment will be done in a simulated offshore environment by performing atmospheric marine corrosion tests. The other experiment will focus on localized corrosion and be performed as electrochemical tests according to standard ASTM G61-81. The chemical composition of each material will be tested by a scanning electron microscope and compared to their corresponding material certificates. Thereafter, an assessment and evaluation of the corrosive properties of the materials will be executed.

The first part of this thesis consists of a literature review, followed by the experimental part of the thesis where tests and tests-procedures are carried out. Thereafter, the results found from the experiments will be presented, followed by a discussion of the results. Finally, a conclusion will be provided, followed by recommendations of further work.

The major limitation of this project is that all the materials delivered from Gateway Stainless AS were tested in the condition that they arrived in. There was not performed any surface treatment on the samples before performing experiments of atmospheric marine corrosion and cyclic polarization. Also, the performance of the experiment's was limited due to time constraints.

2 Literature review

2.1 Introduction to corrosion

Corrosion is defined as the chemical or electrochemical reaction between a material and its environment, which causes the material to deteriorate. Most materials are in some degree exposed to a variety of environments. These interactions impair the materials usability as a result of the deterioration of its mechanical properties, e.g., physical properties such as ductility and strength, and appearance [3]. Corrosion can also be defined as metallurgy in reverse, since the corrosion process returns metals to their thermodynamically stable natural state as compounds (ores), such as oxides or sulphides. These are then metallurgically transformed to metal by supplying energy. To understand the process of metallurgy in reverse, the corrosion cycle of iron is illustrated below in figure 1. There are many forms of corrosion, the most common one is known as rust (iron oxide) and it occurs when iron reacts with oxygen and water [4].

Corrosion is a major cost for society, from estimation it has been found that about 40% of the steel produced is made to replace corroded steel. From a study called IMPACT done by NACE in 2016, it was estimated that the global cost of corrosion was about 3.4% of the global Gross Domestic Product (GDP) of a generic country and 3-4% of the Gross National Product (GNP) of industrialized countries, where 15-35% of these costs could be avoidable [4]. Fundamental laws of thermodynamics cannot be reversed to avoid the process of corrosion, however feasible solutions can be applied to materials to reduce their corrosive rates to acceptable levels, but this must be done in an environmentally safe and cost-effective manner [3].

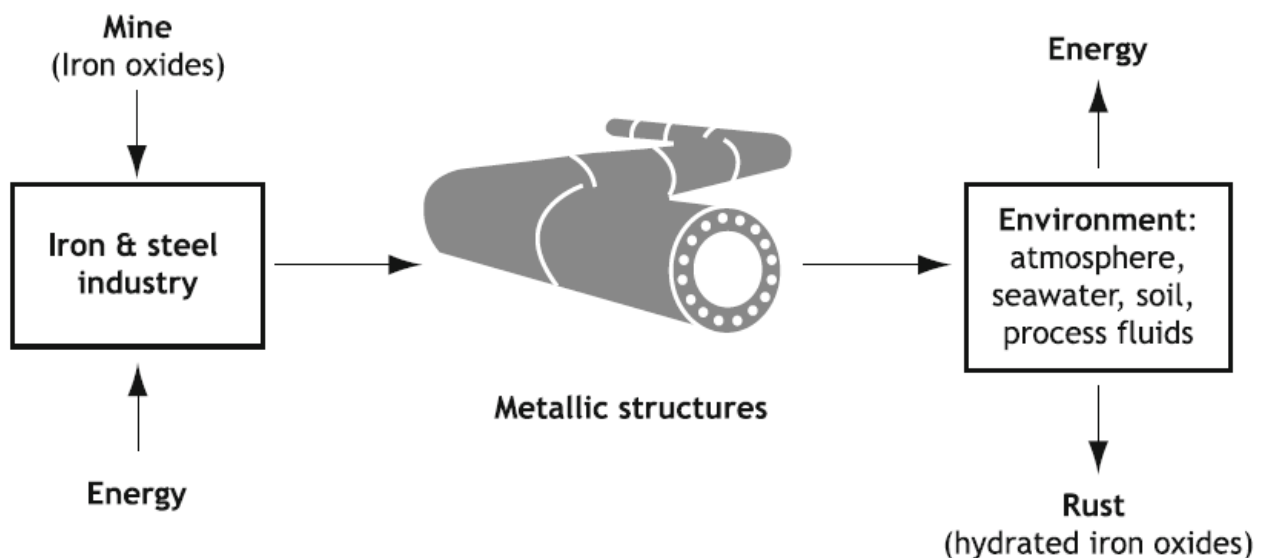


Figure 1: Illustration of corrosion as metallurgy in reverse [4]

2.2 Classification of corrosion

There is no unique way to classify the different types of corrosion, but it can be divided into two major categories commonly known as general and localized corrosion [5].

2.2.1 General corrosion

General corrosion, also known as uniform corrosion, occurs when the surface of a metal is exposed to an electrochemical reaction in environments such as liquid electrolyte, gas electrolyte or hybrid electrolyte [5]. This type of corrosion spreads uniformly over the entire area of the exposed surface and causes surface thinning (i.e. metal loss) [3]. Anodes and cathodes are created on the metal surfaces due to differences in composition or orientation between small areas which facilitates the corrosion process. General corrosion is most often caused by the misapplication of materials in corrosive environments. It is relatively easy to assess the effect of metal loss, often making this type of corrosion tolerable [6]. In table 1 below are some examples of general corrosion forms listed.

2.2.2 Localized corrosion

Localized corrosion occurs when the surface area of a metal is exposed to a suitable electrolyte and specific parts of the surface corrodes. This type of corrosion is more difficult to control than general corrosion [5]. The localized attack is intense, causing a rapid corrosion rate while the rest of the surface corrodes at a lower rate. Localized corrosion is caused by an inherent property of the component material or by some environmental effect [7]. Listed in table 1 below are some examples of localized corrosion forms.

Table 1: Corrosion forms in general and localized corrosion [5]

General corrosion:	Localized corrosion:
<ul style="list-style-type: none">• Atmospheric corrosion• Galvanic corrosion• High-temperature corrosion• Liquid-metal corrosion• Molten-salt corrosion• Biological corrosion• Stray-current corrosion	<ul style="list-style-type: none">• Crevice corrosion• Filiform corrosion• Pitting corrosion• Oral corrosion• Biological corrosion• Selective leaching corrosion

2.3 Mechanisms of corrosion

As previously stated in section 2.1, an electrochemical reaction must take place for corrosion to occur. An essential condition to initiate electrochemical reactions is the formation of a corrosion cell. The corrosion cell consists of an anode, a cathode, an electrolyte and a metal path. The anode is the more reactive metal and it is represented as the negative terminal of the cell. Oxidation occurs at the anode which means that the electrons are released (-). The cathode is represented as the positive terminal of the cell. Reduction occurs at the cathode which means that the electrons are consumed (+). The electrochemical reaction happens within the electrolyte, which is a conductive solution (e.g. salt solution) where conventional flow goes from the anode (-) to the cathode (+). Oxidation reactions represents entry of metal ion into the solution, by dissolution, hydration or by complex formation, and causes metal loss at the area of the anode [8].

Consider a simplified corrosion case of the reaction between iron and water. The overall reaction can be written as:



The overall reaction can be broken down into the oxidising anodic reaction (Eq. 2.2) and the reducing cathodic reaction (Eq. 2.3). The corrosion process is illustrated below in the figure 2 [9].

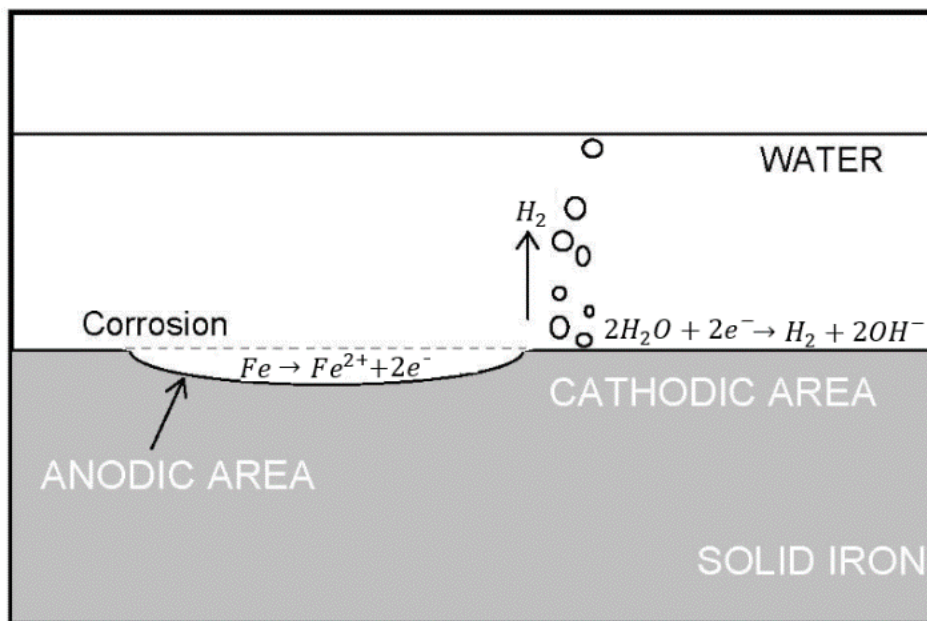


Figure 2: Illustration of the corrosion process of iron [9]

2.4 Polarisation

A metal that is not in equilibrium with its solution of ions has different electrode potential from the equilibrium potential. Polarisation is the amount that differs from the equilibrium potential and it is an essential parameter that allows useful statements to be made about the rates of corrosion process. Polarisation can in practical situations be defined as the potential change away from some other arbitrary potential, and as the free corrosion potential in mixed potential experiments [10].

The polarisation formula is defined as [11]:

$$\eta = E - E_{eq} \quad (2.4)$$

, where E is the resultant potential and E_{eq} is the equilibrium potential.

2.5 Mixed potential theory

Mixed potential theory can be applied to metals and alloys to predict the rate of corrosion in a given environment. There are two assumptions to this theory; 1) electrochemical reactions are composed of two or more partial anodic and cathodic reactions. 2) There cannot be any accumulation of charges [8]. Consider a case where iron is immersed in an acidic solution. The metal constitutes as a multielectrode as four reactions can occur; iron dissolution to form ferrous ions Fe^{2+} , the reverse of this process in which ferrous ions attaining electrons to form Fe , hydrogen ions in solution forming hydrogen gas or the reverse of this process. Figure 3 below is known as an “Evans diagram”, it illustrates the four reactions in potential versus current density. The two solid lines are feasible reactions and are drawn by extrapolation, giving an intersection at the corrosion potential (E_{corr}) and its current density (i_{corr}). This intersection is where the anodic reactions are equal to the cathodic reactions. If the potential is held below E_{corr} , dissolution process of iron will decrease and if held above it will increase [8, 12].

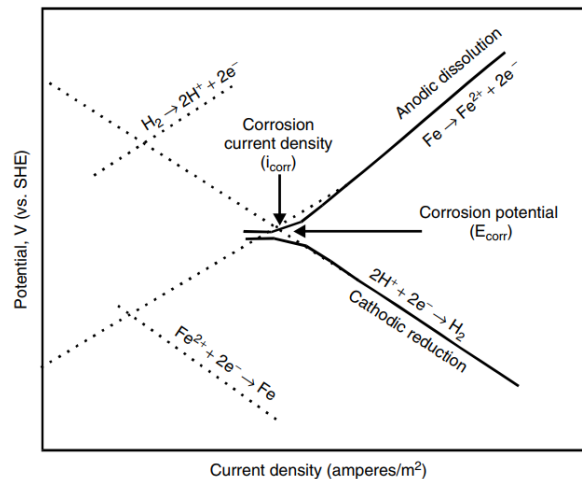


Figure 3: Evans diagram for iron immersed in an acidic solution [12]

From the Evans diagram in figure 3, four important parameters can be found: the corrosion potential (E_{corr}), the corrosion current density (i_{corr}), and the anodic (β_a) and cathodic (β_c) Tafel constants. Straight lines are obtained in the diagram by moving the potential away from the corrosion potential by a set value of $\pm\Delta E$, polarization can be determined with different current (i_{app}), as expressed below [12].

$$\text{For positive slope, } +\Delta E: \quad \eta_a = E - E_{corr} = \beta_a \log\left(\frac{i_{app}}{i_{corr}}\right) \quad (2.5)$$

$$\text{For negative slope, } -\Delta E: \quad \eta_c = \beta_c \log\left(\frac{i_{app}}{i_{corr}}\right) \quad (2.6)$$

2.6 Passivation and passivity

Stainless steels have a thin chromium rich oxide layer that protects against corrosion. The corrosion resistance depends strongly on the surface condition, and the protective film must be thin and continuous to have the mechanical and physical properties that is desired for the given material. Passivation is the formation of layers on the metal surface, while passivity (also called protective film/layer) is the condition when the protection properties of these layers causes an interruption of corrosion. The formation of these protective films on metal surfaces occurs either by precipitation of insoluble corrosion products or directly by the anodic reaction [4].

2.7 Pitting corrosion

Pitting corrosion is one of the most common forms of localized corrosion. The localized attack occurs on certain areas of the material surface, in which craters or pits are produced by the dissolution of small metal volumes. Pitting is considered as a dangerous and destructive form of corrosion since it is difficult to detect, predict and design against. Even small pits can cause the failure of an entire engineering system [11]. In the marine environment, ions such as chloride (Cl^-), bromide (Br^-), iodide (I^-) and thiosulfate ($S_2O_3^-$), in considerable amounts tends to cause pitting of steels [8]. Stainless steels are used in diverse applications for their corrosion resistance, nevertheless they are susceptible to pitting corrosion due to the breakdown of the protective passive film covering the metal. A passive film can repair itself with oxygen which implies that low oxygen environments causes poor corrosion resistance, i.e. the passive film breaks down faster than it can self-repair [13].

Consider a case of stainless steel in seawater. The passive film has a scratch where pitting corrosion has initiated, and the pit continues to propagate. There is usually an extremely corrosive micro-environment developed within the pit, which consists of hydrochloric acid. Inside the pit the pH is lowered significantly, together with an increase in chloride ion concentration, as a result of electrochemical reactions. This causes an increase in pitting growth and will eventually lead to failure of the structure. Shown below in figure 4 are some typical pitting shapes which can occur on the metal surface [13].

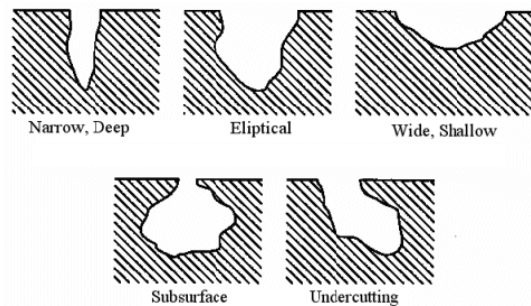


Figure 4: Pitting shapes, ASTM-G46 [13]

2.7.1 Principle of pitting corrosion

According to Z. Ahmad there are three conditions for pitting to initiate: “(1) the passive metal surrounding the anode is not subject to pitting as it forms the cathode and it is the site for reduction of oxygen. (2) The corrosion products which are formed at the anode cannot spread on to the cathode areas. Therefore, corrosion penetrates the metal rather than spread, and pitting is initiated. (3) There is a certain potential characteristic of a passive metal, below which pitting cannot initiate. This is called pitting potential, E_p .” [8]. The formation of an anode is essential for pitting corrosion to commence. A local corrosion cell is generated once the anode has formed. The following events may cause an anode formation; non-homogeneous environment (impurities, grain boundaries, rough surface, etc.), mechanical damage such as scratches, localized stress in form of dislocations, second phase particles emerging on the metal surface, or the formation of an active-passive cell with a large potential difference [8, 13].

The pitting reactions on a metal with a passive film is shown below and illustrated in figure 5. The environment consists of chloride and oxygen. An anodic reaction (Eq. 2.7) occurs inside the pit and is balanced by the cathodic reaction (Eq. 2.8) of oxygen at the surface level. At the beginning of the reaction, the whole surface is exposed to the electrolyte containing oxygen, which leads to reduction of oxygen inside the pit. As the metal continues to dissolve, the system needs to obtain charge neutrality. To accomplish this, an excess of positive ions M^+ and negative ions Cl^- migrate from the electrolyte. The product of this is the formation of hydrolysis (Eq. 2.9), ions of H^+ and Cl^- prevents repassivation and lowers the pH in the pit [8].

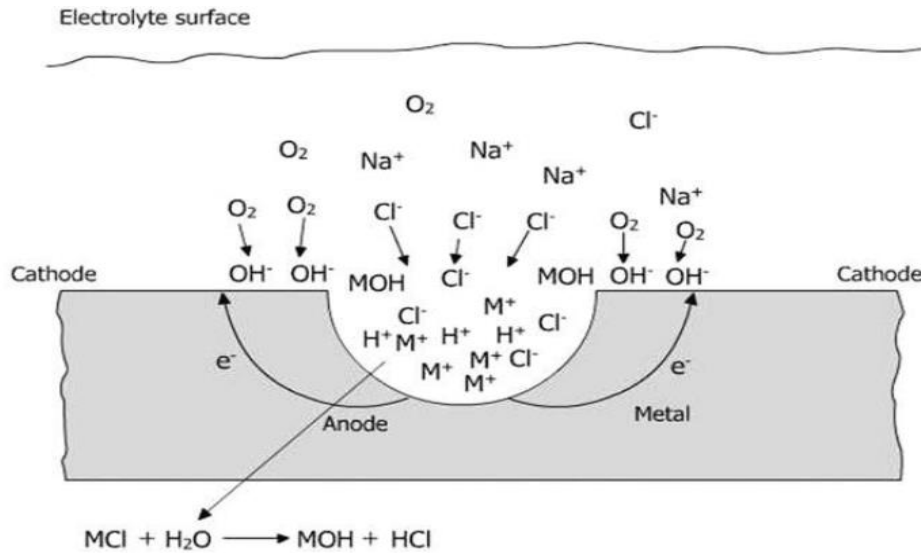
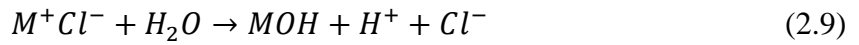


Figure 5: Illustration of pitting corrosion on a metal in chloride solution [8]

2.8 Crevice corrosion

Crevice corrosion is another common form of localized corrosion, with similar characteristics to pitting corrosion. Both corrosion types have similar propagation mechanisms, but different initiations. Crevice corrosion occurs in an occluded region, between a passive metallic surface and another surface, exposed to an electrolyte [14]. Most often it takes place in environments that contains chloride solutions [15]. The surfaces are in close proximity to each other and has a typical average separation gap between $0.1\mu\text{m}$ to $100\mu\text{m}$. An idealized illustration of crevice corrosion is shown in figure 6 below. Occluded regions can be found in many diverse engineering structures such as joints, flanges, metal surfaces under coatings and environmentally assisted cracks in metallic materials. It is difficult to design against crevice corrosion since many engineering structures have two or more materials very near each other, thus excluding the electrolyte from the occluded regions is often impossible. In general, the crevice attack rate increases with tighter occluded regions (i.e. smaller gaps between the surfaces). The corrosive rate is much higher within the occluded region than on the exposed surfaces. There are two parameters that characterizes a crevice: the gap g and the length l . These parameters also affect the initiation and propagation of corrosion [14].

Crevice corrosion can be divided into three fundamental processes: (1) Electrochemical reactions which includes dissolution and reduction reactions. (2) Homogeneous chemical reactions which includes hydrolysis, precipitation and homogeneous oxidation/reduction reactions of dissolved metal. (3) Mass transport by diffusion and convection which leads to large differences in concentration and electrochemical potential between the exposed surface and occluded region, due to the restriction of mass transportation in the occluded region [14].

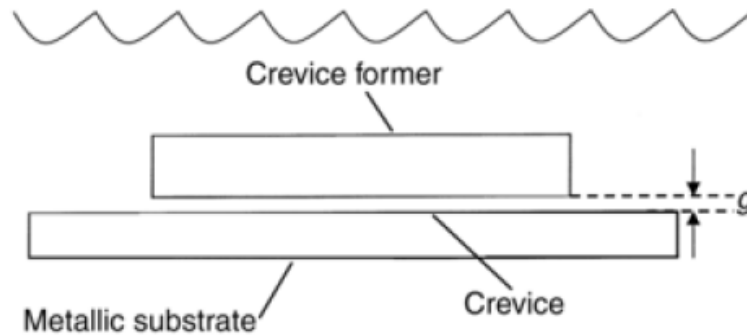


Figure 6: Idealized geometry of crevice corrosion [14]

2.8.1 Principle of crevice corrosion

The same initial anodic- (Eq. 2.7) and cathodic (Eq. 2.8) reaction as described in pitting corrosion (see section 2.7.1) applies for crevice corrosion. The metallic surface will be exposed to uniform corrosion, including the outside of the crevice. The crevice reactions on a metal with a passive film and another surface is illustrated in figure 7 below in an environment consisting of chloride and oxygen. The oxygen inside crevice area becomes consumed by the cathodic reaction, causing negative ions of Cl^- and OH^- to diffuse into the crevice to maintain charge balance. Resulting in metal chloride hydrolyses which lowers the pH and accelerates the corrosion attack [16].

Hydrolysis inside the crevice can be written as [8]:

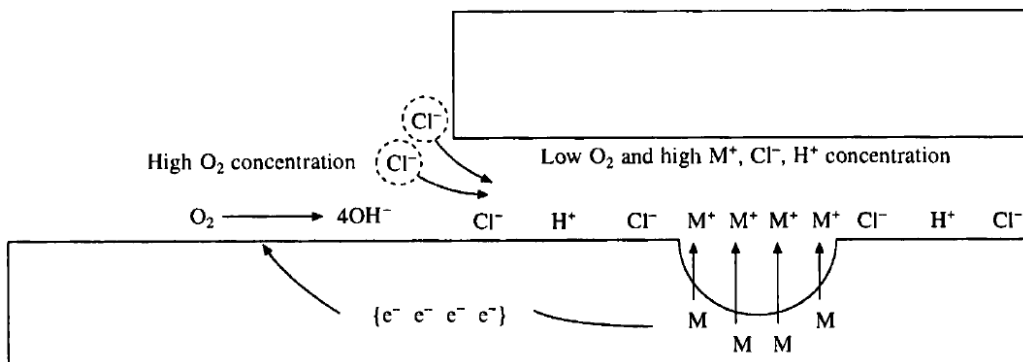
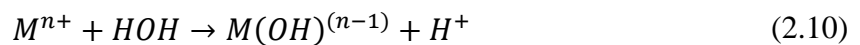


Figure 7: Mechanism of crevice corrosion [16]

2.9 Austenitic stainless steels

The most common type of stainless steel is the austenitic steel. It is a highly corrosion resistant, ductile, non-magnetic steel with austenitic structure (FCC). Austenitic stainless steels are primarily made up of iron, with chromium and nickel as alloying elements (16-26% Cr, 7-22% Ni). Other elements can also be added to the grades for improving the corrosion resistance. The most common type of austenitic stainless steel is known as 304 (UNS S30400) and it serves as a basis for other alloys of the 300-grade series. 304 is often called “18-8” stainless steel, due to nominal composition of 18% chromium and 8% nickel. Another common type is the grade 316 (UNS S31600), which has molybdenum additions for reducing pitting and crevice corrosion. Austenitic stainless steels have up to 0.1% carbon, the carbon content serves to strengthen the alloys. Many steels are made as dual-certified alloys, which means that an additional low-carbon grade is made from the original grade, e.g., 316L (UNS S31603) and 316 (UNS 31600). The low-carbon grade (316L) has reduced yield strength [3, 17]. The chemical composition and properties of 304 and 316L are given in below in table 2 and table 3.

2.9.1 Properties of 304 and 316L

Table 2: Chemical composition of 304 and 316L [18, 19]

UNS	Name	C	Mn	P	S	Si	Cr	Ni	N	Mo
S30400	304	0.07	2.00	0.045	0.030	0.75	17.5-19.5	8.00-10.5	0.1	-
S31603	316L	0.03	2.00	0.045	0.030	0.75	16.0-18.0	10.0-14.0	0.1	2.00-3.00

Note: Percentage by weight. Maximum value unless range is specified.

Table 3: Mechanical and physical properties of 304 and 316L [18, 19]

Name	Yield Strength [MPa]	Ultimate Tensile Strength [MPa]	Percent Elongation in 51 mm	Hardness, Max. Brinell
304	205	515	40	201
316L	170	485	40	217

Name	Density [g/cm ³]	Elastic Modulus [GPa]	Linear co-eff. of Thermal Expansion [cm/cm/°C]	Thermal Conductivity [W/m*K]	Specific Heat [J/kg*K]	Electrical Resistivity [μΩ*cm]
304	7.90	200	16.6 x 10 ⁻⁶ [20-100°C]	16.3 [100°C]	500 [20°C]	72 [20°C]
316L	8.027	200	16.5 x 10 ⁻⁶ [20-100°C]	14.6 [100°C]	450 [20°C]	74 [20°C]

Note: Minimum mechanical properties required.

2.10 Duplex stainless steels

Duplex stainless steels (DSS) are also primarily made up from iron, with chromium and nickel as alloying elements. The microstructure of DSS consists of a dual phase, one phase of ferritic (BCC) steels and another phase of austenitic (FCC) steels. The ferritic-austenitic phase is achieved by lowering the nickel content compared to austenitic steels. By comparing DSS to austenitic stainless steels there are several advantages, namely, higher mechanical strength, superior corrosion resistance, and a lower price due to low nickel content. DSS are less suitable than austenitic steels above 250°C and below -50°C due to the brittle behaviour of ferrite at these temperatures [3, 20]. A common grade among DSS is the type 2205 (UNS S32205), it is high in Ni and Mo additions. Lean versions of this grade exist with lower Mo and Ni contents, such as 2304 (UNS S32304) and 2003 (UNS S32003) [2]. The chemical composition and properties of 2003, 2304 and 2205 are given in below in table 4 and table 5.

2.10.1 Properties of 2003, 2304 and 2205

Table 4: Chemical composition of 2003, 2304 and 2205 [21, 22, 23]

UNS	ATI	C	Mn	P	S	Si	Cr	Ni	N	Mo
S32003	2003	0.030	2.00	0.030	0.020	1.00	19.5- 22.5	3.00- 4.00	0.14- 0.20	1.50- 2.00
S32205	2205	0.030	2.00	0.030	0.020	1.00	22.0- 23.0	4.50- 6.50	0.14- 0.20	3.00- 3.50
S32304	2304	0.030	2.50	0.040	0.030	1.00	21.5- 24.5	3.00- 5.50	0.05- 0.20	0.05- 0.60

Note: Percentage by weight. Maximum value unless range is specified.

Table 5: Mechanical and physical properties of 2003, 2304 and 2205 [21, 22, 23]

Name	Yield Strength [MPa]	Ultimate Tensile Strength [MPa]	Percent Elongation in 50 mm	Hardness, Max. BHN
2003	485	695	25	293
2205	450	655	25	293
2304	400	600	25	290

Name	Density [g/cm ³]	Elastic Modulus [GPa]	Mean co-eff. of Thermal Expansion [cm/cm*°C]	Thermal Conductivity [W/m*K]	Specific Heat [J/kg*K]
2003	7.78	210	13.8 x 10 ⁻⁶ [20-93°C]	17 [100°C]	510 [23°C]
2205	7.82	200	13.5 x 10 ⁻⁶ [20-100°C]	14.6 [100°C]	-
2304	7.80	200	13 x 10 ⁻⁶ [20-100°C]	13 [100°C]	-

Note: Minimum mechanical properties required.

2.11 The effect of alloying elements

2.11.1 Chromium

Chromium (Cr) is an essential alloying element in stainless steels, it is a ferrite former and insures the natural development of a stable, passive oxide film on the material surface. The film develops at approximate 10% Cr, stainless steels can have a maximum composition of 30% Cr. Higher composition gives increased corrosion resistance, but at the costs of mechanical properties, fabrication, weldability and suitability for applications in thermal exposures. Low chromium content allows only for mild atmospheric protection. Therefore, it is more efficient for stainless steels to add other alloying elements for improved chromium oxide film performance instead of adding more chromium [24, 25].

2.11.2 Nickel

Nickel (Ni) is an austenite former and it stabilizes the austenite structure which enhances mechanical properties such as toughness, ductility and weldability, and fabrication characteristics. In stainless steels, the Ni content can be up to 40% and the amount required to retain austenite structure depends on the carbon (C) content. The alloying effects of nickel are important because it promotes repassivation of the chromium oxide film and increases the resistance to acids [24, 25].

2.11.3 Molybdenum

Molybdenum (Mo) is a ferrite former and it stabilizes the chromium oxide film in the presence of chlorides. The alloying effects of molybdenum are important since it improves the resistance to localized corrosion such as pitting and crevice corrosion. Mo content added for stainless steels is usually up to 6 - 7% [24, 25].

2.11.4 Nitrogen

Nitrogen (N) stabilizes the austenite structure and enhances localized corrosion resistance. Nitrogen is an important alloying element since it strengthens the steel. In duplex grade steels it diminishes chromium and molybdenum segregation while increasing the corrosion resistance of austenitic phase. Nitrogen is normally added up to 0.3% in duplex (ferritic-austenitic) grade steels and up to 0.5% in austenitic stainless steels [24, 25].

2.11.5 Pitting resistance equivalent number

Pitting resistance equivalent (PRE) number is used as an estimation to calculate the resistance to localized corrosion by chlorides. Higher values of PRE give greater resistance. Stainless steels with PRE value of 40 or greater is regarded as truly seawater resistant. The common formula for PRE number is defined as [24, 25]:

$$PRE\ number = \%Cr + 3.3\%Mo + 16\%N \quad (2.11)$$

Table 6: Typical PRE numbers for stainless steels [18, 23]

Name	PREN
304	19*
316L	24*
2003	30*
2205	36*
2304	26*

Note: * is based on typical values from formula (2.11)

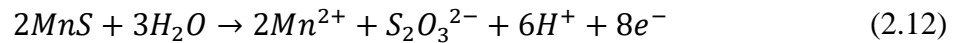
2.12 Atmospheric marine corrosion

The marine atmosphere is a very aggressive environment to metals. Seawater is characterized by its high salt content, that is, on average 35 parts per thousand which approximates to the weight in grams of dry salts contained in 1000g of seawater. Seawater is chloride (Cl⁻) dominant in ions, but the salinity also depends on other ions with less concentrations such as bromide (Br⁻) and iodide (I⁻). The marine environment can be divided into two groups, which are, splash zones and salt detectable zones. Splash zones, also called spray zones, are where metal surfaces are exposed to alternating wetting and drying conditions with deposition of salts from the sea. Salt detectable zones are found close the shore where salts in the wind are blown onto metal surfaces. Important factors in the marine environment that contributes to corrosion are temperature, oxygen content, pH of seawater, marine growth and salinity [26].

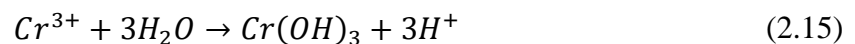
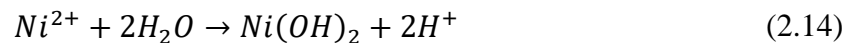
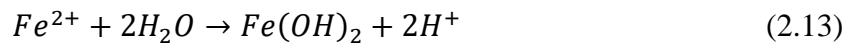
Seawater is usually alkaline, and the pH lies between 8.1 and 8.3 in the surface layers of the ocean. Often, seawater will contain hydrogen sulphide (H_2S), which accelerates the corrosion of most ferrous and non-ferrous alloys. Hydrogen sulphide is produced by the metabolism of sulphate-reducing bacteria, and its presence causes a reduction in pH (i.e. the water becomes more acidic). Temperature variations in seawater affects the pH, the rate of evaporation of moisture from the

surface and the rate of corrosion. It is expected that a high temperature accelerates the chemical process of dissolution. However, high temperatures are not always the cause of an increase in the corrosion rate, other factors such as difference in oxygen content and marine growths can play a key role in the marine environment [26].

Chloride ions in seawater breaks down the passive film on metals, pitting corrosion of 304 and 316L may initiate with the dissolution of manganese sulphide (MnS) inclusions. The MnS dissolves by the following reaction [27, 28]:



Reaction (Eq. 2.12) causes the pH to lower at the inclusion, which leads to dissolution of metals (Fe, Ni, Cr). Some of the metal ions continues to lower the pH due to hydrolysis, their reactions are written as [27, 28]:



2.13 Electrochemical testing

Electrochemical tests are usually performed in a laboratory and used to find the basic corrosion-influencing factors, such as corrosion potential, passivation, oxidation power, anodic and cathodic characteristics, thermodynamic- and kinetic parameters. Test procedures are generally performed with guidelines provided from standards, which gives the results a high reproducibility. Polarization curves can be obtained by the potentiostatic method, usually provided in Evans diagrams. This method requires a potentiostat, a working electrode (W), a reference electrode (RE), a counter electrode (CE) and an electrolyte. This is illustrated in the standard polarization cell shown in figure 8 below [2].

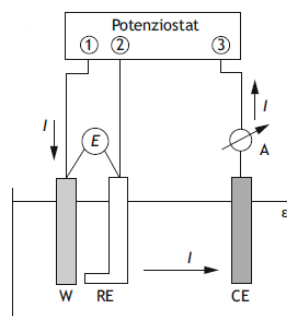


Figure 8: Standard polarization cell [4]

2.13.1 Method for Cyclic Potentiodynamic polarization

Cyclic potentiodynamic polarization (CPDP) tests are used on iron- nickel- and cobalt-based alloys to determine their susceptibility to localized corrosion, such as pitting and crevice corrosion. Initially the test specimen is prepared and the rest potential (E_r) is measured between the working electrode (specimen) and the reference electrode, this is called the open circuit potential (OCP). The general shape of a CPDP curve is shown below in figure 9, the potential increases (forward) and decreases (reverse) following the arrows indicated on the curve. The most important parameters for evaluating pitting corrosion behaviour is the pitting potential (E_{pit}) and the repassivation potential (E_{rep}) with respect to the corrosion potential (E_{corr}). The pitting potential indicates the minimum potential of pitting initiation, passing this potential will initiate the growths of new pits. The repassivation potential is found at the intersection of the reverse- and forward curve, it indicates the potential at which pitting corrosion is stopped [29].

In the CPDP curve hysteresis tends to occur, which is when the forward- and reverse curve does not overlay with each other. The amount of hysteresis, which is the difference of pitting potential and repassivation potential ($E_{pit} - E_{rep}$), indicates the amount of pitting corrosion. The materials resistance to localized corrosion is based on E_{rep} measured to E_{corr} . If $E_{rep} > E_{corr}$, propagation of active pits stops. The region between E_{rep} and E_{corr} is called perfect passivity and the passive film is stable, i.e. neither crevice or pitting will initiate or propagate. In the region between E_{pit} and E_{rep} prior pitting will propagate, but not nucleate. If E_{corr} lies between E_{pit} and E_{rep} , fully repassivation of pits fails and the pits continues to propagate [29].

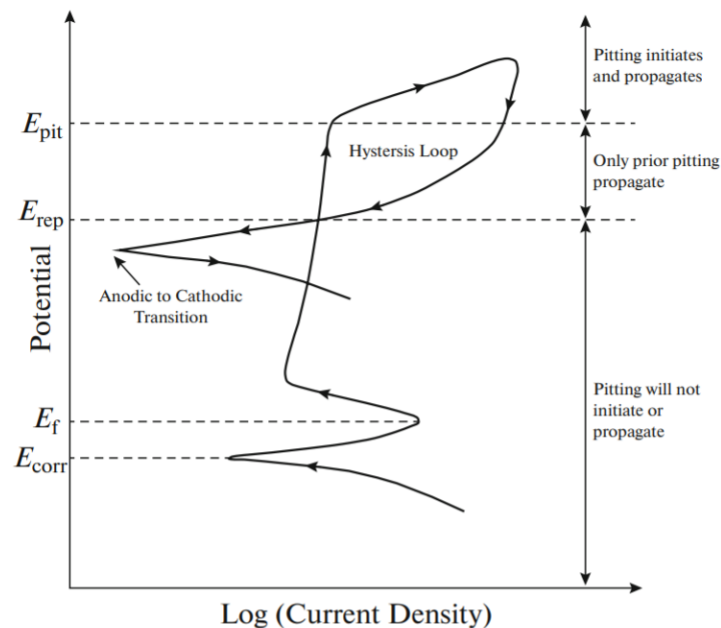


Figure 9: General CPDP curve and corrosion parameters [29]

2.14 X-ray

2.14.1 Energy dispersive spectroscopy analysis

Energy dispersive spectroscopy (EDS) is used to determine the elemental composition of a sample, which includes both qualitative and quantitative analysis (i.e., it finds the elements and the amount of each element in a sample). EDS uses a solid-state detector consisting of a lithium doped silicon crystal to capture emitted X-rays (as photons or Auger-electrons) from the sample. X-rays occur when the electron beam hits the surface of the sample. The characteristic X-rays are studied on an emission spectrum, where the energy is given in voltage for each of the emitted X-rays. The quantitative analysis is called ZAF and uses a known standard composition to compare with the sample. Both standard and sample should be almost equal to get feasible results. Also, parameters such as current, acceleration voltage and outlet angle should be kept constant for both standard and sample. A more accurate alternative to EDS is wavelength dispersive spectrometer (WDS), which measures specific elements from incoming wavelengths of X-rays using Bragg's Law [30].

2.14.2 Characteristic X-rays

In an atom, the electrons are found in different discrete energy levels called K-, L- and M-shells, where K is the inner shell. These energy levels are given by the atom's quantum number. Characteristic X-rays develop when incoming electrons from the electron gun interact with the orbital electrons (in the K-, L- and M-shell) in the atom of the test sample. If the electron current has enough energy, it can ionize the atom. The atom then loses an electron in one of the shells, causing it to be in an excited state. In an excited state, the atom has an empty spot requiring an electron. To return to its original state, it must send an electron from one of the outer shells into the empty spot. This process results in emission of photons or Auger electrons. The transition from the L- to K-shell emits a K_{α} -photon and the transition from M- to K-shell emits a K_{β} -photon [30].

With different energy levels in the shells of the atom, the emitted photons have an energy matching the difference between the initial and the final shell that the electron lands in. This is measured as wavelength by Moseley's law, written as [30]:

$$\lambda = \frac{K}{(Z - \sigma)^2} \quad (2.16)$$

, where K and σ are constants, and Z is the atomic number. Each of the wavelengths of the characteristic X-rays belongs to certain atoms (given by atom number), this makes the detection of characteristic X-rays correspond to elements within the test sample. As shown in the equation (Eq. 2.16), the wavelength decreases as the atomic number increases [30].

3 Materials and methods

To investigate the corrosion properties of stainless steels in simulated offshore environment, it was carried out experiments of atmospheric marine corrosion and cyclic polarization on the samples. The main objective was to investigate and compare the corrosive properties of LDSS 2003 and 2304, using 2205, 304 and 316L as reference samples. The purpose was to study visual effects, change of mass, and important parameters for pitting corrosion behaviour, on the samples exposed to a simulated offshore environment. In the atmospheric marine corrosion experiment, it was attempted to generate general and localized corrosion on the samples. The cyclic polarization experiment was performed according to ASTM G61-86, and important parameters such as pitting potential, repassivation potential and corrosion potential was carried out from the samples. A scanning electron microscope was used to find the chemical compositions of the materials and used to inspect the surface layer of each material before testing.

3.1 Material certification

The materials, provided by Gateway Stainless AS, were delivered as rectangular hollow tubes with different dimensions. The tubes were manufactured, quality assured and tested by Stalatube in Finland. The material certificates give information about the materials grades, surface finish, mechanical properties and compositions, and can be found in Appendix A. In table 7 below, the test materials grades are shown with its belonging mechanical properties. The composition is shown in table 8 below with the belonging PRE-values, calculated from formula (2.11).

Table 7: Mechanical properties of the materials

Grade	Name	Test round	Yield Strength Rp0.2 [N/mm ²]	1% Proof Strength Rp1.0 [N/mm ²]	Tensile Strength Rm [N/mm ²]	Elongation A5 %	Hardness HB
EN 1.4301	304	Test 1	325	384	621	46	85
		Test 2	330	387	627	47	84
EN 1.4404	316L	Test 1	333	374	617	51	187
		Test 2	336	373	616	52	178
UNS S32003	2003	Test 1	586	-	779	27	-
		Test 2	-	-	-	-	-
EDX 2304	2304	Test 1	613	681	789	32	246
		Test 2	606	671	771	34	244
EN 1.4462	2205	Test 1	637	719	844	33	258
		Test 2	625	707	833	33	251

Table 8: Composition and PRE-value of the materials

Name	C	Mn	P	S	Si	Cr	Ni	N	Mo	PRE (Eq. 2.11)
304	0.016	1.120	0.036	0.005	0.400	18.110	8.060	0.046	-	18.846
316L	0.021	0.920	0.037	0.001	0.460	17.100	10.000	0.036	2.020	24.342
2003	0.013	1.740	0.025	-	0.350	22.200	3.700	0.170	1.780	30.794
2304	0.015	1.330	0.029	0.001	0.520	23.740	4.270	0.176	0.530	28.305
2205	0.021	1.360	0.026	0.001	0.330	22.220	5.680	0.189	3.140	35.606

Note: Percentage by weight.

3.2 Preparing the test materials

The test materials were delivered as tubes, as shown below in figure 12. Two different horizontal metal cutting band saws were used to cut the tubes into smaller plates. The tubes were first cut into smaller sized tubes with similar lengths of 5 cm by the Rusch metal cutting band saw, as shown in figure 10 below. The smaller tubes were then cut into small plates with different lengths (width was kept as 5 cm) by the Pilous ARG 220 plus band saw as seen in figure 11. After the cutting process, the edges of the plates were treated by a metal file to remove most of the burr created from cutting (i.e. sharp edges and burr were trimmed down). This is shown in figure 13, where the sample was fastened by a clamp. The samples were then ready for atmospheric marine corrosion testing, one test sample is shown in figure 14.



Figure 10: Rusch horizontal metal cutting band saw Figure 11: Pilous ARG 220 plus band saw

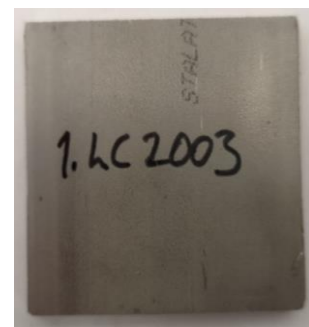


Figure 12: Stainless steel tubes

Figure 13: Metal file used on a sample

Figure 14: Sample ready for testing

3.3 Atmospheric marine corrosion test

In the atmospheric marine corrosion experiment, three rounds of testing were performed (named 1., 2., 3.). The samples were exposed to a simulated offshore environment and subjected to different temperatures for each testing round. In the first round, the test period consisted of 8 weeks in room temperature of 20°C, the second round and third round consisted of 4 weeks in a heating cabinet with a temperature of 40°C and 60°C. Each type of material had two samples for every test round to test their corrosive properties against general- and localized corrosion, where one of the samples were taped across its surface to provide crevice or pitting initiation. The samples were named AC for general corrosion and LC for localized corrosion. During the test rounds, the lower half of the samples was immersed in seawater. The samples were sprayed with salt-spray (seawater) two times a day on the surfaces (front side facing up) to simulate the splash zone in the marine environment.

The test set-up is illustrated below in figure 15, where each material had their own small plastic containers to store seawater. The material was supported by a small piece of wood so that it could be half immersed in seawater. The seawater used was gathered from the North Sea, close to shore in Fiskepiren, Stavanger. During each round of testing there was evaporation of seawater, the containers were filled up every third day so that the samples would stay half immersed. The heating cabinet provided by Multi Phase Meters is shown below in figure 16 and the inside with the samples in containers in figure 17. The samples were weighted to find their mass before and after the testing rounds, and visual inspection was performed after testing. A total of 30 samples were tested for general and localized corrosion, given in table 9 below is an overview of the materials and sample names.



Figure 15: Samples ready for general and localized corrosion testing



Figure 16: Heating cabinet



Figure 17: Samples inside the heating cabinet

Table 9: Material types with sample names

Test type	No.	Temperature (Duration)	SS 304	SS 316L	LDSS 2003	LDSS 2304	DSS 2205
General atmospheric marine corrosion	1	20°C (8 weeks)	1.AC304	1.AC316L	1.AC2003	1.AC2304	1.AC2205
	2	40°C (4 weeks)	2.AC304	2.AC316L	2.AC2003	2.AC2304	2.AC2205
	3	60°C (4 weeks)	3.AC304	3.AC316L	3.AC2003	3.AC2304	3.AC2205
Localized atmospheric marine corrosion	1	20°C (8 weeks)	1.LC304	1.LC316L	1.LC2003	1.LC2304	1.LC2205
	2	40°C (4 weeks)	2.LC304	2.LC316L	2.LC2003	2.LC2304	2.LC2205
	3	60°C (4 weeks)	3.LC304	3.LC316L	3.LC2003	3.LC2304	3.LC2205

3.4 Scanning electron microscope

The scanning electron microscope, SEM ZIESS SUPRA 35VP, was used to provide the chemical compositions and surface images of each material. Each material had to be cut as 1cm X 1cm plates and cleaned with Acetone and Ethanol before testing. The samples cut for testing can be seen in the figure 18 below, where 2304, 304, 2003, 2205 and 316L corresponds to sample names: 04, 4, 3, 5 and L. After cleaning the samples, they were mounted on a rotary sample stub and inserted in the SEM specimen chamber. The chamber was then depressurized to provide vacuum inside it. During examination, the working distance was set to 10mm and acceleration voltage was set to 20kV. Adjustments of brightness, contrast and focus were made to fine tune the image. Energy dispersive spectrometer (EDS) data was provided by the EDAX software and the SEM is shown in figure 19 below. During the imaging of the samples surfaces it was observed that they

contained some contamination (dark spots). After some trials with EDS scanning on different point and areas, it was decided that the samples should also be retested with a polished surface to remove some of the contaminations.



Figure 18: Samples cut for SEM-analysis

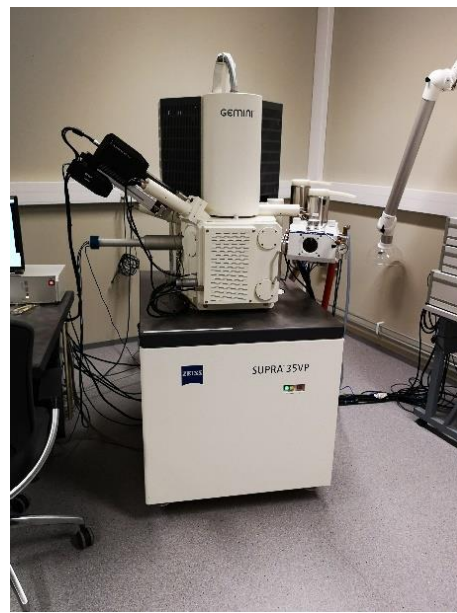


Figure 19: SEM ZIESS SUPRA 35VP

3.5 ASTM G61-86 test

The standard ASTM G61-86 was used to determine the materials relative susceptibility to localized corrosion in a chloride environment. This standard covers a test procedure for conducting cyclic potentiodynamic polarization measurements, and the test provides corrosion properties such as pitting potential, repassivation potential and corrosion potential. The tests were performed with some deviations from the standard. There was performed two experiments, one ordinary according to standard and one modified with a lower sodium chloride content. The purpose of the modified experiment was to investigate the different materials corrosion properties in a low chloride environment. The standard is stated as:

ASTM G61-86 (Reapproved 2018) - Standard Test Method for Conducting Cyclic Potentiodynamic Polarization Measurements for Localized Corrosion Susceptibility of Iron-, Nickel-, or Cobalt-Based Alloys [31]

3.5.1 Preparation

The samples were cut into small rectangular shapes with the same length so that they would fit through the lid of the beaker and easily expose the same area to the chloride environment. Some pre-experiments by trial were performed to get to know the testing procedure and the Gamry software.

3.5.2 Equipment

- Working Electrode (Sample)
- Counter Electrode
- Reference Electrode
- Gamry Potentiostat
- Beakers
- Sartorius digital weight scale
- Plastic tubes
- Nitrogen tank
- Parafilm
- PTFE tape
- Ultrasonic cleaner

3.5.3 Test procedure

The given test procedure is for one sample, there was performed 3 parallel test per material, i.e., 15 tests for the ordinary experiment and 15 tests for the modified experiments. Before testing, the Gamry instrument was calibrated as shown in figure 20. The samples names are given in table 10 and the polarization cell can be seen in figure 21. The test procedure was performed as follows:

1. The sample was cleaned in an ultrasonic bath containing distilled water for 5 minutes and set to dry.
2. 34 g of NaCl, measured by Sartorius digital weight scale, was dissolved in 920 mL distilled water to create a 3.56 % (by weight) sodium chloride solution.
3. The sodium chloride solution was set to reach room-temperature of 20°C.
4. 900 mL of the sodium chloride solution was transferred into a beaker.
5. 1 cm² of the sample was measured as the exposure area and the rest of the sample was taped.
6. The lid was placed on top of the beaker and sealed by parafilm, then the electrodes and nitrogen tube were placed in the belonging positions into the lid and connected to the Gamry potentiostat. The working electrode (sample) was placed above solution level. All openings through the lid was sealed by tape.
7. The solution was set to purge with nitrogen gas to remove oxygen from the solution for 5 minutes.
8. The working electrode (sample) was then lowered into the solution.

9. Gamry software was then started, and the open circuit potential (OCP) was set to run for 5 minutes.
10. After obtaining the OCP, the cyclic polarization scan was set to run with forward and reverse scan-rate of 1 mV/s. Apex E and Apex I was set to 1,5 V and 15 mA/cm².
11. The data from the tests was stored and evaluated.

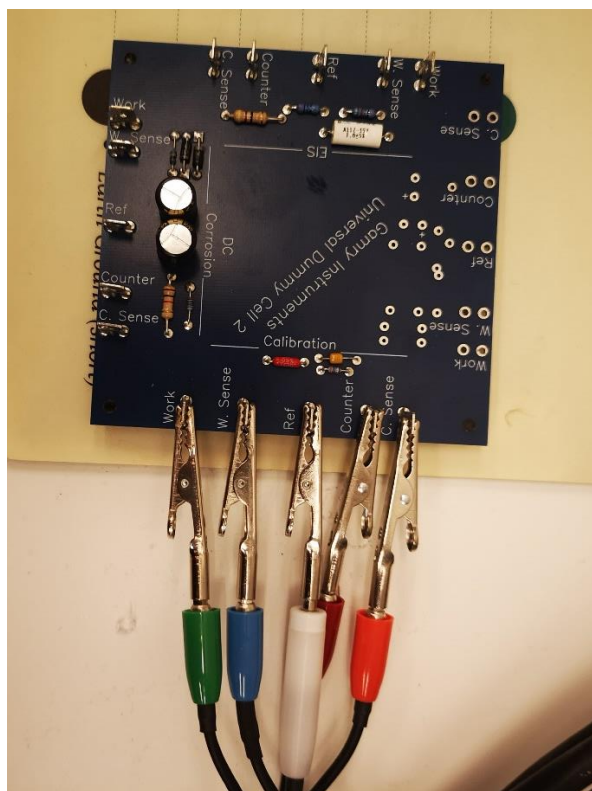


Figure 20: Calibration of Gamry instrument

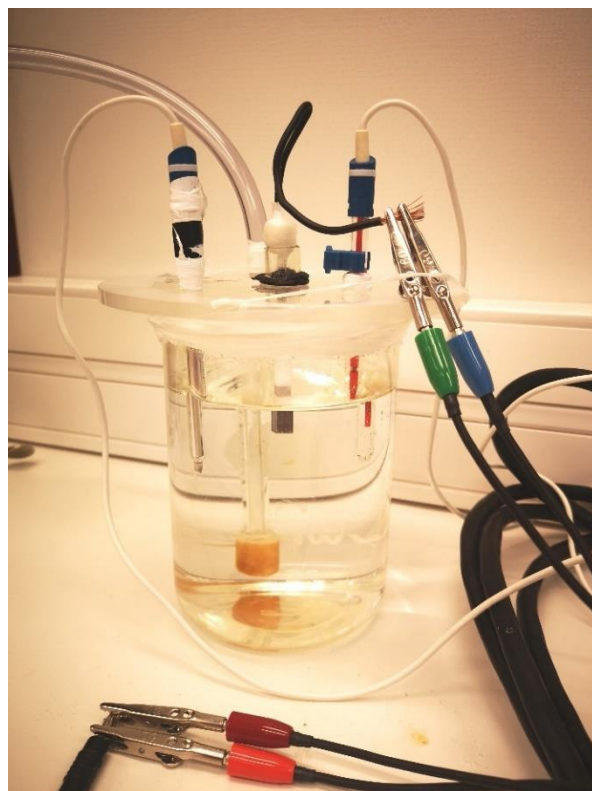


Figure 21: Polarization cell

Table 10: Ordinary and modified test samples with names

Test type	Condition	No.	SS 304	SS 316L	LDSS 2003	LDSS 2304	DSS 2205
Ordinary	34 g NaCl in 920 mL distilled water	1	1P304	1P316L	1P2003	1P2304	1P2205
		2	2P304	2P316L	2P2003	2P2304	2P2205
		3	3P304	3P316L	3P2003	3P2304	3P2205
Modified	10 g NaCl in 920 mL distilled water	1	1M304	1M316L	1M2003	1M2304	1M2205
		2	2M304	2M316L	2M2003	2M2304	2M2205
		3	3M304	3M316L	3M2003	3M2304	3M2205

The experimental setup and hardware settings in the Gamry software are shown below in figure 22 and figure 23.

Chart	Experimental Setup	Experimental Notes	Open Circuit Voltage	Hardware Settings
Initial E (V)	<input type="text" value="-0.5"/>	<input checked="" type="radio"/> vs. E _{ref}	<input type="radio"/> vs. E _{gc}	
Apex E (V)	<input type="text" value="1.5"/>	<input checked="" type="radio"/> vs. E _{ref}	<input type="radio"/> vs. E _{gc}	
Final E (V)	<input type="text" value="-0.25"/>	<input checked="" type="radio"/> vs. E _{ref}	<input type="radio"/> vs. E _{gc}	
Test Identifier	<input type="text" value="Cyclic Polarization Scan"/>			
Date	<input type="text" value="30.4.2019"/>			
Time	<input type="text" value="16:38:26"/>			
Forward Scan (mV/s)	<input type="text" value="1"/>		Reverse Scan (mV/s)	<input type="text" value="1"/>
Sample Period (s)	<input type="text" value="1"/>		Apex I (mA/cm ²)	<input type="text" value="15"/>
Sample Area (cm ²)	<input type="text" value="1"/>			
Density (g/cm ³)	<input type="text" value="7.87"/>			
Equiv. Wt	<input type="text" value="27.92"/>			
Conditioning	<input type="checkbox"/> Off	<input type="text" value="15"/> Time(s)	<input type="text" value="0"/> E(V)	
Init. Delay	<input type="checkbox"/> Off	<input type="text" value="300"/> Time(s)	<input type="text" value="0.1"/> Stab.(mV/s)	
IR Comp	<input type="checkbox"/> Off			
Equil. Time (s)	<input type="text" value="0"/>			
Open Circuit (V)	<input type="text" value="-0.347453"/>			

Figure 22: Experimental Setup in Gamry software

Chart	Experimental Setup	Experimental Notes	Open Circuit Voltage	Hardware Settings
Potentiostat	PCI4G750-51101		Pstat Model	Series-G 750
Control Mode	Potentiostat		Current Convention	Anodic
Control Amp Speed	Medium		I/E Stability	Nom
I/E AutoRange	<input checked="" type="checkbox"/> On		I/E Range	75 mA
Ich Auto Range	<input checked="" type="checkbox"/> On		Vch Auto Range	<input checked="" type="checkbox"/> On
Ich Range	3 V		Vch Range	30 V
Ich Filter	5 Hz		Vch Filter	5 Hz
Ich Offset Enable	<input type="checkbox"/> Off		Vch Offset Enable	<input type="checkbox"/> Off
Ich Offset (V)	<input type="text" value="0"/>		Vch Offset (V)	<input type="text" value="0"/>
Positive Feedback IR Comp	<input type="checkbox"/> Off		Positive Feedback Resistance	<input type="text" value="0"/>
I/E Range Lower Limit	75 nA		Ach Range	3 V
DC Calibration Date	24.4.2019		AC Calibration Date	24.4.2019
Framework Version	5.67			

Figure 23: Hardware Settings in Gamry software

3.5.4 Interpretation of the polarization plots

In all the samples, the pitting potential (E_{pit}) is measured at a current of $200\ \mu\text{A}$, just above the occurrence of a sharp increase in anodic current of the forward scan. The repassivation potential (E_{rep}) is measured at a current of $2\ \mu\text{A}$ of the reverse scan for all samples, except samples of duplex where the repassivation is set at the maximum point [32]. This is illustrated below in figure 24 and figure 25.

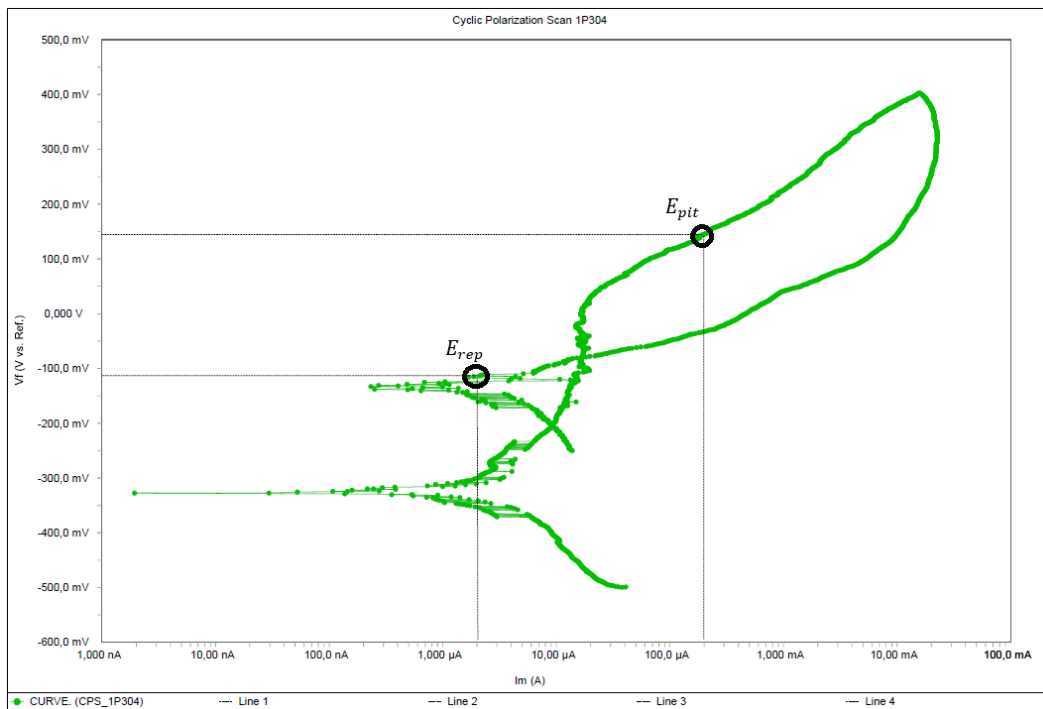


Figure 24: Pitting- and repassivation potential of SS 304 plot

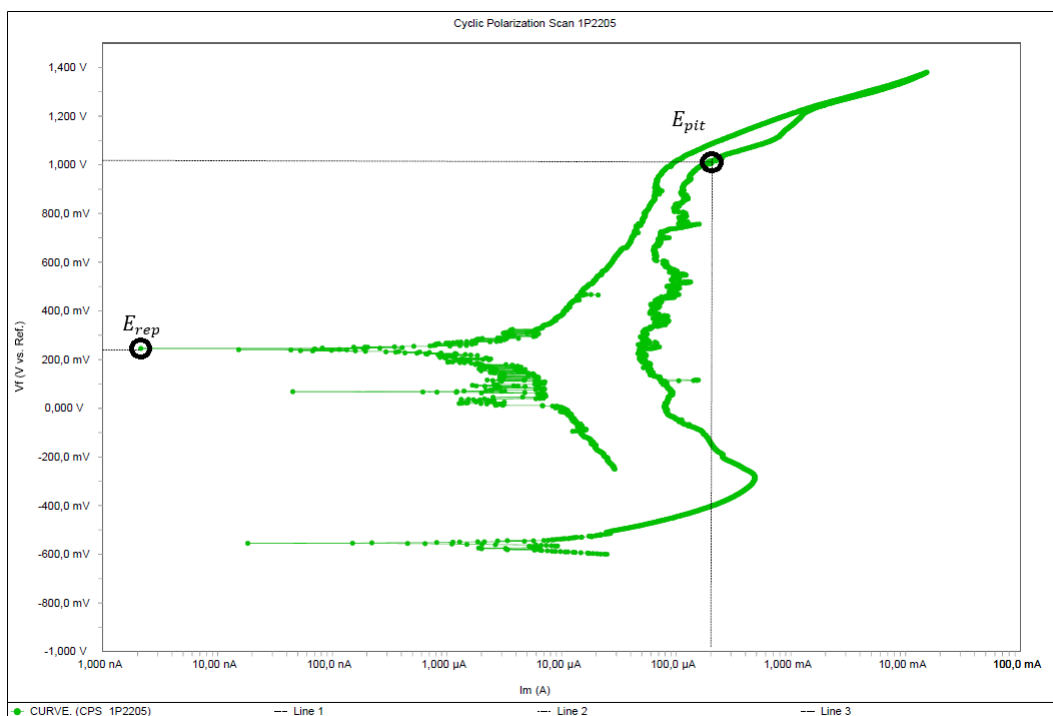


Figure 25: Pitting- and repassivation potential of DSS 2205

3.5.5 Deviation from standard

Temperature:

The standard states that the temperature of the solution should be $25 \pm 1^\circ\text{C}$. The temperature of the solution was $20 \pm 3^\circ\text{C}$.

Specimen preparation:

The recommendation from the standard is to wet grind and wet polish the sample with 240-grit and 600-grit SiC paper. Prior to assembly, the sample is to be ultrasonically degreased for 5 minutes in detergent and water, and then rinsed in distilled water. This was performed differently; the sample was only cleaned by an ultrasonic bath with distilled water for 5 minutes.

Oxygen removal of the solution:

The standard recommends that the solution is to be purged with an appropriate gas to remove oxygen for a minimum 60 minutes. The solution was purged with nitrogen gas for 5 minutes.

Immersion of the specimen:

The standard states that the specimen should be immersed in the solution for 60 minutes before initiating open circuit potential and polarization. This was not done as the experiment was started after purging of the solution.

Specimen holder:

According to the standard, a suitable holder designed for the exposure of 1 cm^2 of the sample should be used. Instead a beaker and a lid were used, sealed by parafilm and tape. The exposure area was the same.

Potential scan-rate:

The standard says that a potential scan rate of $0.6\text{ mV}/h \approx 0.167\text{ mV}/s$, this was performed with a scan rate of $1\text{ mV}/s$.

Modified experiment:

The modified experiment was performed the same way as the ordinary experiment, but with a lower sodium chloride solution; 10 g of NaCl dissolved in 920 mL distilled water.

4 Results

4.1 Evaluation of samples after atmospheric marine corrosion testing

The results obtained from atmospheric marine corrosion testing are shown in table 11, where it is marked with an X if the samples have corroded. Test round 3 had the most aggressive environment to the samples, which also caused almost all the samples to corrode. Test round 2 had very little effect on the samples and only three samples showed signs of general corrosion. Test round 1 had caused some samples to corrode. During testing of each round there was observed a generation of salt layer on the surfaces of the samples, this was washed off by spring water before the weight test and then pictures of the samples were taken. The salt layer on the samples are shown in figure 26 below. There was not observed any form of localized corrosion on the samples, pictures of the samples before and after testing are found in Appendix B. There was not recorded any deviations of mass before and after testing, which can be seen in Appendix C.

Table 11: Result of general- and localized corrosion on the samples

Sample	Round 1 (samples 1.)		Round 2 (samples 2.)		Round 3 (samples 3.)	
	General corrosion	Localized corrosion	General corrosion	Localized corrosion	General corrosion	Localized corrosion
AC304	X				X	
LC304	X		X		X	
AC316L			X		X	
LC316L	X				X	
AC2003					X	
LC2003						
AC2304	X				X	
LC2304			X		X	
AC2205	X				X	
LC2205						

Note: X indicates visible corrosion on the surface



Figure 26: Salt layer on samples after testing of round 1

The percentage of the corroded surfaces were estimated by applying a 20x20 grid, such as illustrated for one sample below in figure 27. The X on each grid point indicates a corroded area by general corrosion of the sample surface. The amount of these corroded areas is divided by the total grid area and then multiplied by 100 to get the estimated percentage of corrosion. In figure 28 below, the percentage of corrosion are shown for each sample from table 11.

The formula used to calculate the percentage of corroded areas of a sample surface is as follows:

$$\text{Percentage of corrosion} = \frac{\text{Amount of corroded areas}}{\text{Total grid area (20x20)}} * 100 \tag{4.1}$$



Figure 27: 20x20 grid illustrated on sample 3.AC 304

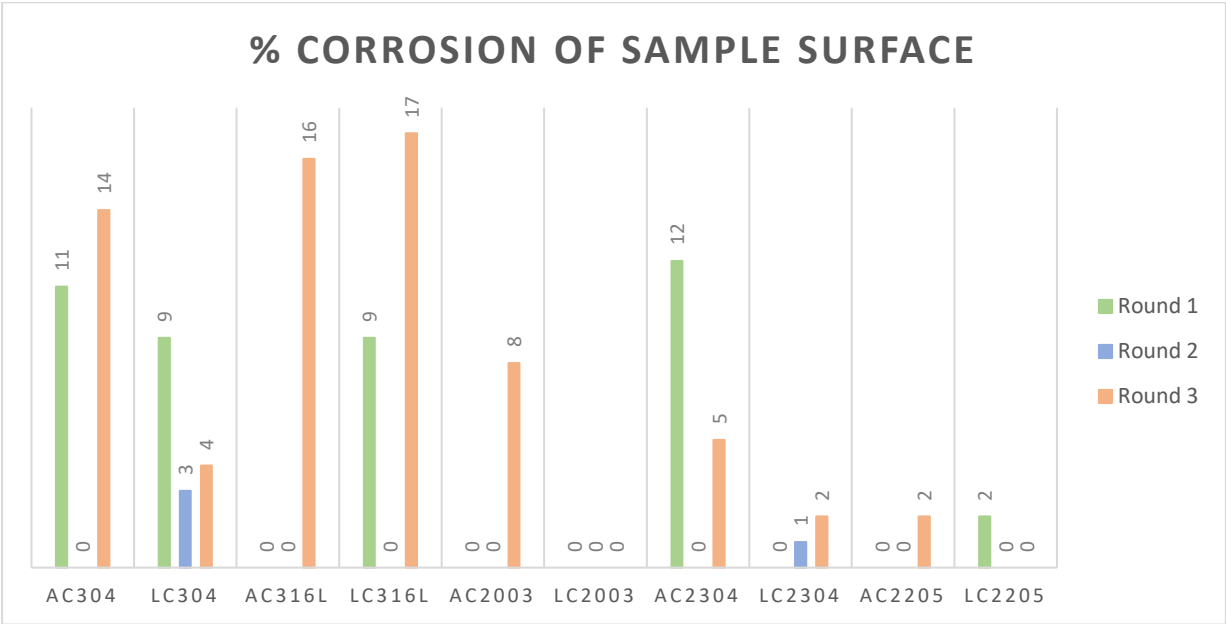


Figure 28: Percent corrosion of the sample surfaces

4.1.1 Samples from test round 1

Some of the samples from test round 1 showed signs of general corrosion initiation, while the other samples showed zero corrosion activities. Samples 1.AC316L, 1.AC2003 and 1.AC2205 tested for general corrosion was not affected by the chloride environment and have not corroded. None of the samples tested for localized corrosion showed initiation of localized corrosion, however sample 1.LC304 had initiated general corrosion above the tape level. General corrosion can also be spotted on sample 1.AC2304 at water level, sample 1.LC316L had begun to initial general corrosion on tape level. Sample 1.LC2205 showed a small area of general corrosion on the burr edge. The front- and backside of the samples are shown below in figure 29 and figure 30.

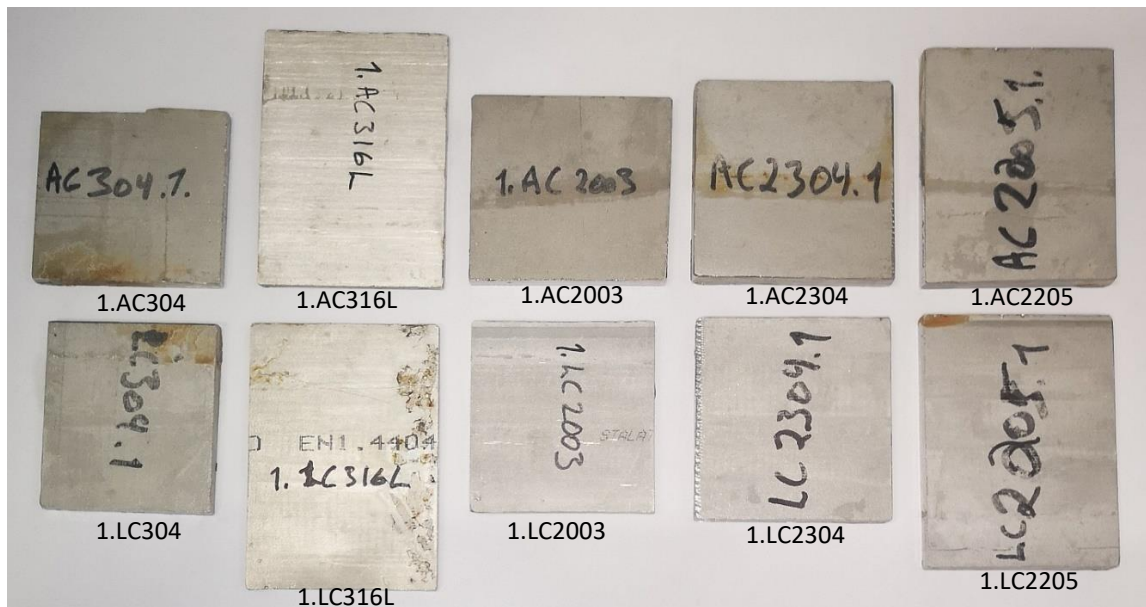


Figure 29: Frontside of the samples after test round 1

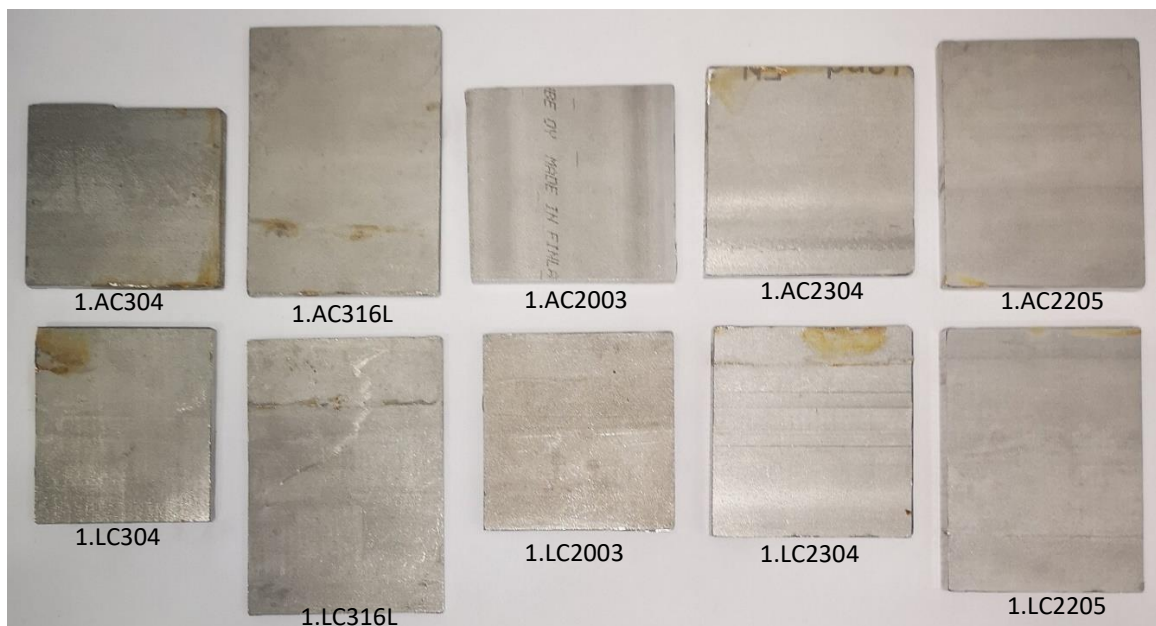


Figure 30: Backside of the samples after test round 1

4.1.2 Samples from test round 2

The result from test round 2 reveals almost no corrosion on the samples. The only samples affected by general corrosion initiation were 2.LC304 and 2.LC2304. Sample 2.AC316L had one small spot of corroded area on both the front- and back-side, these spots were less than 0.2% corrosion by using a 20x20 grid. This can be seen below in figure 31 and figure 32.



Figure 31: Frontside of the samples after test round 2

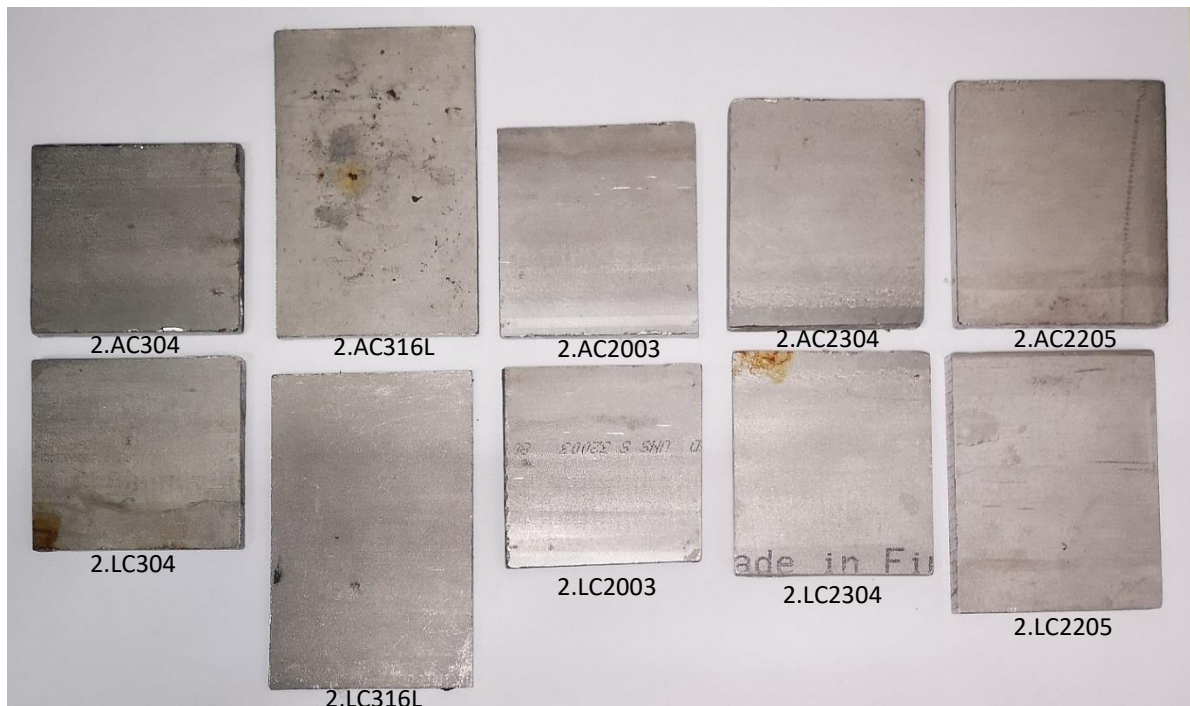


Figure 32: Backside of the samples after test round 2

4.1.3 Samples from test round 3

The samples gathered from test round 3 appears to be the most corroded samples of all the test rounds due to high temperature. All samples were affected by general corrosion, except samples 3.LC2003 and 3.LC2205. Samples 3.AC304 and 3.LC304 have general corrosion on the burr edges, which can be seen on the backside of the samples. This was also observed with the frontside of sample 3.AC2003. Samples 3.AC2304 and 3.AC2205 were little affected by corrosion and have only initiated small areas of general corrosion on their surfaces. The front- and backside of the samples are shown in figure 33 and figure 34 below.

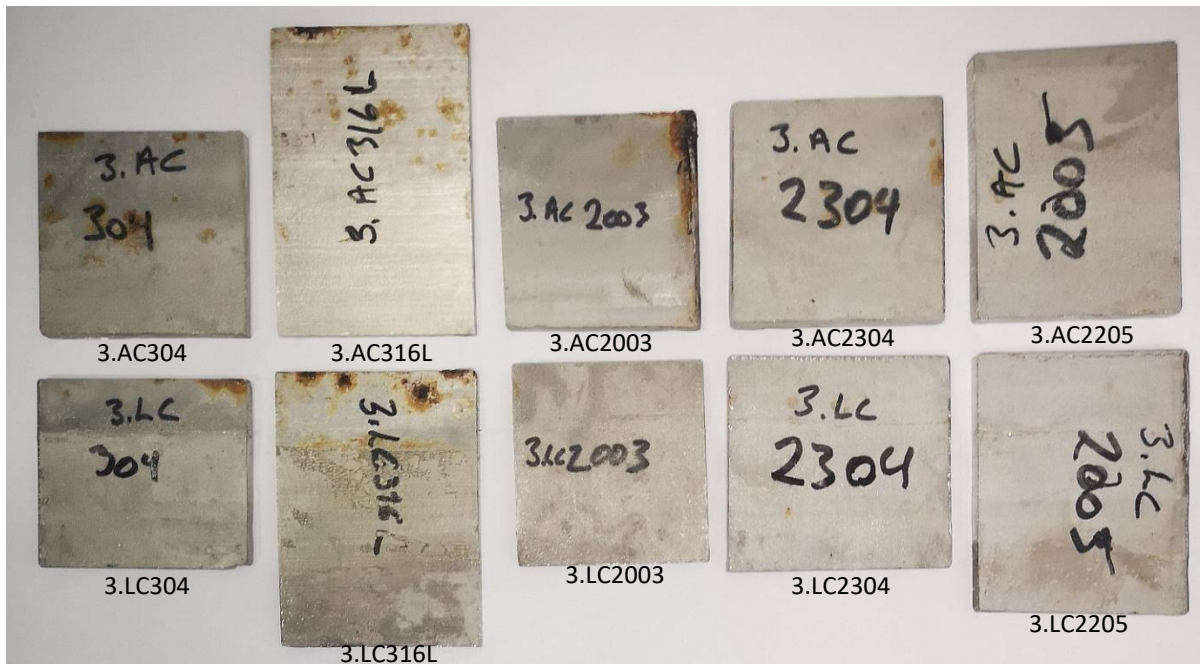


Figure 33: Frontside of the samples after test round 3

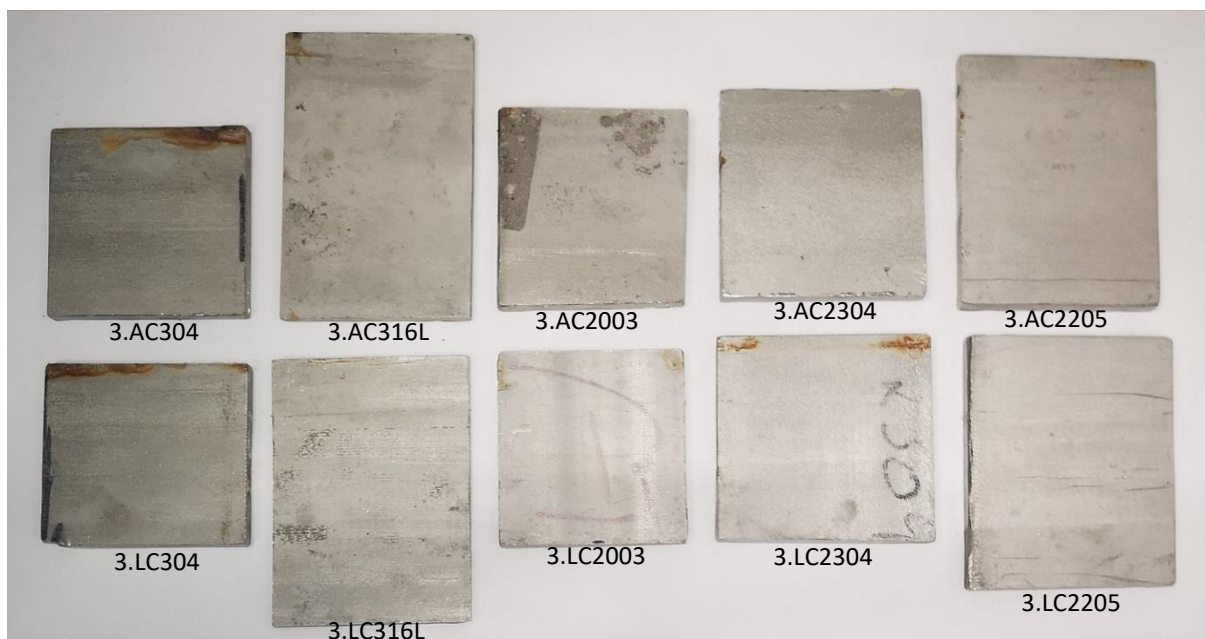


Figure 34: Backside of the samples after test round 3

4.2 Analysis of materials using SEM

EDS analysis were performed on different points and areas on the samples, and as mentioned in section 3.4, it was observed some impurities on the surfaces of the samples such as high carbon and nitrogen content. Therefore, it was decided that each sample should also be tested with a polished surface to see if some of the contaminated areas could be removed, i.e. each sample was tested twice as unpolished and polished surfaces.

In Appendix F, the surface images of the samples are shown with a magnification of 10-100 μm . Some of the spots on the images of the surfaces are dark (black) and was checked with EDS spot-analysis, it was found that these dark spots were contaminated areas.

The different elements in the sample composition were identified by an EDS spectrum, as shown in figure 35. The EDS spectrum shows the different energy levels of the characteristic X-rays, some of the peaks were identified by the EDAX software while other peaks were left blank. The blank peaks were found by looking at the suggestions of the EDAX software and the periodic table containing X-ray energy reference. As post processing of the results, all the peaks were checked with their belonging energy levels. The compositions of each material are given in the tables in sections 4.2.1-4.2.5 below, where the EDS scan was performed as area analysis over the sample surface, shown in Appendix D.

The results from EDS shows that carbon and nitrogen values are much higher than the certificate and that they are difficult to measure. Elements such as sulphur and phosphorous were also difficult to measure. Chromium content in 304 and 316L were found to be around 1-2 weight % higher than the certificates and around 1 weight % lower in 2003 and 2205. Molybdenum was found to be 0.1-1 weight % lower in all samples except sample of 304 which does not contain it. Other elements show little difference in values compared to their certificate values.

Due to the difficulties of measuring elements regarding pitting resistance equivalent numbers by formula (2.11), it is observed that the PRE values become much higher than they should be for each material grade. PRE number is calculated based on chromium, molybdenum and nitrogen contents, and this can be seen in chapter 3.1, table 8, which contains the PRE values according to material certificates.

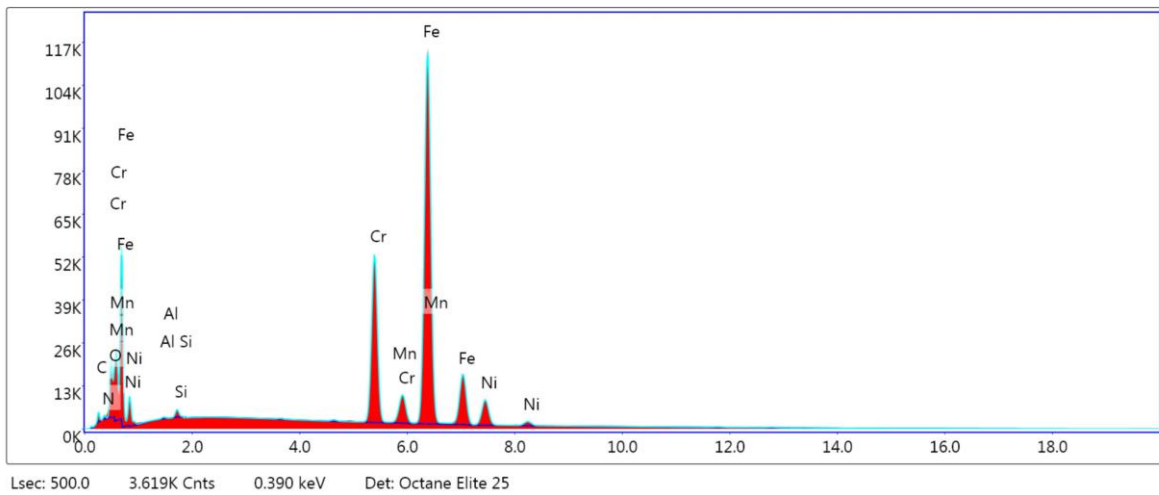


Figure 35: EDS spectrum from one sample

4.2.1 EDS scan of 304

Table 12: Composition of sample 304

Sample 304	Unpolished surface	Polished surface	Material certificate
Element	Weight %	Weight %	Weight %
C K	1.59	0.40	0.016
Mn K	1.37	1.59	1.120
P K	-	0.02	0.036
S K	-	0.11	0.005
Si K	0.37	0.38	0.400
Cr K	20.18	20.07	18.110
Ni K	6.74	7.20	8.060
N K	0.32	-	0.046
O K	1.44	-	-
Fe K	67.90	68.81	-
Cu K	-	0.36	-
V K	-	0.51	-
Al K	0.09	0.02	-
Sn L	-	0.53	-
Total	100	100	-

4.2.2 EDS scan of 316L

Table 13: Composition of sample 316L

Sample 316L	Unpolished surface	Polished surface	Material certificate
Element	Weight %	Weight %	Weight %
C K	1.08	0.56	0.021
Mn K	1.19	0.89	0.920
P K	-	-	0.037
S K	-	0.28	0.001
Si K	0.28	0.40	0.460
Cr K	18.43	18.94	17.100
Ni K	8.63	8.97	10.000
N K	0.02	-	0.036
Mo L	1.20	0.97	2.020
O K	1.21	-	-
Fe K	66.39	68.71	-
Cu K	-	0.24	-
Al K	1.58	0.02	-
Total	100.01	99.98	-

4.2.3 EDS scan of 2003

Table 14: Composition of sample 2003

Sample 2003	Unpolished surface	Polished surface	Material certificate
Element	Weight %	Weight %	Weight %
C K	3.08	0.24	0.013
Mn K	1.43	1.80	1.740
P K	-	-	0.025
S K	-	0.25	-
Si K	0.33	0.25	0.350
Cr K	21.35	24.34	22.200
Ni K	3.25	3.15	3.700
N K	0.38	-	0.170
Mo L	1.09	0.72	1.780
O K	2.08	-	-
Fe K	66.36	68.59	-
Cu K	-	0.34	-
Al K	0.24	0.01	-
Sn L	-	0.12	-
Ca K	0.41	-	-
V K	-	0.19	-
Total	100	100	-

4.2.4 EDS scan of 2304

Table 15: Composition of sample 2304

Sample 2304	Unpolished surface	Polished surface	Material certificate
Element	Weight %	Weight %	Weight %
C K	1.58	0.13	0.015
Mn K	1.30	1.88	1.330
P K	-	-	0.029
S K	-	-	0.001
Si K	0.35	0.34	0.520
Cr K	23.96	26.08	23.740
Ni K	3.62	3.79	4.270
N K	0.43	-	0.176
Mo L	0.43	0.34	0.530
O K	1.68	-	-
Fe K	65.84	66.63	-
Cu K	-	0.30	-
Al K	0.41	-	-
Sn L	-	0.50	-
Ca K	0.38	-	-
Total	99.98	99.99	-

4.2.5 EDS scan of 2205

Table 16: Composition of sample 2205

Sample 2205	Unpolished surface	Polished surface	Material certificate
Element	Weight %	Weight %	Weight %
C K	2.58	0.37	0.021
Mn K	1.29	1.43	1.360
P K	-	-	0.026
S K	-	0.39	0.001
Si K	0.24	0.22	0.330
Cr K	21.79	24.44	22.220
Ni K	5.07	5.07	5.680
N K	0.32	0.09	0.189
Mo L	2.49	1.50	3.140
O K	1.63	-	-
Fe K	64.01	66.10	-
Nb K	-	-	0.009
Cu K	-	0.13	0.230
Co K	-	0.13	0.130
Al K	0.15	-	-
Ca K	0.43	0.11	-
Total	100	99.98	-

4.3 Analysis of ASTM G61-86 test

The results from cyclic polarization scans are shown in table 17 below, where the obtained corrosion potential, pitting potential and repassivation potential are shown for each sample. These values are also plotted below as diagrams for easier comparison, where pitting potentials are shown in figure 36, open circuit potentials in figure 37 and repassivation potentials in figure 38. It was observed from testing that the lower sodium chloride solution in the modified experiment resulted in higher pitting potentials than the ordinary experiment.

Some of the initial scan points were varied of the test rounds due to difference in open circuit potentials. According to ASTM G61-81, the open circuit potential is the corrosion potential. Pitting-, open circuit- and repassivation potentials were obtained by the mean value of each polarization plots.

Positive hysteresis loops were observed in all samples, except the samples of DSS 2205. There were also observed small negative hysteresis loops at the beginning of the reverse scans of the lean duplex samples, which then turned into positive hysteresis loops at lower currents. The open circuit potentials are shown in Appendix E. Some fluctuations of both open circuit potential (OCP) and cyclic polarization scan (CPS) were also observed during testing, the three samples plotted for each material, in each graph are coloured as green for sample 1, red for sample 2 and blue for sample 3.

Table 17: Results of cyclic polarization scans

Test type	Samples (1, 2 & 3)	Initial E [mV]	Final E [mV]	OCP E_{corr} [mV]	Pitting potential E_{pit} [mV]	Repassivation potential E_{rep} [mV]
Ordinary	P304	-500	-250	-280	171	-129
	P316L	-500	-250	-358	353	-102
	P2003	-500	-250	-297	1009	-73
	P2304	-500	-250	-269	732	-76
	P2205	-600	-250	-497	1038	378
Modified	M304	-500	-250	-241	377	-71
	M316L	-500	-250	-216	462	-105
	M2003	-600	-250	-300	1032	28
	M2304	-600	-250	-382	838	-66
	M2205	-600	-250	-344	1108	230

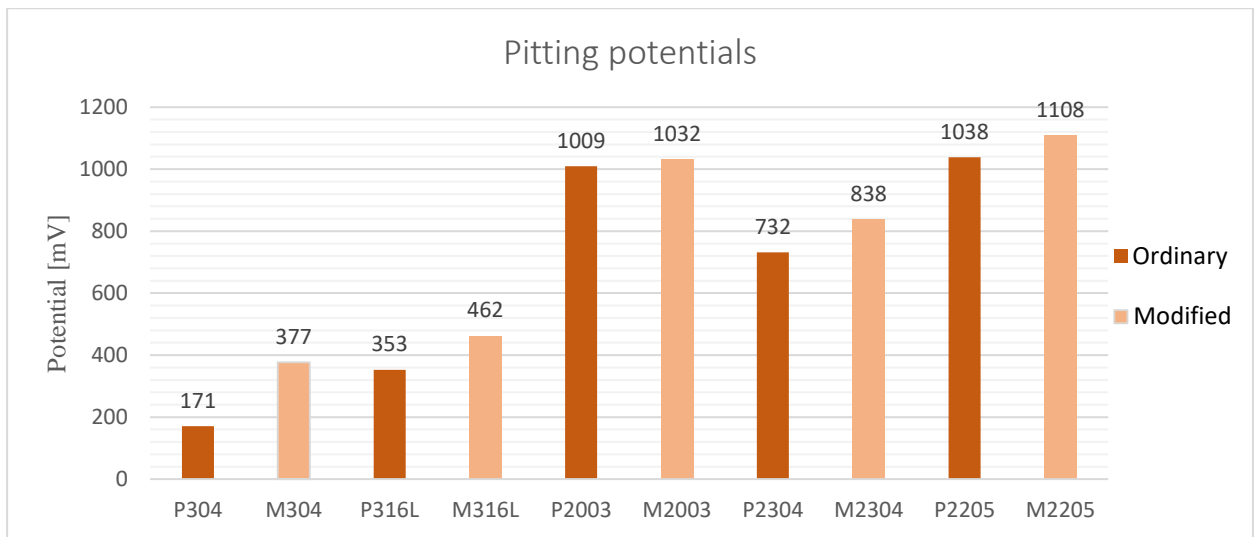


Figure 36: Pitting potentials of the samples

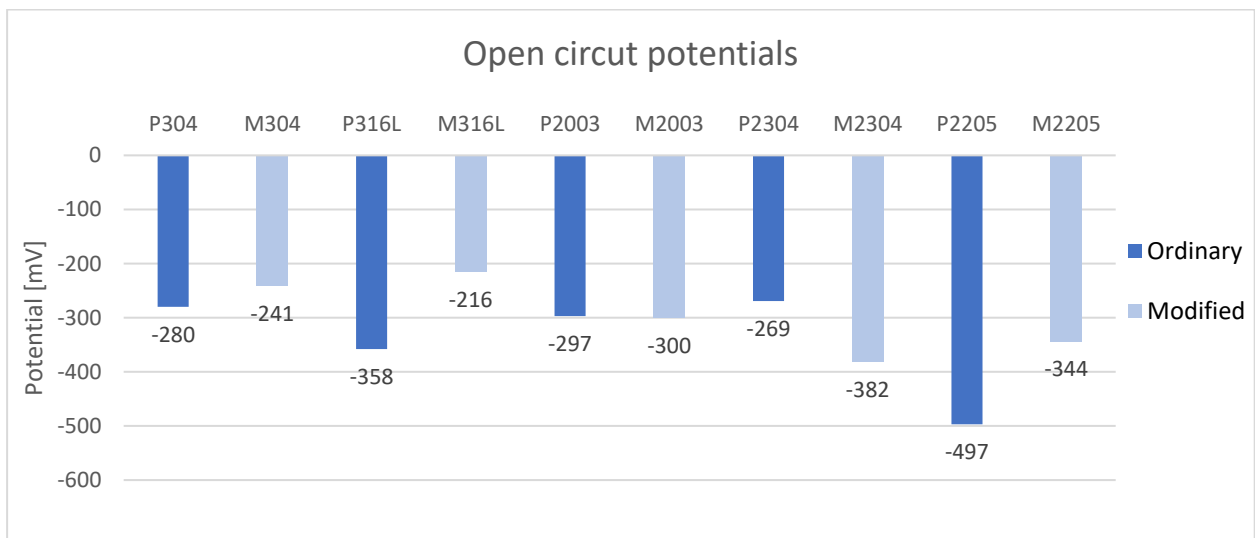


Figure 37: Open circuit potentials of the samples

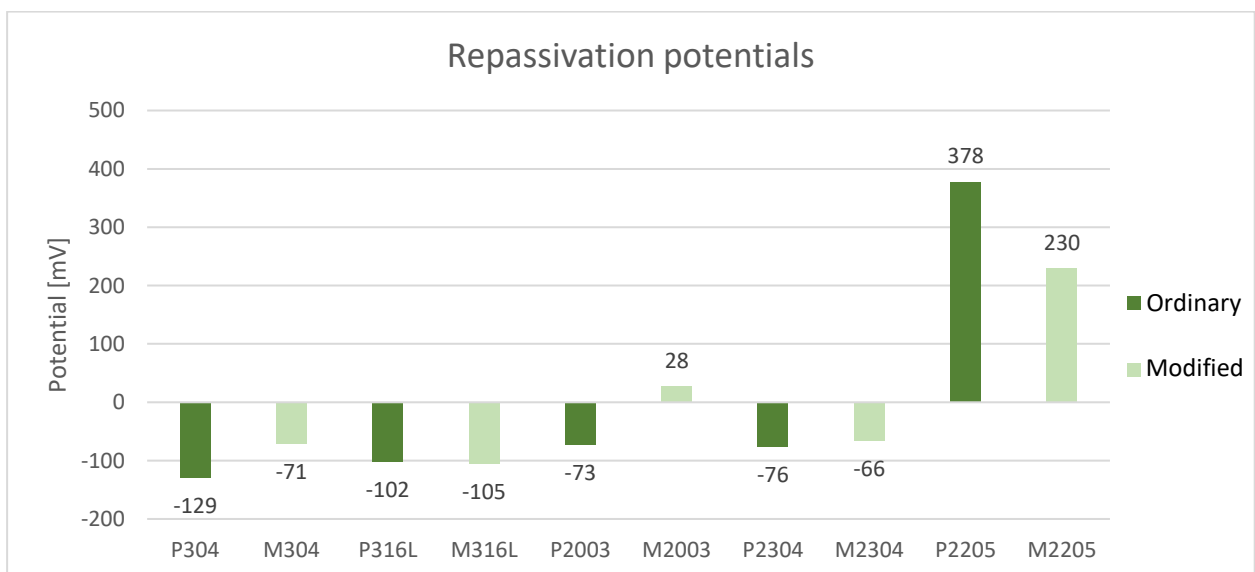


Figure 38: Repassivation potentials of the samples

4.3.1 Polarization scan of 304

As shown below in the ordinary and modified polarization plots (figure 39 and figure 40), there are large hysteresis areas for all the samples which indicates a susceptibility of localized corrosion. In the ordinary scan, sample 1P304 and 3P304 showed repeatable results and sample 2P304 had some deviation as pitting potential occurred in two states. The values of pitting-, repassivation potential of the P304 scan are 171 mV and -129 mV.

In the modified scan it was observed some fluctuations in samples 2M304 and 3M304, while sample 1M304 showed the lowest pitting potential. Pitting- and repassivation potentials of the M304 scan are 377 mV and -71 mV.

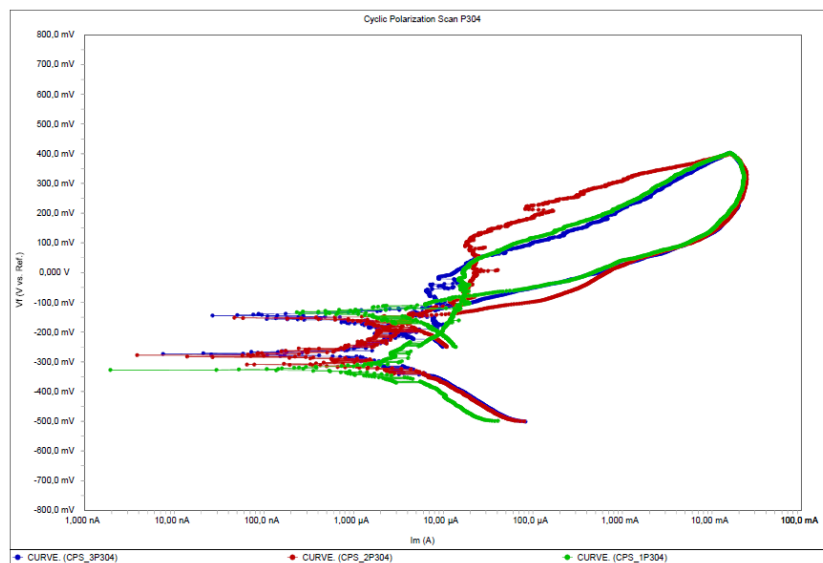


Figure 39: CPS ordinary P304

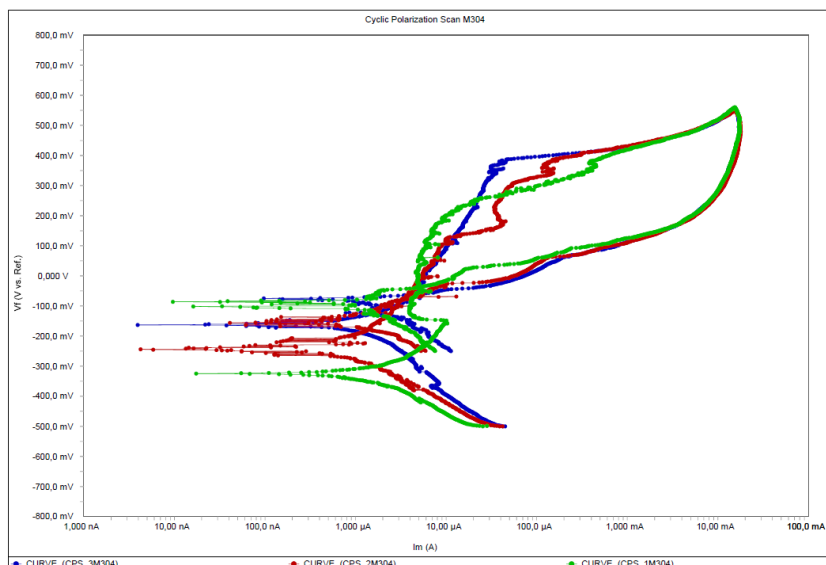


Figure 40: CPS modified M304

4.3.2 Polarization scan of 316L

In the ordinary polarization scan, shown in figure 41, there was observed some fluctuations between the samples. Samples 1P316L and 2P316L showed similar trends in pitting- and repassivation potential, while sample 3P316L was difficult to interpret. The pitting- and repassivation potential for P316L are measured as 353 mV and -102 mV.

From the results of the modified scan in figure 42, the pitting- and repassivation potentials of the M316L scan are 462 mV and -105 mV. The samples in this scan showed repeatability, sample 3M316L had some fluctuations and a larger pitting potential than the others. Both ordinary and modified scans have large areas of positive hysteresis loops, leading to poor resistance against localized corrosion in chloride environments.

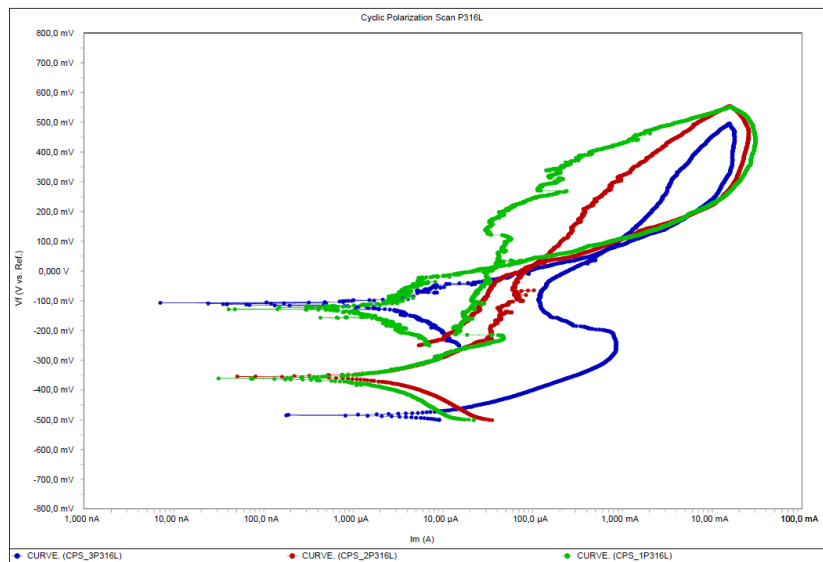


Figure 41: CPS ordinary P316L

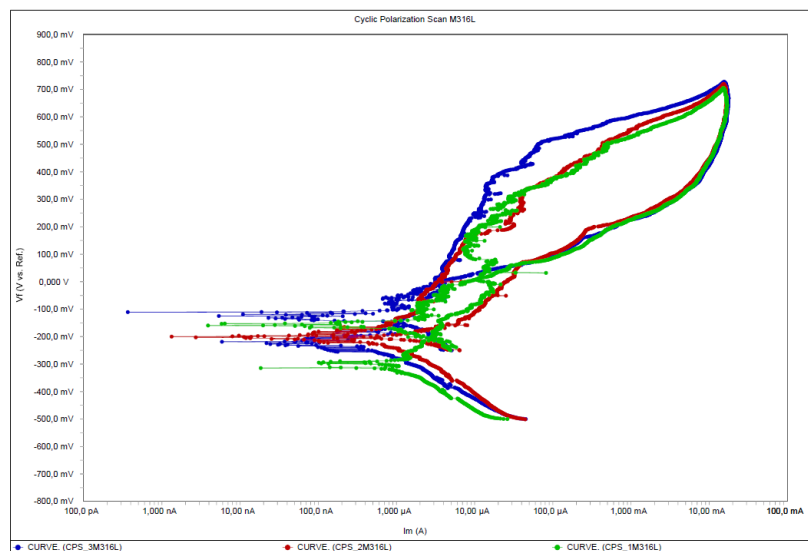


Figure 42: CPS modified M316L

4.3.3 Polarization scan of 2003

The scans of both ordinary and modified scans shows similarities between the samples with some fluctuations, as shown in figure 43 and figure 44. After a rapid increase in anodic current the hysteresis becomes negative, and at a lower current it becomes positive with a small hysteresis area, which occurred in all the samples of 2003. This indicates that the material is susceptible to localized corrosion, the pitting- and repassivation potentials of P2003 are measured to 1009 mV and -73 mV. In the modified experiment, sample 1M2003 showed a difference in the forward scan due to fluctuation. Pitting- and repassivation of M2003 was measured to be 1032 mV and -300 mV.

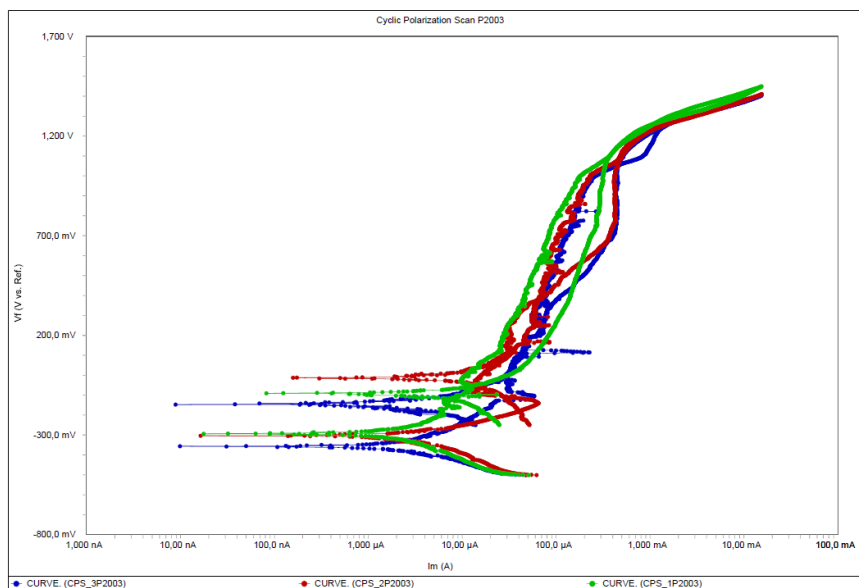


Figure 43: CPS ordinary P2003

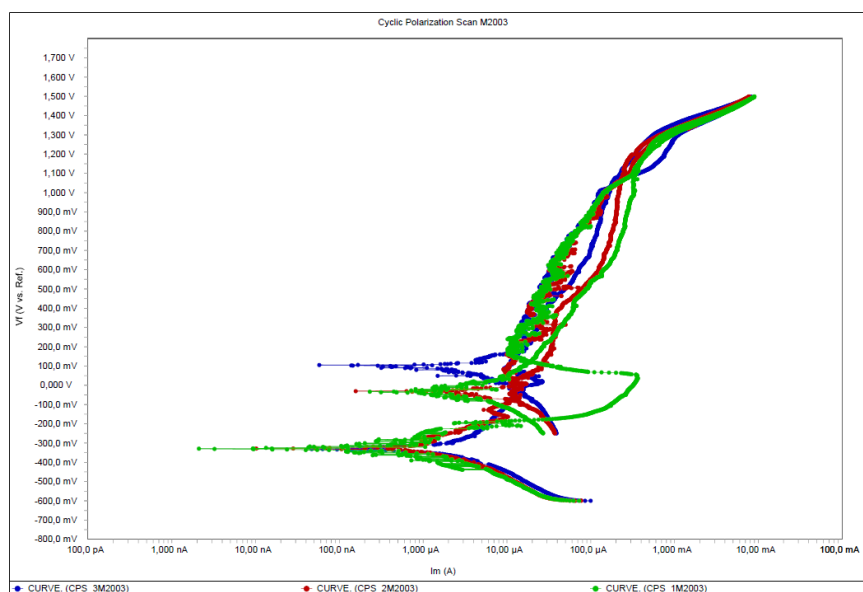


Figure 44: CPS modified M2003

4.3.4 Polarization scan of 2304

The hysteresis loops of all the samples of P2304 and M2304 shows similarities, as seen in figure 45 and figure 46. The hysteresis loops become negative after a rapid increase in current and positive in the reverse scan with large areas, which indicates poor pitting resistance. In the ordinary scan, potentials of pitting and repassivation was obtained to be 732 mV and -76 mV. The modified scan showed a pitting- and repassivation potential of 838 mV and -66 mV.

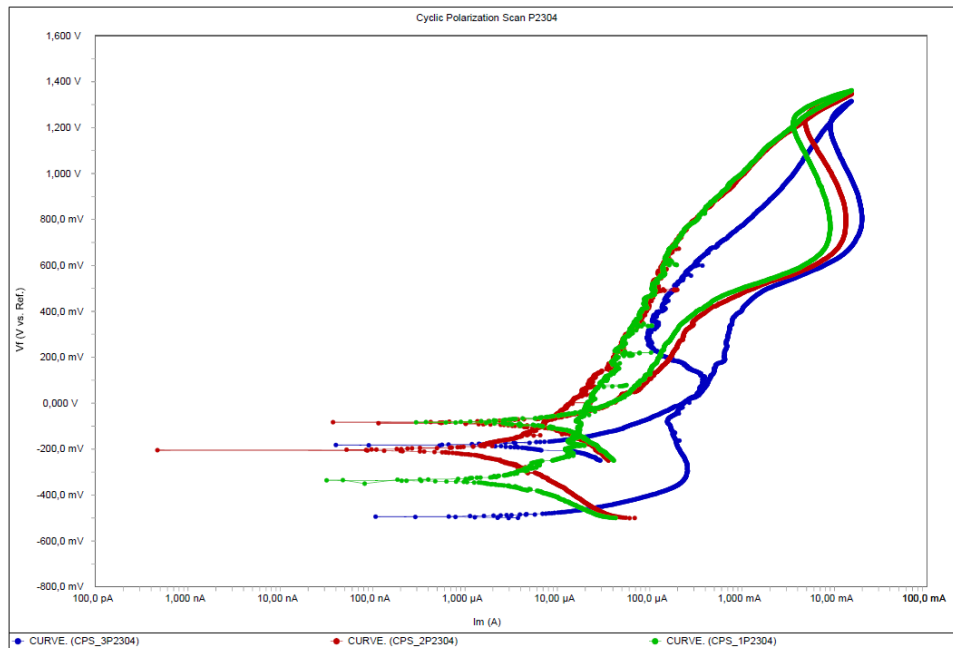


Figure 45: CPS ordinary P2304

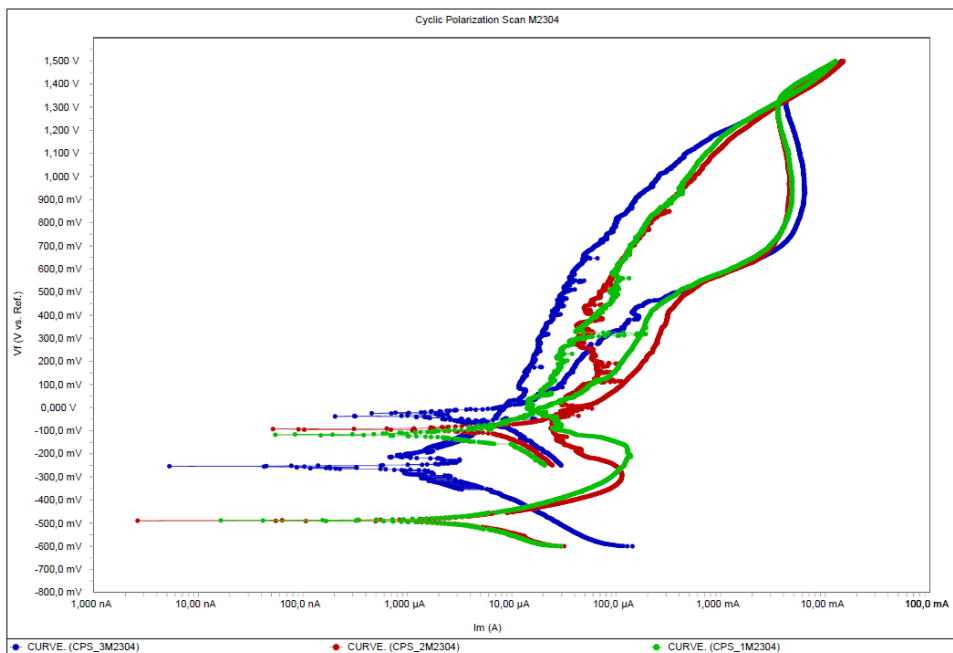


Figure 46: CPS modified M2304

4.3.5 Polarization scan of 2205

In the ordinary scan, sample 3P2205 and 1P2205 showed no hysteresis loop, while sample 2P2205 showed a negative hysteresis loop as seen in figure 47. This indicates that the material has a very good resistance to localized corrosion. The pitting potential was measured to be 1038 mV and was the highest recorded pitting potential among all the materials of the ordinary scans. Repassivation potential was found to be 378 mV.

The modified scan showed similar results, where sample 1M2205 and sample 3M2205 showed negative hysteresis loops while sample 2M2205 had no hysteresis loop as seen in figure 48. All the samples of the modified and ordinary scans show high pitting potentials with proximities to each other. Pitting- and repassivation potential of M2205 was measured to be 1108 mV and 230 mV.

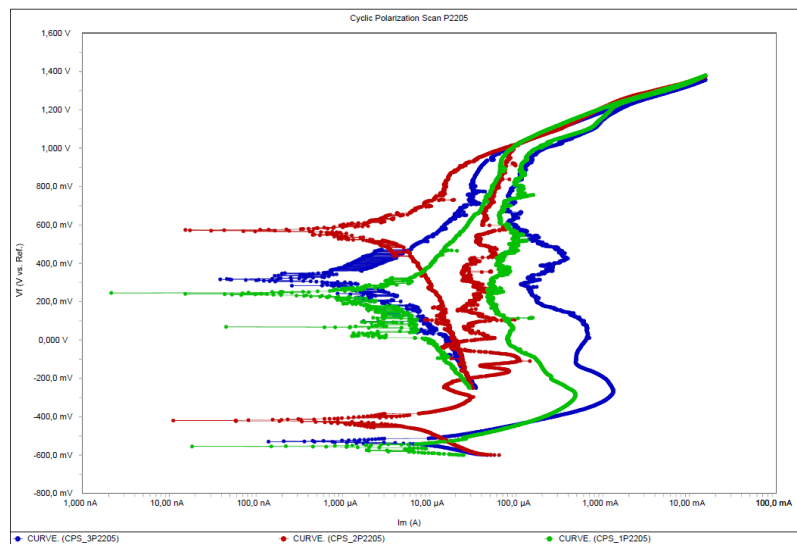


Figure 47: CPS ordinary P2205

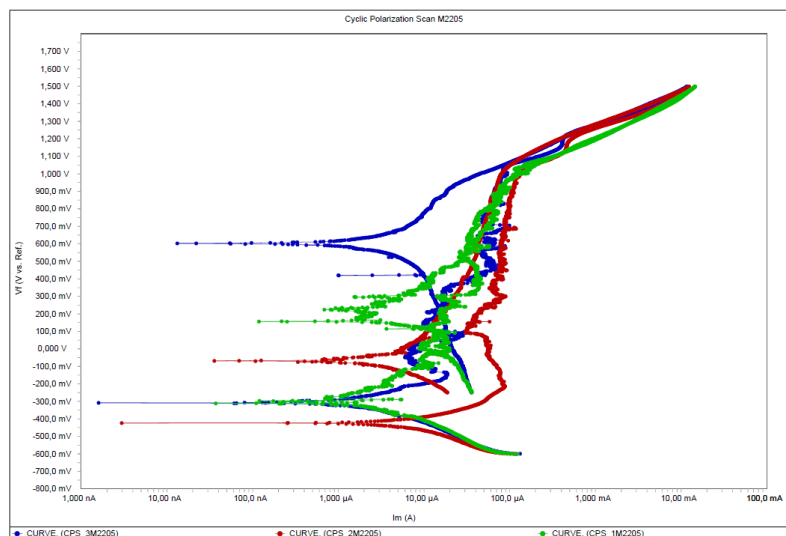


Figure 48: CPS modified M2205

4.3.6 Comparison of 2304 and 2003

In the ordinary scan of figure 49 below, sample 2P2304 (marked as blue) is plotted against 2P2003 (marked as red). The polarization plot is plotted with a line function to make it easier to compare the two samples. The plot shows the difference in the passive anodic current and that 2P2003 has a larger pitting potential. It also shows that the positive hysteresis loop for 2P2304 is larger than for 2P2003.

Figure 50 below shows the modified scan with samples 2M2304 (marked as blue) and 2M2003 (marked as red). It has similarities to the ordinary scan. 2M2304 also has a larger area of positive hysteresis loop and a lower pitting potential than 2M2003.

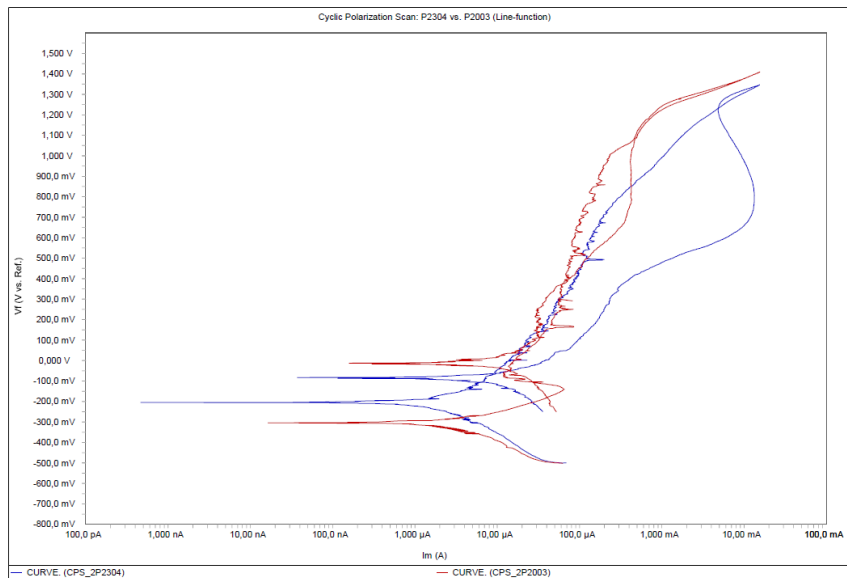


Figure 49: CPS samples; 2P2304 vs. 2P2003

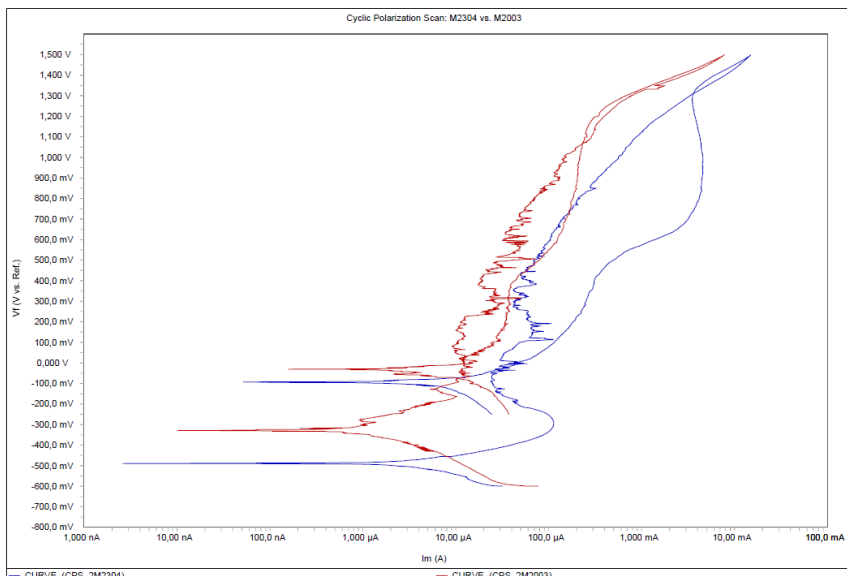


Figure 50: CPS samples; 2M2304 vs. 2M2003

5 Discussion

5.1 Atmospheric marine corrosion testing

The materials were exposed to three test rounds with different temperatures in a chloride environment of seawater. The seawater was obtained from the Northern Sea, close to shore. The pH of the seawater was not measured and was assumed to be of around 8. There could be some deviations from this assumption since it can be more pollution in the seawater closer to shore than in the open sea. As mentioned in chapter 2.12, the pH of the seawater is also an important factor in the corrosive rate of the samples and should have been checked prior testing.

From the results of all the test rounds with different conditions, it was difficult to compare the materials to each other due to the lack of dissolution of material. One of the reasons for the absence of both general and localized corrosion on the samples is because of the lack of exposure time to the chloride environment; as it was seen by visual inspection an initiation of corroded areas on many of the samples. Test round 2 and 3 were performed parallel to test round 1, but with half of the exposure period to save time. The results would have been more comparable if all the test rounds were performed with an equal exposure period.

As mentioned in chapter 4.1, the first round of testing was performed for 8 weeks in a room temperature of around 20°C. The room temperature may have deviated with $\pm 3^\circ\text{C}$ during day/night-time, this may have had a little effect on the corrosion rate of the samples. The results from the first round of exposing the materials to the simulated offshore environment shows that general corrosion occurred on the surfaces of some of the samples. Although the amount of corrosion observed was very small, the materials that showed the best results against the environment were 2003 and 2205.

The second round of testing was performed for 4 weeks in a heating cabinet with a temperature of 40°C. Very little to almost no corrosion was observed on the samples after testing. Only samples 304, 2304 and 316L showed some very small areas of general corrosion on their surfaces. 2003 and 2205 were observed to not be affected by the chloride environment.

The third round of testing was also performed in a heating cabinet with temperature of 60°C for 4 weeks. This round of testing contained the most corroded samples of general corrosion, where 8 of the 10 samples showed initiated corrosion although the corroded areas were small. From the results of this test, the materials of duplex and lean duplex (2205, 2304 and 2003) performed best against the corrosion test since there were not observed much corroded areas on their surfaces (mostly at their burr edges).

The samples were sprayed with salt-spray (seawater) two times per day on their front-sides (surface) during testing. Evaporation of the seawater in the containers occurred and the water level was refilled so that the samples stayed half immersed. The salt-spraying could have been performed more often during testing to provide more exposure time to the electrolyte of the upper half of the samples. Also, the samples could have been sprayed on both sides (i.e., front and back-sides) to provide more exposure areas. There was not observed any difference in mass before and after testing, which could be due to a lack of time exposing the samples to the chloride environment. The digital weight scale used to find the samples mass only had two decimals, measured by gram. A different digital weight scale with more decimals should have been used which could have provided a difference in mass of some of the corroded samples.

It was observed general corrosion on many of the samples and some showed an initiation of corrosion on spots on their surfaces. If the testing had been performed for a longer period, there would be a noticeable amount of dissolution of mass after testing. After close inspection of the samples tested for localized corrosion, none of the samples were affected by the tape which tried to initiate crevice or pitting between the tape and the surface. General corrosion was also observed on many of the samples tested for localized corrosion, but with a longer testing period the results may have been different.

From the theory about crevice corrosion in chapter 2.8, a reason for the tape not working as a former for localized corrosion may be because of it was wrapped around the samples too much, which may have not let any exposure of the electrolyte within the tape and the surface. Also, the top of the tape on the surface of the samples were above water level, this should have been performed different by having the top of the tape at or below water level. Then, the localized initiation area would become more exposed to the electrolyte and an acceleration of the corrosion process would have occurred.

Some of the burr created after cutting the samples were difficult to remove. It was observed that the burr side of some samples, which were trimmed down with a metal file, corroded more than on their surfaces. This may be by the cause of some burr was remaining on the samples or that the cut side of the material was damaged due to cutting and metal-filing. The burr areas on the materials may have had its passive layer broken down, causing an increase in corrosion of these areas as they become anodic. Another method of removing the burr and sharp edges after cutting could have been used to provide smoother sides and edges that may have changed the outcome of corrosion test.

5.2 Material compositions

The chemical compositions of each material were found by a scanning electron microscope using EDS analysis. The results matched well with the certificates with some deviations. Some of the elements were difficult to measure as they either became too high or too low in weight % contents. Both carbon and nickel were elements that came out the analysis too high to compare it to their belonging certificates. The reason of this may be due to impurities on the surfaces of the samples, causing contaminated areas. Spot analysis were also used on the samples before performing area analysis of the entire surfaces, which found that these impurities, shown as dark (black) spots, contained elements with large deviations from the rest of the surface.

Other elements such as sulphur and phosphorous were also difficult to measure. These elements came out the analysis too low. In the certificates, these elements are very low compared to the rest of the alloying elements. The X-rays captured of sulphur and phosphorous may not be properly captured by the EDS detector due to restrictions. Another reason for them not to be corresponding to the certificates could be because of emitted energy levels (X-rays) of other elements with similar energy spectra overlaps them in the EDS spectrum, causing other elements to be larger in content than they should be.

It was observed that the polished samples may have reduced contaminated areas as it showed reduced carbon and nitrogen content. Some of the elements became more accurate, according to the certificates, while others had more deviations. This may be because some of the passive layer or elements near the passive layer were removed during polishing, since chromium and molybdenum were more accurate in the first round of testing, i.e., as unpolished samples.

The used acceleration voltage was set to 20 kV, which covers all the energy spectra of the alloying elements from the certificates (as stated in the period table containing X-ray energy references). However, the acceleration voltage could be set to lower and higher values (e.g., 15 kV and 25 kV), which may provide an easier detection of low and high energy elements that are difficult to measure, such as carbon, nitrogen, silicone, phosphorous, sulphur and molybdenum.

EDS has its restrictions regarding element analysis and another test method should also be performed on the samples so that elements from both tests could be verified against the material certificates. Other methods such as Wave dispersive spectrometer (WDS) could also be used for more accurate results, especially for comparing important elements such as molybdenum, chromium and nitrogen for PRE value.

5.3 Corrosion potentials

From the plots of the cyclic polarization scans found in sections 4.3.1 to 4.3.5 it is shown that the results are reproducible with some deviations between the three parallel samples for each material. The occurrence of these deviations may be by the cause of outer noise disturbing the system or by not performing the experiment exact as the test-procedure of standard ASTM G61-86 states.

As mentioned in section 3.5.5, the experiments were performed with some deviations from ASTM G61-86 that could have had some impact on the outcome of the experiments. These are discussed below:

- The temperature of the solution was performed with $20 \pm 3^\circ\text{C}$ (room-temperature) instead of $25 \pm 1^\circ\text{C}$. The solution was made ready a day before testing and was let to achieve room-temperature before testing. This may have affected the potentials from the results.
- For specimen preparation, the standard recommends removing impurities by wet grinding and polishing the samples with 240-grit and 600-grit SiC paper. This was not performed and could have changed the results of the potentials, as there were observed impurities on the surfaces as mentioned in section 3.4. The samples were cleaned with an ultrasonic bath of distilled water for 5 minutes prior testing, which removed degrease from the surfaces.
- Before testing, the solution was purged for 5 minutes with nitrogen gas to remove oxygen from the solution, instead of 60 minutes which the standard states. This was done to save time, but it could also have affected the outcome of the experiments by letting the solution or environment have some oxygen remaining in it. Also, the standard states that the specimen should be immersed in the solution for 60 minutes before running OCP, followed by cyclic polarization scan. This was performed differently to save time as the OCP was set to run for 5 minutes right after specimen immersion. This may have caused some disturbances in the OCP values found in Appendix E, as some of the OCP-curves shows not to have been fully stabilized.
- According to the standard, the specimen holder should have been designed to expose 1 cm^2 of the sample into the electrolyte. This was performed differently with a beaker and a lid, sealed by parafilm and tape. However, the exposure area of the sample remained the same.
- The standard states that scan rate should be set to 0.167 mV/s , but the scan rate used was 1 mV/s to save time. This may have caused some disturbances of the anodic/cathodic reactions during the forward- and reverse scan, as well as affecting some of the potentials of the plot.

Two experiments were performed with similar test-procedures, one ordinary according to ASTM G61-86 and one modified with a lower sodium chloride solution. The purpose of the modified experiment was to see if the materials showed any different behaviours in a lower sodium chloride solution. It was observed from testing that the modified experiment with lower sodium chloride solution resulted in higher pitting potentials in all the samples, while hysteresis loops remained similar as to the ordinary experiment. The higher potentials observed in the low sodium chloride solution may be the cause of a weaker electrolyte that limits its ability to conduct electric current, requiring more current to initiate dissolution of metal.

From section 2.13.1, pitting corrosion on the samples are evaluated based on the polarization plots in which contains information about potentials and hysteresis. The most important parameters to look for are the pitting potential and the repassivation potential, with respect to the corrosion potential. The amount of hysteresis, which is the difference of pitting potential and repassivation potential, indicates the amount of pitting corrosion. The results from the experiments of cyclic polarization shows that most of the materials contained positive hysteresis, except the duplex grade 2205. This indicates that 2205 did not reveal any form of pitting corrosion and can be considered as the best material in regards of pitting resistance, it was also found that it contained the highest values among the pitting potentials.

The material grades of lean duplex showed higher pitting potentials than the grades of austenitic stainless steels. The results from cyclic polarization was as expected based on the literature study, from table 7 in chapter 3.1, the pitting resistance equivalent number ranks the materials resistance against pitting corrosion. Higher PRE values indicate better resistance. Below in table 18, the ranking of the materials resistance against pitting corrosion is given the in order from 1 to 5. The ranking is based on pitting potentials, hysteresis, corrosion potentials and PRE values, where 1 indicates the best material against pitting and 5 the worst. The ranking order also matches the materials corresponding PRE values.

Table 18: Ranking of the materials based on cyclic polarization and PRE values

Material	Ranking	Pitting potential: Ordinary experiment	Corrosion potential: Ordinary experiment	PRE according to certificate from table 7
2205	1	1038 mV	-497 mV	35.606
2003	2	1009 mV	-297 mV	30.794
2304	3	732 mV	-269 mV	28.305
316L	4	353 mV	-358 mV	24.342
304	5	171 mV	-280 mV	18.846

6 Conclusion and recommendations

The following conclusions are drawn based on the results obtained:

- Lean duplex grade 2003 is superior to 2304 in terms of resistance against pitting corrosion, which may be due to 2003 having more molybdenum additions and a higher PRE number.
- The order of the materials resistance against localized corrosion, based on the results from cyclic polarization, from best to worst are given in the following order: 2205, 2003, 2304, 316L and 304. This order also agrees with the materials PRE numbers.
- A sodium chloride (NaCl) solution lower than 3.56 % (by weight) in cyclic polarization experiments provides higher pitting potentials of the materials.
- Corrosion behaviour is temperature dependent, as the results from the highest temperature round of testing in the atmospheric marine environment have the most corroded samples.
- The atmospheric marine corrosion experiment needed a longer test period, as it was observed that the samples had begun to corrode and did not get to achieve large enough corrosion areas on their surfaces to give a noticeable dissolution of mass.
- The chemical compositions of the materials were found to fit their corresponding material certificates with some deviations.

Further work with recommendations provided based on this study are mentioned below:

- It could be interesting to perform similar experiments as to this project by further investigating only new grades of lean duplex grades against different types of corrosion, e.g. 2304 (UNS S32304), 2003 (UNS S32003) and 2101 (UNS S32101).
- For investigations of chemical compositions of different materials, more methods should be used to compare with the material certificates. A more accurate method such as wave dispersive spectrometer could also be used if deviations arises in determining elements.
- It could be interesting performing cyclic polarization studies on lean duplex materials in different acidic solutions and with temperature variations.
- It is recommended when testing against localized corrosion that the gap between the sample surface and the tape (or another material) is most often exposed to the electrolyte to accelerate the corrosion process.
- An alternative method could be used to break down the passive layers of the materials to achieve localized or general corrosion faster when testing in atmospheric marine environment.

7 References

- [1] S. Aribó, R. Barker, X. Hu and A. Neville, “Erosion–corrosion behaviour of lean duplex stainless steels in 3.5% NaCl solution,” *Wear, Volume 302, Issues 1-2*, pp. 1602-1608, 2012.
- [2] J. Charles, “Duplex Stainless Steels: A Review after DSS '07 held in Grado,” *Steel Research International*, 79, pp. 455-465, 2008.
- [3] V. Cicek and B. Al-Numan, *Corrosion Engineering and Cathodic Protection Handbook*, Beverly: Scrivener Publishing, 2017.
- [4] P. Pedferri, *Corrosion Science and Engineering*, Cham: Springer International Publishing, 2018.
- [5] N. Perez, *Electrochemistry and Corrosion Science*, Boston: Kluwer Academic Publishers, 2004.
- [6] “NACE International,” [Online]. Available: <https://www.nace.org/General-Attack-Corrosion/>. [Accessed 29 01 2019].
- [7] “NACE International,” [Online]. Available: <https://www.nace.org/Corrosion-Central/Corrosion-101/Testing-for-Localized-Corrosion/>. [Accessed 01 29 2019].
- [8] Z. Ahmad, *Principles of Corrosion Engineering and Corrosion Control*, Boston: Elsevier Science & Technology Books, 2006.
- [9] “Corr Science,” 2011. [Online]. Available: <http://www.corrscience.com/products/corrosion/intro-to-corrosion/principles-of-corrosion/>. [Accessed 25 02 2019].
- [10] K. Tretheway and J. Chamberlain, *Corrosion for Science and Engineering Second edition*, Harlow: Longman, 1995.
- [11] P. R. Roberge, *Corrosion Engineering Principles and Practice*, eBook: McGraw-Hill, 2008.

- [12] J. K. Wessel, *Handbook of Advanced Materials: enabling new designs*, Hoboken, New Jersey: Wiley-Interscience, 2004.
- [13] N. Bensalah, *Pitting Corrosion*, Rijeka: InTech, 2012.
- [14] R. G. Kelly, "Crevice Corrosion, Corrosion: Fundamentals, Testing, and Protection, Vol 13A," in *ASM Handbook*, Materials Park OH, ASM International, 2003, pp. 242-247.
- [15] Z. Szklarska-Smialowska, *Pitting and Crevice Corrosion*, Houston: NACE International, 2005.
- [16] H. S. Khatak and B. Raj, *Corrosion of Austenitic Stainless Steels: Mechanism, Mitigation and Monitoring*, Cambridge: Woodhead Publishing Limited, 2002.
- [17] R. Heidersbatch, *Metallurgy and Corrosion Control in Oil and Gas Production Second Edition*, Hoboken, NJ: Wiley, 2018.
- [18] "ATI," 17 02 2014. [Online]. Available: https://www.atimetals.com/Products/Documents/datasheets/stainless-specialty-steel/austenitic/ati_302_304_304l_305_tds_en2_v1.pdf. [Accessed 15 04 2019].
- [19] "ATI," 18 02 2014. [Online]. Available: https://www.atimetals.com/Products/Documents/datasheets/stainless-specialty-steel/austenitic/ati_316_316l_317_317l_tds_en2_v1.pdf. [Accessed 15 04 2019].
- [20] J. Nilsson, "Super Duplex Stainless Steels," in *Material Science and Technology vol 8*, Sandviken, Sweden, The Institute of Materials, 1992, pp. 685-700.
- [21] "ATI," 29 06 2015. [Online]. Available: https://www.atimetals.com/Products/Documents/datasheets/stainless-specialty-steel/duplex/ati_2205_tds_en_v4.pdf. [Accessed 15 04 2019].
- [22] "ATI," 18 03 2013. [Online]. Available: https://www.atimetals.com/Products/Documents/datasheets/stainless-specialty-steel/duplex/ati_2003_tds_en_v2.pdf. [Accessed 15 04 2019].

- [23] “ATI,” 17 02 2014. [Online]. Available:
https://www.atimetals.com/Products/Documents/datasheets/stainless-specialty-steel/duplex/ati_2304_tds_en_v1.pdf. [Accessed 15 04 2019].
- [24] G. Rørvik, *Materialoversikt for rustfrie stål- og nikkel-legeringer*, Trondheim: SINTEF Materialteknologi, 1997.
- [25] S. D. Cramer and B. S. Cavino, “Corrosion of Wrought Stainless Steels, Corrosion: Materials, Vol 13B,” in *ASM Handbook*, Materials Park OH, ASM International, 2005, pp. 54-77.
- [26] K. A. Chandler, *Marine and Offshore Corrosion*, London: Butterworth & Co Ltd, 1985.
- [27] Y. Tsutsumi, A. Nishikata and T. Tsuru, “Pitting corrosion mechanism of Type 304 stainless steel under a droplet of chloride solutions,” *Corrosion Science, Volume 49, Issue 3*, pp. 1394-1407, 2007.
- [28] W. Lv, C. Pan, W. Su, Z. Wang, S. Liu and C. Wang, “Atmospheric corrosion mechanism of 316 stainless steel in simulated marine atmosphere,” *Corrosion Engineering, Science and Technology, Volume 51, Issue 3*, pp. 155-162, 2016.
- [29] S. Esmailzadeh, M. Aliofkhazraei and H. Sarlak, “Interpretation of Cyclic Potentiodynamic Polarization Test Results for Study of Corrosion Behaviour of Metals: A Review,” *Protection of Metals and Physical Chemistry of Surfaces, Vol. 54, No. 5*, pp. 976-989, 2018.
- [30] J. Hjelen, *Scanning elektron-mikroskopi*, Trondheim: SINTEF, NTH, 1986.
- [31] ASTM_G61-86, *Standard Test Method for Conducting Cyclic Potentiodynamic Polarization Measurements for Localized Corrosion Susceptibility of Iron-, Nickel-, or Cobalt-Based Alloys*, West Conshohocken: ASTM International, 2018.
- [32] M. Kutz, *Handbook of Environmental Degradation of Materials, Third Edition*, Oxford: William Andrew, 2018.

Appendix A: Material Certificates



INSPECTION CERTIFICATE EN 10204 3.1 1/1

Date 26.02.2019

Gateway Stainless AS
Nedre Eiker vei 8
Ole Steens gate 10
NO-3045 Drammen
NORWAY

YOUR ORDER NO.
REFERENCE
Sample tubes

EXTENT OF DELIVERY	STAINLESS STEEL TUBES	
Quantity	Dimension	Finish
1 m	150x150x5 mm	unpolished

Coil-No.	Grade of material
89S701880	EN 1.4301

CHEMICAL COMPOSITION (according to certificate of steel mill)

C %	Si %	Mn %	P %	S %	Cr %	Ni %	Mo %
0,016	0,400	1,120	0,036	0,005	18,110	8,060	-
Ti %	Nb %	Cu %	N %	Others %	Al %	Mg %	Co %
-	-	-	0,046	-	-	-	-

TESTING RESULTS (Coil)

Sample-No.	YIELD STRENGTH Rp0.2 N/mm2	1% PROOF STRENGTH Rp1.0 N/mm2	TENSILE STRENGTH Rm N/mm2	ELONGATION A5 %	HARDNESS HRB
Test 1	325	384	621	46	85
Test 2	330	387	627	47	84

Material acc. to EN 10088-2:2014; ASTM A240-15b; ASTM A554-16 (if included)

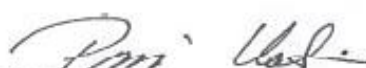
Eddycurrent test acc. to Stalatube norm. (Not applied to 'press brake' tubes)

Tubes are produced according to Stalatube technical data sheet

Country of Mfg: FINLAND
Country of Melt: CHINA

STALATUBE OY

Lahti
26.02.2019


Pasi Uotinen
Quality Manager

Stalatube Oy

Taivalkatu 7, 15170 LAHTI
FINLAND

Domicile Lahti
www.stalatube.com

Tel: +358 3 882 190
Fax: +358 3 882 1914

VAT FI15685444
Trade-Reg.No: FI1568544-4

Date 27.02.2019

Gateway Stainless AS
Nedre Eiker vei 8
Ole Steens gate 10
NO-3045 Drammen
NORWAYYOUR ORDER NO.
REFERENCE
Sample tubes

EXTENT OF DELIVERY	STAINLESS STEEL TUBES	
Quantity	Dimension	Finish
1 m	100x100x3,00 mm	Stalazzo

Coil-No.	Grade of material
917645	EN 1.4404

CHEMICAL COMPOSITION (according to certificate of steel mill)

C %	Si %	Mn %	P %	S %	Cr %	Ni %	Mo %
0,021	0,460	0,920	0,037	0,001	17,100	10,000	2,020
Ti %	Nb %	Cu %	N %	Others %	Al %	Mg %	Co %
-	-	-	0,036	-	-	-	0,250

TESTING RESULTS (Coil)

Sample-No.	YIELD STRENGTH Rp0.2 N/mm2	1% PROOF STRENGTH Rp1.0 N/mm2	TENSILE STRENGTH Rm N/mm2	ELONGATION A50 %	HARDNESS HB
Test 1	333	374	617	51	187
Test 2	336	373	616	52	178

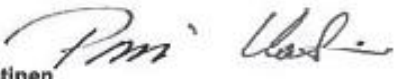
Material acc. to EN 10088-2:2014; ASTM A240-15b; ASTM A554-16 (if included)

Eddycurrent test acc. to Stalatube norm. (Not applied to 'press brake' tubes)

Tubes are produced according to Stalatube technical data sheet

Country of Mfg: FINLAND
Country of Melt: FINLAND

STALATUBE OY

Lahti
27.02.2019
Pasi Uotinen
Quality Manager

Stalatube OyTaivalkatu 7, 15170 LAHTI
FINLANDDomicile Lahti
www.stalatube.comTel: +358 3 882 190
Fax: +358 3 882 1914VAT FI15685444
Trade-Reg.No: FI1568544-4

Date 21.01.2019

Gateway Stainless AS
Nedre Eiker vei 8
Ole Steens gate 10
NO-3045 Drammen
NORWAYYOUR ORDER NO.
REFERENCE
Finn Martin

EXTENT OF DELIVERY	STAINLESS STEEL TUBES
Quantity	Dimension Finish
336 m	80x80x5,00 mm pickled

Coil-No.	Grade of material
10202C746/754	Lean Duplex UNS S 32003

CHEMICAL COMPOSITION (according to certificate of steel mill)

C %	Si %	Mn %	P %	S %	Cr %	Ni %	Mo %
0,013	0,350	1,740	0,025	0,000	22,200	3,700	1,780
Ti %	Nb %	Cu %	N %	Others %	Al %	Ca %	Mg %
-	-	-	0,170	-	-	-	-

TESTING RESULTS (Coil)

Sample-No.	YIELD STRENGTH Rp0.2 N/mm2	1% PROOF STRENGTH Rp1.0 N/mm2	TENSILE STRENGTH Rm N/mm2	ELONGATION A50 %	HARDNESS HB
Test 1	586	-	779	27	-
Test 2	-	-	-	-	-

Material acc. to MDS-D35 rev01c. Tubes acc. to MDS-YD37 rev01c.

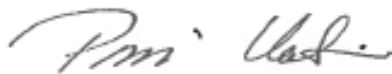
Dimensional tolerances acc. to EN 10219-2:2006

DPI 10% tested and passed. 100% visually inspected. EN ISO 5817-C

Country of Mfg: FINLAND

Country of Melt: UNITED STATES OF AMERICA

STALATUBE OY

Lahti
21.01.2019Paal Uotinen
Quality Manager

Stalatube OyTaivaikatu 7, 15170 LAHTI
FINLANDDomicile Lahti
www.stalatube.comTel: +358 3 882 190
Fax: +358 3 882 1914VAT F115685444
Trade-Reg.No: F11568544-4

Date 26.02.2019

Gateway Stainless AS
Nedre Eiker vei 8
Ole Steens gate 10
NO-3045 Drammen
NORWAYYOUR ORDER NO.
REFERENCE
Sample tubes

EXTENT OF DELIVERY STAINLESS STEEL TUBES

Quantity	Dimension	Finish
1 m	150x100x6,00 mm	unpolished

Coil-No.	Grade of material
584660-001	Lean duplex EDX 2304

CHEMICAL COMPOSITION (according to certificate of steel mill)

C %	Si %	Mn %	P %	S %	Cr %	Ni %	Mo %
0,015	0,520	1,330	0,029	0,001	23,740	4,270	0,530
Ti %	Nb %	Cu %	N %	Others %	Al %	Mg %	Co %
-	-	0,280	0,176	-	-	-	-

TESTING RESULTS (Coil)

Sample-No.	YIELD STRENGTH Rp0.2 N/mm2	1% PROOF STRENGTH Rp1.0 N/mm2	TENSILE STRENGTH Rm N/mm2	ELONGATION A5 %	HARDNESS HB
Test 1	613	681	789	32	246
Test 2	606	671	771	34	244

Material acc. to MDS-D35 revF01. Tubes acc. to MDS-YD37 revF01. PREN min.28

Dimensional tolerances acc. to EN 10219-2:2006

DPI 10% tested and passed. 100% visually inspected acc. EN ISO 5817-C

Country of Mfg: FINLAND
Country of Melt: SWEDEN

STALATUBE OY

Lahti
26.02.2019
Pasi Uotinen
Quality Manager

Stalatube OyTaivalkatu 7, 15170 LAHTI
FINLANDDomicile Lahti
www.stalatube.comTel: +358 3 882 190
Fax: +358 3 882 1914VAT FI15685444
Trade-Reg.No: FI1568544-4

Date 21.01.2019

Gateway Stainless AS
Nedre Eiker vei 8
Ole Steens gate 10
NO-3045 Drammen
NORWAYYOUR ORDER NO.
REFERENCE
Finn Martin**EXTENT OF DELIVERY STAINLESS STEEL TUBES**

Quantity	Dimension	Finish
24,4 m	4"x4"x.250"	unpolished

Coil-No.	Grade of material
570349-003	EN 1.4462

CHEMICAL COMPOSITION (according to certificate of steel mill)

C %	Si %	Mn %	P %	S %	Cr %	Ni %	Mo %
0,021	0,330	1,360	0,026	0,001	22,220	5,680	3,140
Ti %	Nb %	Cu %	N %	Others %	Al %	Mg %	Co %
-	0,009	0,230	0,189	-	-	-	0,130

TESTING RESULTS (Coil)

Sample-No.	YIELD STRENGTH Rp0.2 N/mm2	1% PROOF STRENGTH Rp1.0 N/mm2	TENSILE STRENGTH Rm N/mm2	ELONGATION A5 %	HARDNESS HB
Test 1	637	719	844	33	258
Test 2	625	707	833	33	251

Material acc. to EN 10088-2:2014; ASTM A240-15b; ASTM A554-16 (if included)

Eddycurrent test acc. to Stalatube norm. (Not applied to 'press brake' tubes)

Tubes are produced according to Stalatube technical data sheet

Country of Mfg: FINLAND
Country of Melt: SWEDEN

STALATUBE OY

Lahti
21.01.2019Pasi Uotinen
Quality Manager**Stalatube Oy**Talvalkatu 7, 15170 LAHTI
FINLANDDomicile Lahti
www.stalatube.comTel: +358 3 882 190
Fax: +358 3 882 1914VAT FI15685444
Trade-Reg.No: FI1568544-4

Appendix B: Pictures of The Samples Before and After Testing

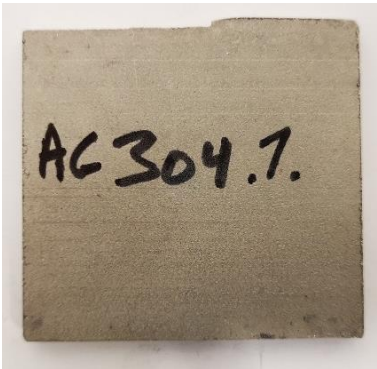


Figure 1: 1.AC304 before testing

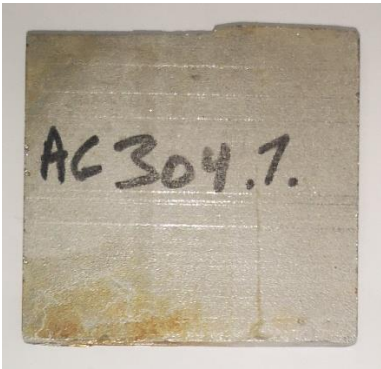


Figure 2: 1.AC304 after testing

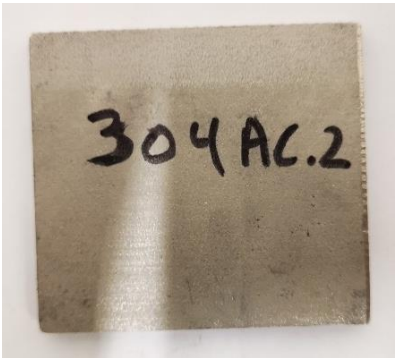


Figure 3: 2.AC304 before testing

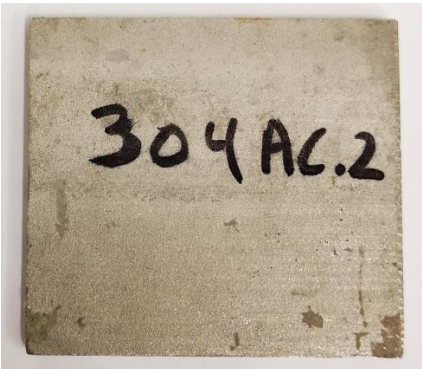


Figure 4: 2.AC304 after testing

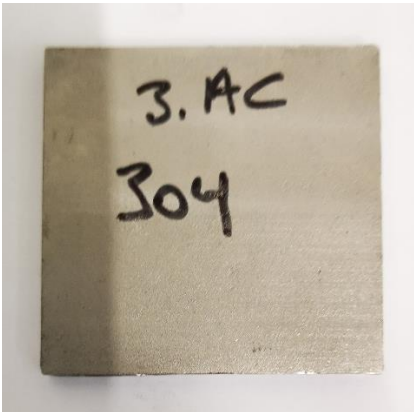


Figure 5: 3.AC304 before testing

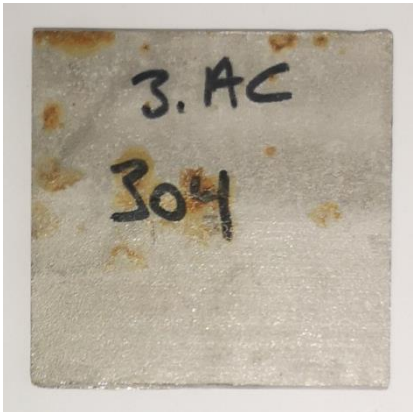


Figure 6: 3.LC304 after testing

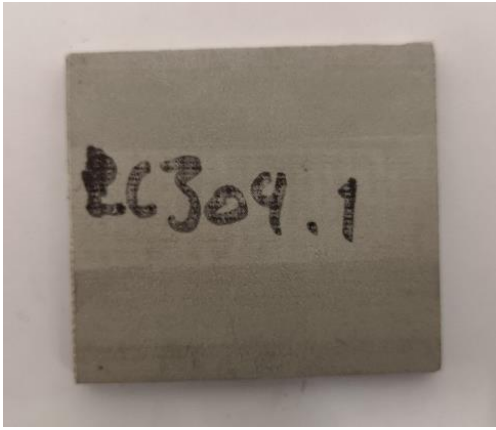


Figure 7: 1.LC304 before testing

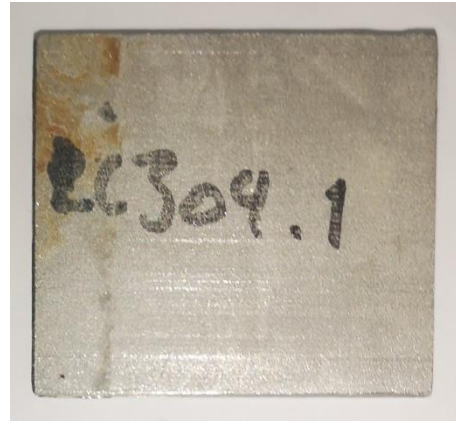


Figure 8: 1.LC304 after testing

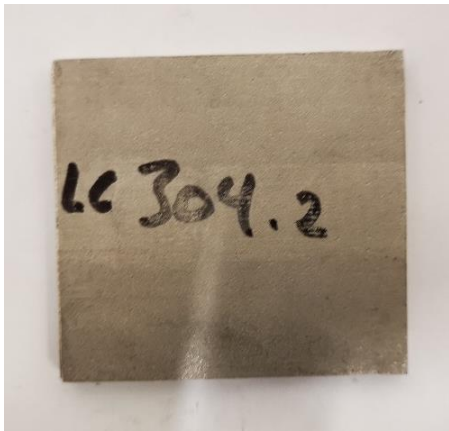


Figure 9: 2.LC304 before testing

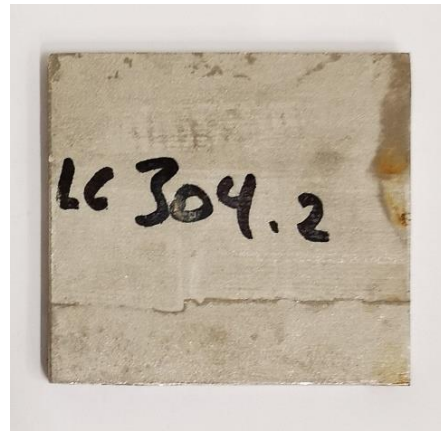


Figure 10: 2.LC304 after testing

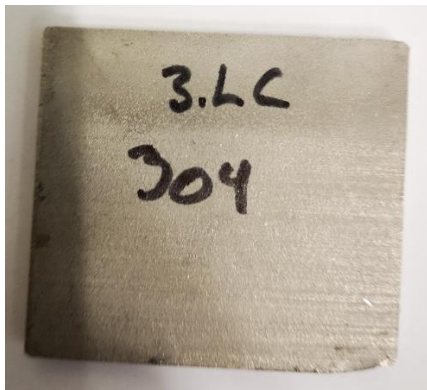


Figure 11: 3.LC304 before testing

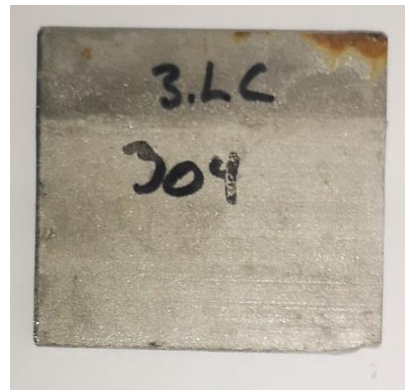


Figure 12: 3.LC304 after testing



Figure 13: 1.AC316L before testing



Figure 14: 1.AC316L after testing



Figure 15: 2.AC316L before testing



Figure 16: 2.AC316L after testing



Figure 17: 3.AC316L before testing

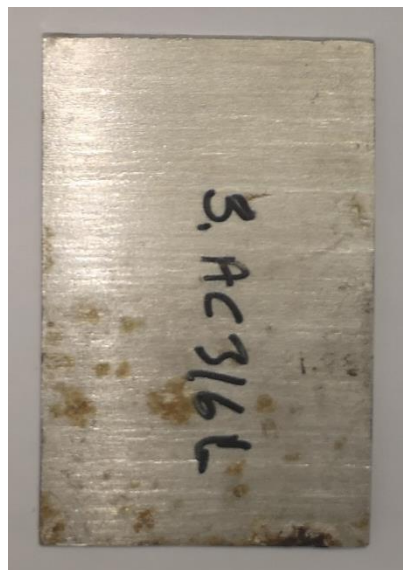


Figure 18: 3.AC316L before testing

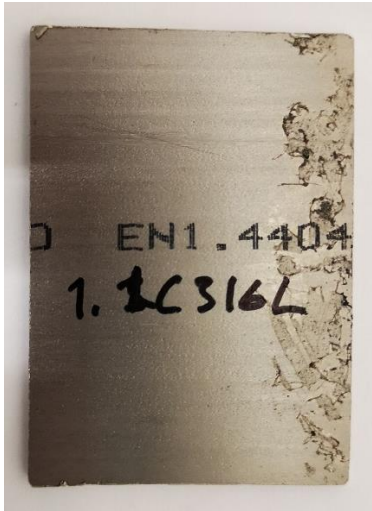


Figure 19: 1.LC316L before testing



Figure 20: 1.LC316L after testing



Figure 21: 2.LC316L before testing



Figure 22: 2.LC316L after testing



Figure 23: 3.LC316L before testing



Figure 24: 3.LC316L after testing



Figure 25: 1.AC2003 before testing



Figure 26: 1.AC2003 after testing

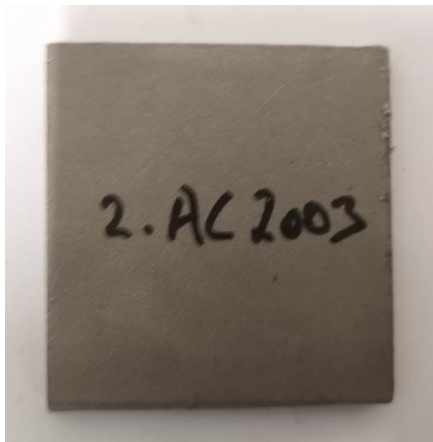


Figure 27: 2.AC2003 before testing

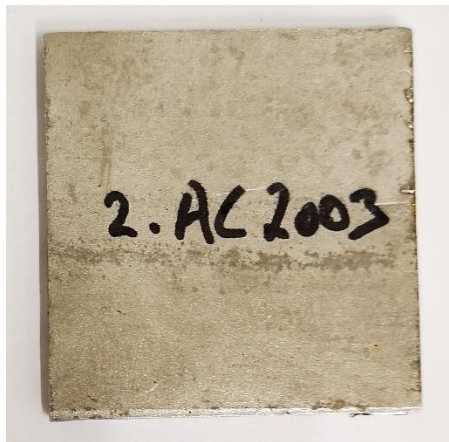


Figure 28: 2.AC2003 after testing

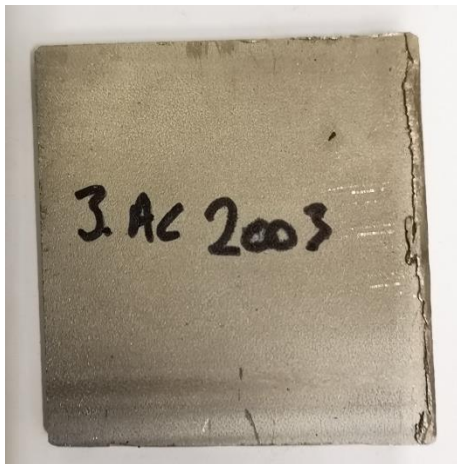


Figure 29: 3.AC2003 before testing

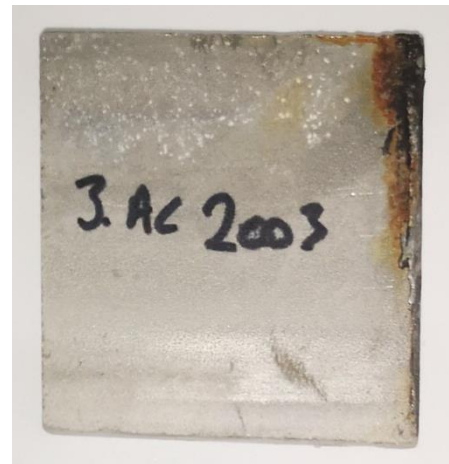


Figure 30: 3.AC2003 after testing



Figure 31: 1.LC2003 before testing

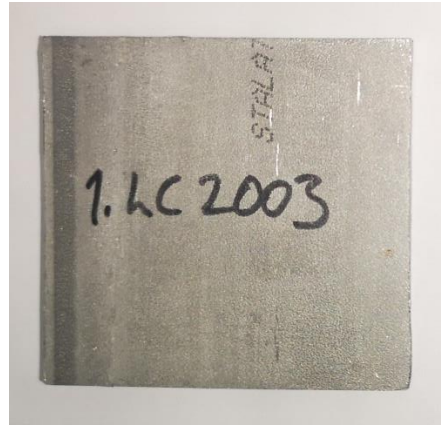


Figure 32: 1.LC2003 after testing

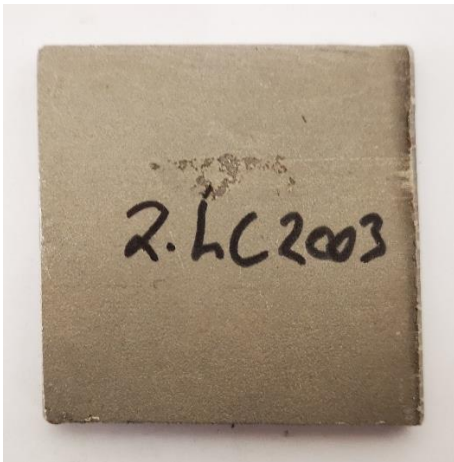


Figure 33: 2.LC2003 before testing

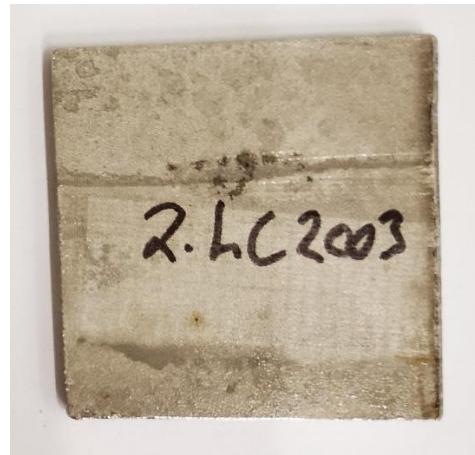


Figure 34: 2.LC2003 after testing

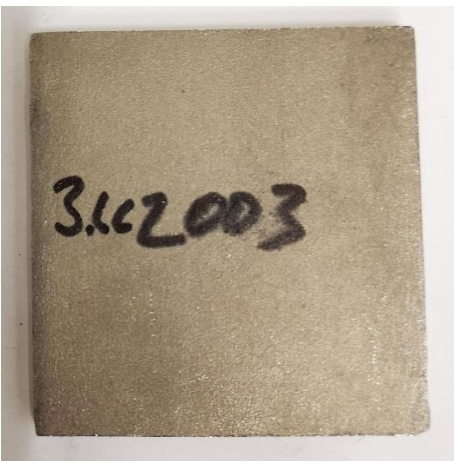


Figure 35: 3.LC2003 before testing

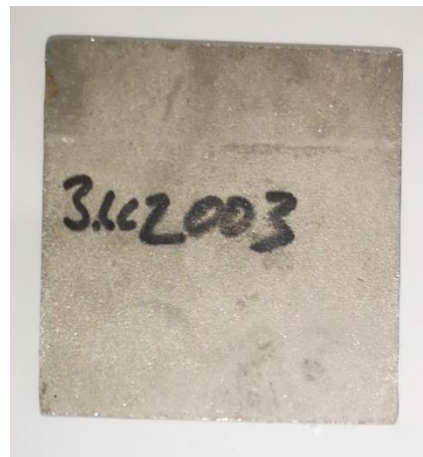


Figure 36: 3.LC2003 after testing



Figure 37: 1.AC2205 before testing

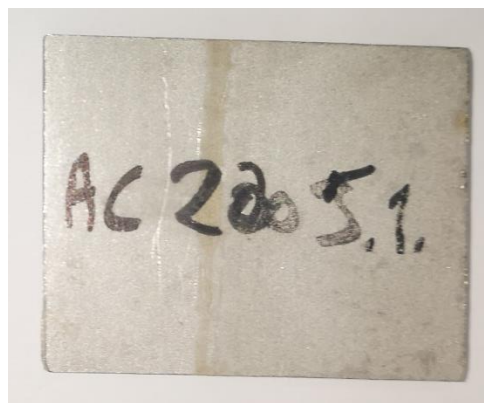


Figure 38: 1.AC2205 after testing

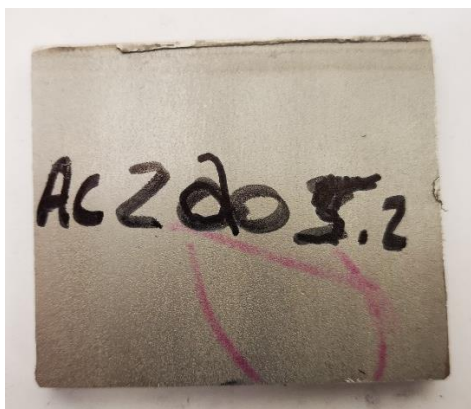


Figure 39: 2.AC2205 before testing

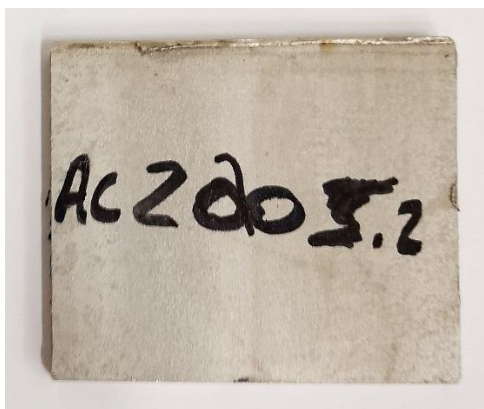


Figure 40: 2.AC2205 after testing

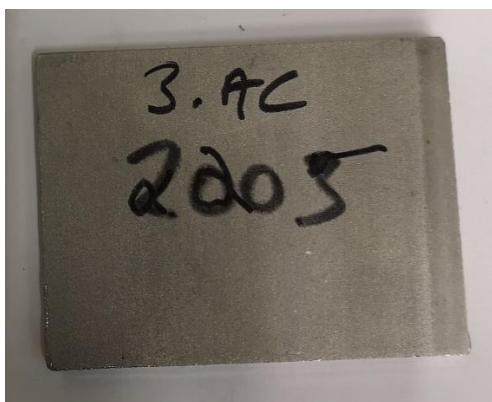


Figure 41: 3.AC2205 before testing

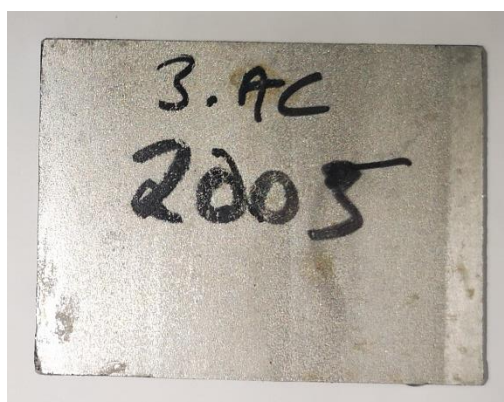


Figure 42: 3.AC2205 after testing

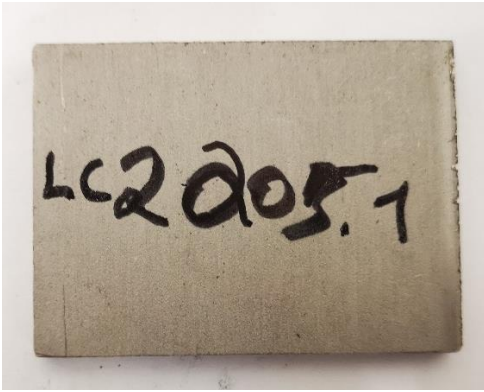


Figure 43: 1.LC2205 before testing

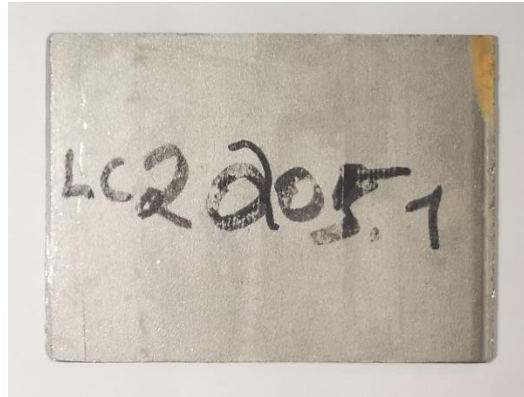


Figure 44: 1.LC2205 after testing

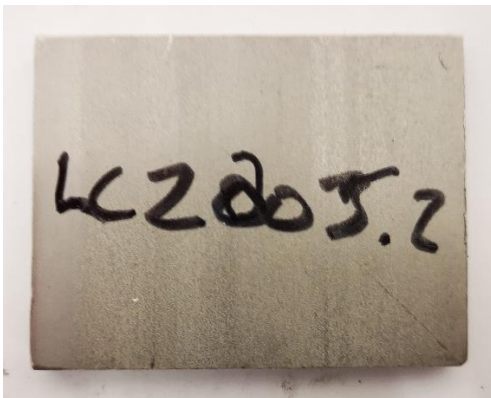


Figure 45: 2.LC2205 before testing

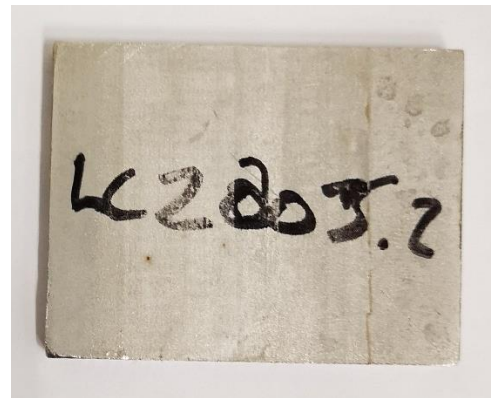


Figure 46: 2.LC2205 after testing

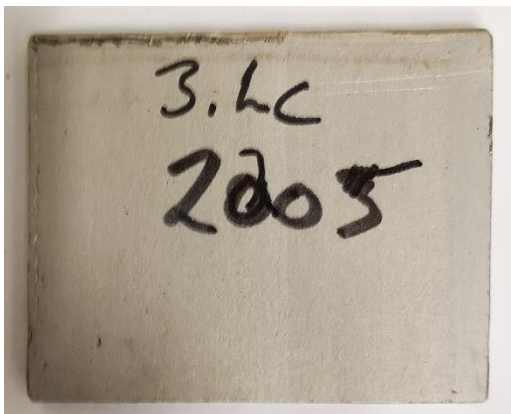


Figure 47: 3.LC2205 before testing

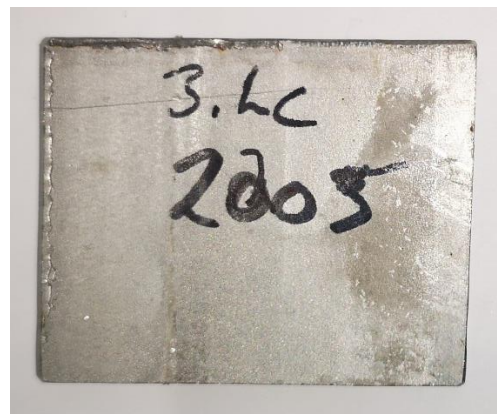


Figure 48: 3.LC2205 after testing

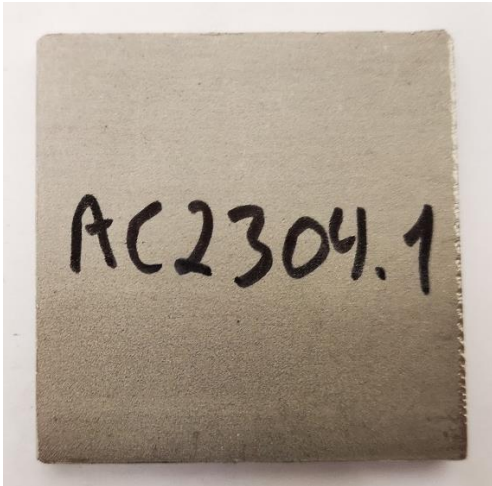


Figure 49: 1.AC2304 before testing

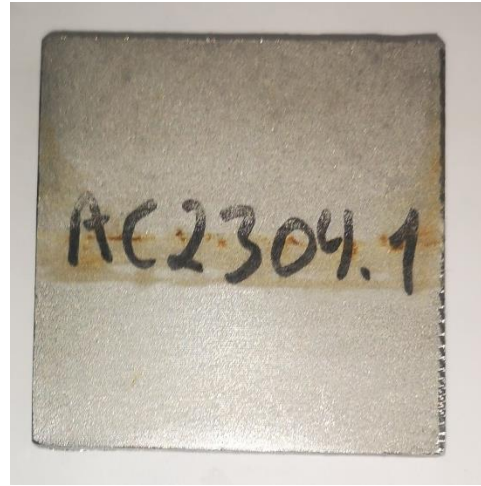


Figure 50: 1.AC2304 after testing

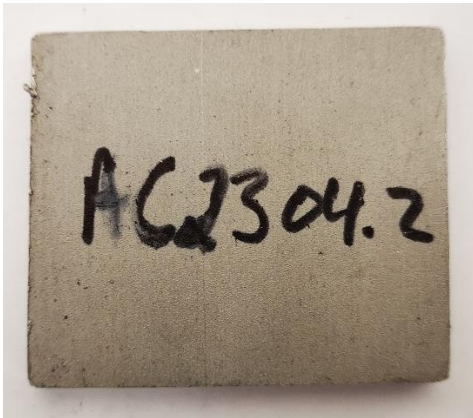


Figure 51: 2.AC2304 before testing

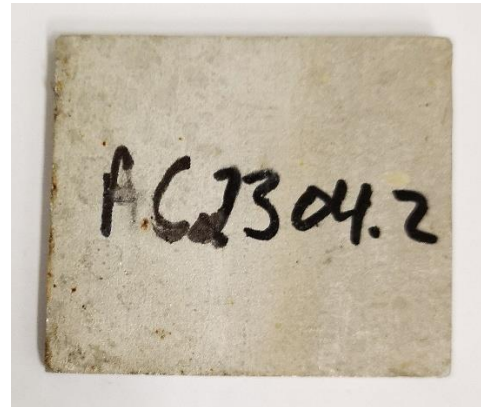


Figure 52: 2.AC2304 after testing

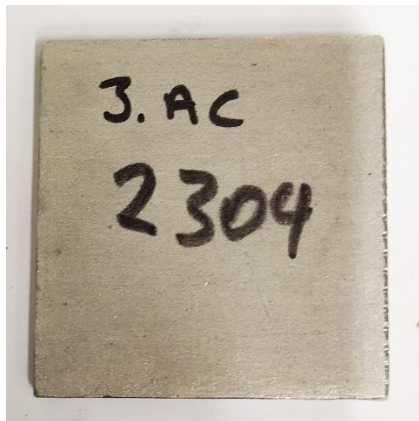


Figure 53: 3.AC 2304 before testing



Figure 54: 3.AC2304 after testing

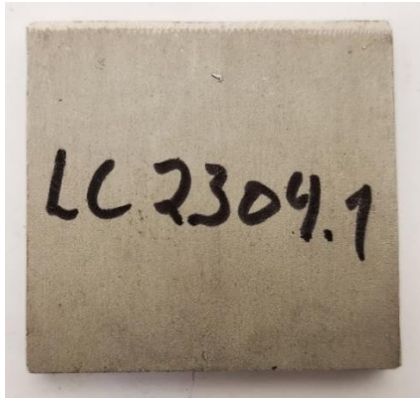


Figure 55: 1.LC2304 before testing

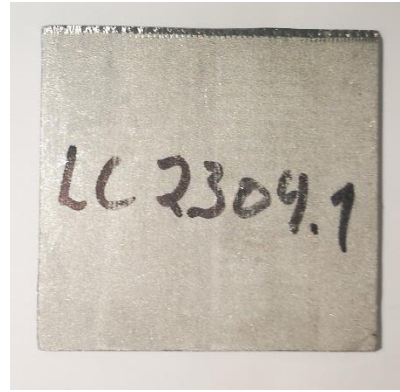


Figure 56: 1.LC2304 after testing

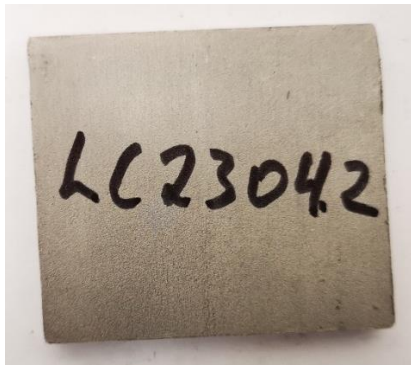


Figure 57: 2.LC2304 before testing

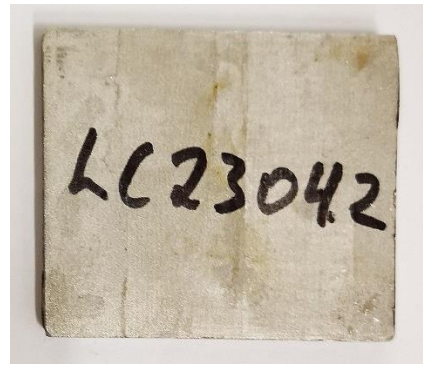


Figure 58: 2.LC2304 after testing

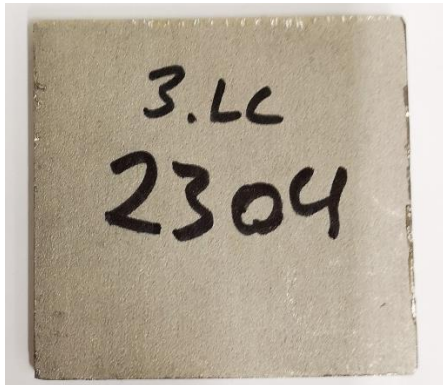


Figure 59: 3.LC2304 before testing

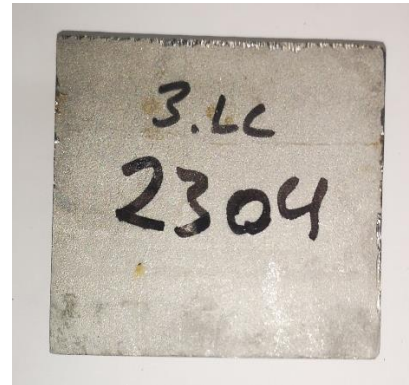


Figure 60: 3.LC2304 after testing

Appendix C: Weight Test Results

Table 1: Sample mass before- and after testing

Samples	Temperature	Test period	Mass before testing [g]	Mass after testing [g]	Deviation [%]
1.AC304	20°C	8 weeks	82.30	82.30	0.0
2.AC304	40°C	4 weeks	84.73	84.73	0.0
3.AC304	60°C	4 weeks	87.07	87.07	0.0
1.LC304	20°C	8 weeks	79.13	79.13	0.0
2.LC304	40°C	4 weeks	84.46	84.46	0.0
3.LC304	60°C	4 weeks	84.29	84.29	0.0
1.AC316L	20°C	8 weeks	76.03	76.03	0.0
2.AC316L	40°C	4 weeks	84.59	84.59	0.0
3.AC316L	60°C	4 weeks	80.41	80.41	0.0
1.LC316L	20°C	8 weeks	78.27	78.27	0.0
2.LC316L	40°C	4 weeks	77.35	77.35	0.0
3.LC316L	60°C	4 weeks	76.49	76.49	0.0
1.AC2003	20°C	8 weeks	97.39	97.39	0.0
2.AC2003	40°C	4 weeks	92.42	92.42	0.0
3.AC2003	60°C	4 weeks	90.18	90.18	0.0
1.LC2003	20°C	8 weeks	89.48	89.48	0.0
2.LC2003	40°C	4 weeks	86.17	86.17	0.0
3.LC2003	60°C	4 weeks	85.67	85.67	0.0
1.AC2205	20°C	8 weeks	142.64	142.64	0.0
2.AC2205	40°C	4 weeks	139.08	139.08	0.0
3.AC2205	60°C	4 weeks	145.74	145.74	0.0
1.LC2205	20°C	8 weeks	146.48	146.48	0.0
2.LC2205	40°C	4 weeks	140.12	140.12	0.0
3.LC2205	60°C	4 weeks	149.02	149.02	0.0
1.AC2304	20°C	8 weeks	125.68	125.68	0.0
2.AC2304	40°C	4 weeks	118.48	118.48	0.0
3.AC2304	60°C	4 weeks	124.64	124.64	0.0
1.LC2304	20°C	8 weeks	121.05	121.05	0.0
2.LC2304	40°C	4 weeks	116.29	116.29	0.0
3.LC2304	60°C	4 weeks	127.91	127.91	0.0

Appendix D: Composition Test Results

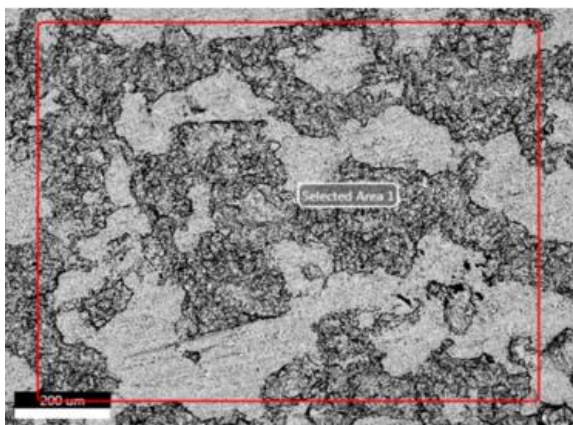
EDAX TEAM

Page1

Martin Berntsen

Author: student
 Creation: 03/12/2019 10:49:34 AM
 Sample Name: SS 304

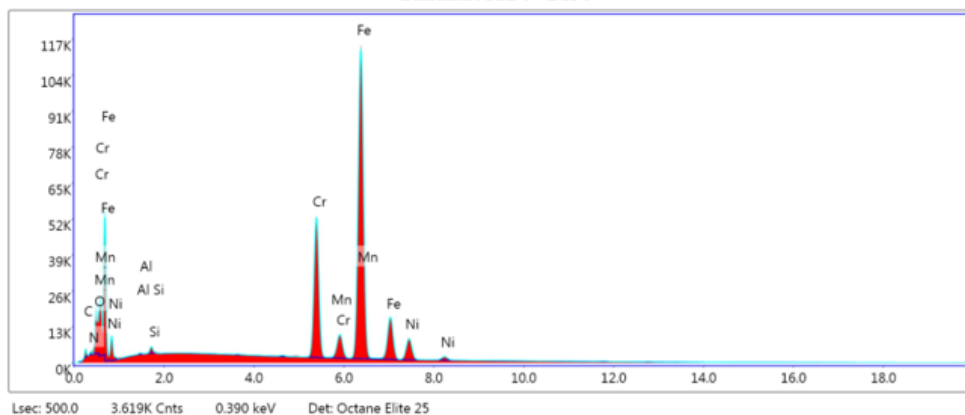
SS 304



Selected Area 1

kV: 20 Mag:300 Takeoff: 37.8 Live Time(s): 500 Amp Time(μs):7.68 Resolution:(eV)125.8

Selected Area 1 - Det 1



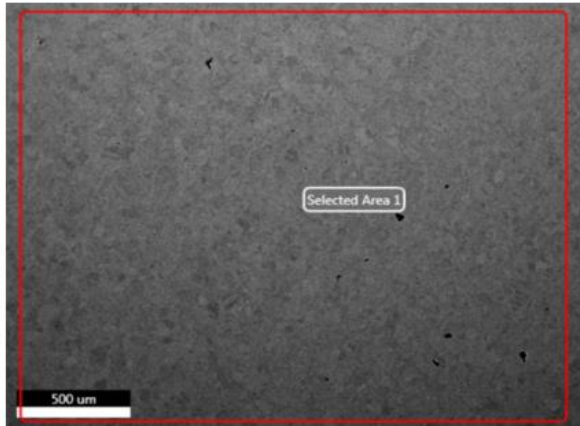
eZAF Smart Quant Results

Element	Weight %	Atomic %	Net Int.	Error %	Kratio	Z	A	F
CK	1.59	6.59	48.08	10.29	0.0046	1.3048	0.2220	1.0000
NK	0.32	1.15	19.40	11.99	0.0013	1.2786	0.3033	1.0000
OK	1.44	4.49	210.19	6.87	0.0083	1.2553	0.4606	1.0000
AlK	0.09	0.17	12.72	17.88	0.0004	1.1271	0.3559	1.0018
SiK	0.37	0.65	70.17	8.24	0.0021	1.1535	0.4818	1.0031
CrK	20.18	19.35	2655.21	1.87	0.2143	0.9895	0.9920	1.0819
MnK	1.37	1.25	154.56	4.08	0.0140	0.9699	0.9931	1.0598
FeK	67.90	60.63	6361.24	1.82	0.6523	0.9866	0.9652	1.0088
NiK	6.74	5.73	463.89	3.03	0.0612	0.9994	0.9030	1.0060

Martin polished

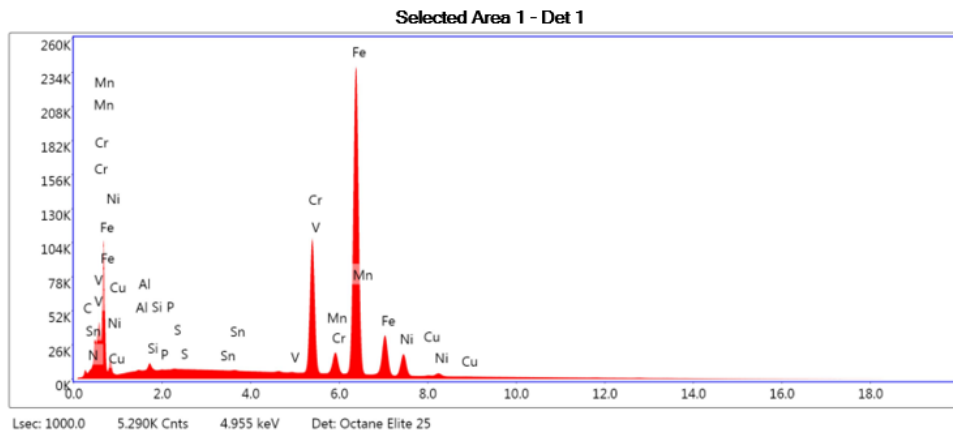
Author: student
 Creation: 05/16/2019 3:36:12 PM
 Sample Name: Sample 304 Polished

SS_304_polished



Selected Area 1

kV: 20 Mag:140 Takeoff: 37.3 Live Time(s): 1000 Amp Time(μs):7.68 Resolution:(eV)125.8



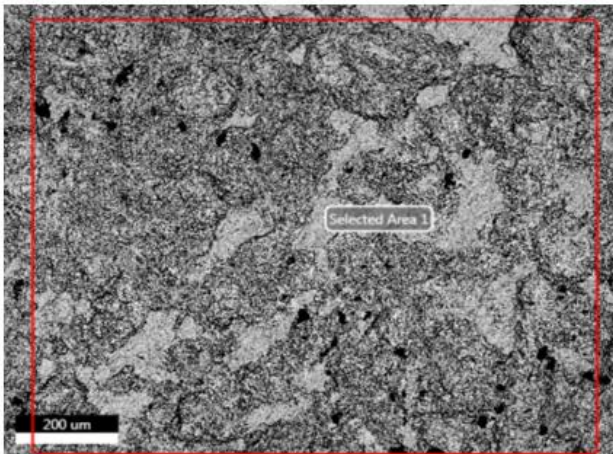
eZAF Smart Quant Results

Element	Weight %	Atomic %	Net Int.	Error %	Kratio	Z	A	F
C K	0.40	1.79	11.94	12.81	0.0011	1.3170	0.2180	1.0000
N K	0.00	0.00	0.00	99.99	0.0000	1.2905	0.3108	1.0000
Al K	0.02	0.04	2.70	62.57	0.0001	1.1379	0.3474	1.0018
Si K	0.38	0.73	72.32	7.85	0.0021	1.1646	0.4725	1.0031
P K	0.02	0.03	3.29	59.16	0.0001	1.1202	0.5917	1.0054
S K	0.11	0.19	24.15	7.38	0.0009	1.1438	0.6982	1.0085
Sn L	0.53	0.24	45.92	3.01	0.0047	0.8424	1.0523	1.0116
V K	0.51	0.55	76.37	4.36	0.0055	0.9836	0.9806	1.1066
Cr K	20.07	20.97	2709.42	1.85	0.2145	0.9997	0.9892	1.0807
Mn K	1.59	1.57	183.26	2.97	0.0163	0.9799	0.9901	1.0587
Fe K	68.81	66.92	6625.55	1.84	0.6665	0.9969	0.9626	1.0094
Ni K	7.20	6.66	508.60	2.89	0.0658	1.0102	0.8992	1.0061
Cu K	0.36	0.31	21.43	14.54	0.0032	0.9607	0.9187	1.0102

Martin Berntsen

Author: student
 Creation: 03/12/2019 11:45:07 AM
 Sample Name: SS 316L

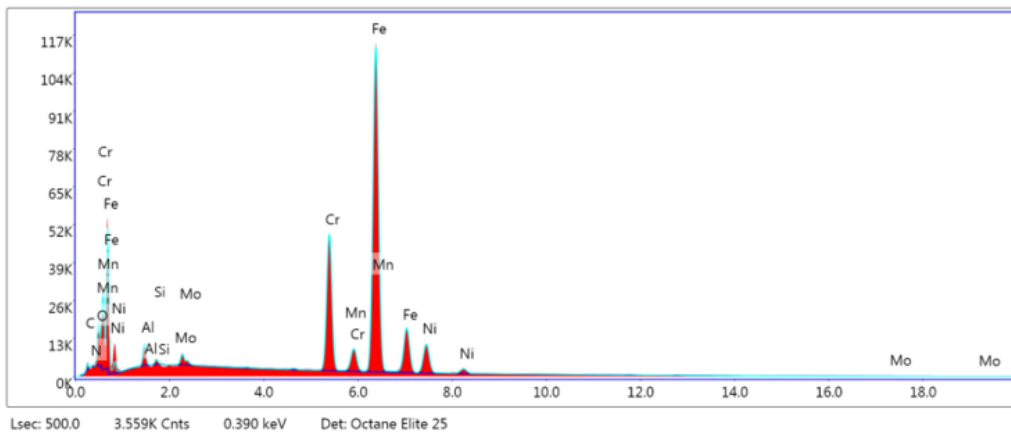
SS 316L



Selected Area 1

kV: 20 Mag:300 Takeoff: 37.3 Live Time(s): 500 Amp Time(us):7.68 Resolution:(eV)125.8

Selected Area 1 - Det 1



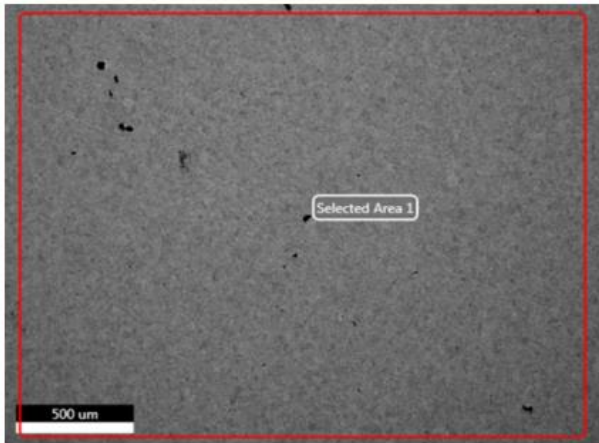
eZAF Smart Quant Results

Element	Weight %	Atomic %	Net Int.	Error %	Kratio	Z	A	F
C K	1.08	4.58	31.16	11.13	0.0030	1.3079	0.2118	1.0000
N K	0.02	0.06	0.96	72.34	0.0001	1.2817	0.2903	1.0000
O K	1.21	3.86	170.18	7.34	0.0067	1.2584	0.4421	1.0000
AlK	1.58	2.98	221.32	8.14	0.0063	1.1299	0.3540	1.0018
SiK	0.28	0.50	52.24	9.30	0.0015	1.1564	0.4729	1.0031
MoL	1.20	0.64	130.16	3.63	0.0091	0.8871	0.8530	1.0018
CrK	18.43	18.09	2448.64	1.92	0.1959	0.9922	0.9891	1.0832
MnK	1.19	1.11	136.18	4.26	0.0122	0.9725	0.9913	1.0629
FeK	66.39	60.67	6314.11	1.83	0.6418	0.9893	0.9663	1.0114
NiK	8.63	7.50	601.78	2.92	0.0787	1.0022	0.9045	1.0063

Martin polished

Author: student
 Creation: 05/16/2019 3:06:59 PM
 Sample Name: Sample 316L polished

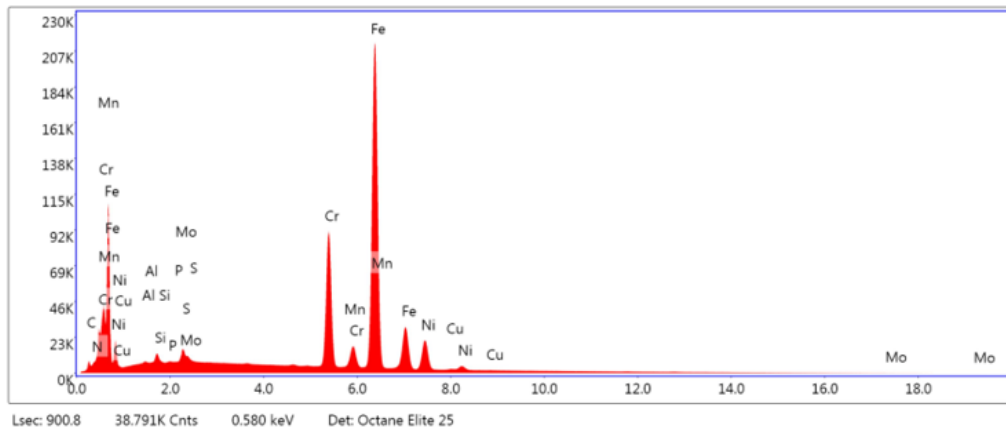
SS_316L_polished



Selected Area 1

kV: 20 Mag:140 Takeoff: 37 Live Time(s): 900.8 Amp Time(μs):7.68 Resolution:(eV)125.8

Selected Area 1 - Det 1



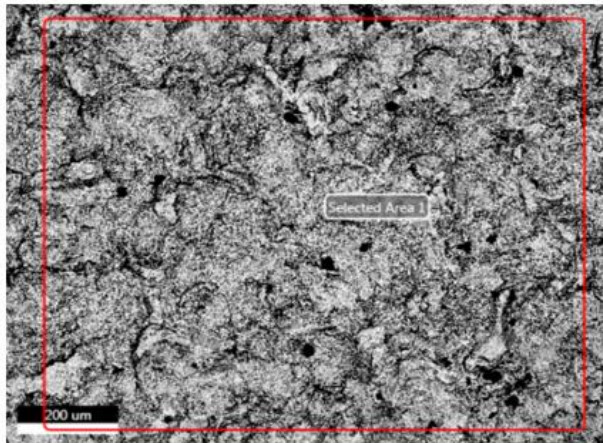
eZAF Smart Quant Results

Element	Weight %	Atomic %	Net Int.	Error %	Kratio	Z	A	F
CK	0.56	2.53	15.98	11.84	0.0016	1.3154	0.2124	1.0000
AlK	0.02	0.05	3.36	62.29	0.0001	1.1365	0.3455	1.0018
SiK	0.40	0.77	74.67	7.86	0.0022	1.1633	0.4703	1.0031
MoL	0.97	0.55	103.67	3.66	0.0074	0.8924	0.8509	1.0018
SK	0.28	0.48	59.83	9.39	0.0023	1.1424	0.6963	1.0083
CrK	18.94	19.71	2494.17	1.88	0.2026	0.9986	0.9887	1.0834
MnK	0.89	0.88	101.17	4.68	0.0092	0.9788	0.9908	1.0638
FeK	68.71	66.56	6469.74	1.82	0.6678	0.9958	0.9650	1.0114
NiK	8.97	8.26	617.37	2.83	0.0820	1.0091	0.9009	1.0060
CuK	0.24	0.21	13.86	17.23	0.0022	0.9596	0.9199	1.0102

Martin Berntsen

Author: student
 Creation: 03/12/2019 10:16:36 AM
 Sample Name: SS 2003

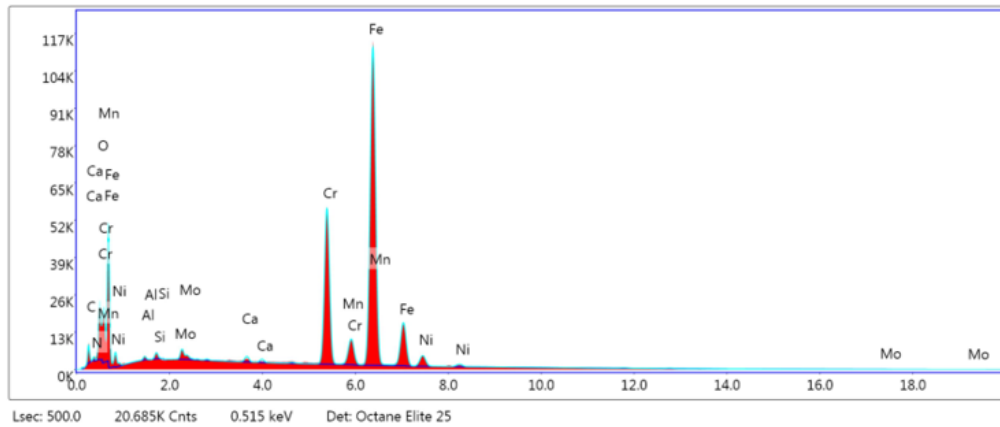
SS 2003



Selected Area 1

kV: 20 Mag:300 Takeoff: 37.7 Live Time(s): 500 Amp Time(μs):7.68 Resolution:(eV)125.8

Selected Area 1 - Det 1



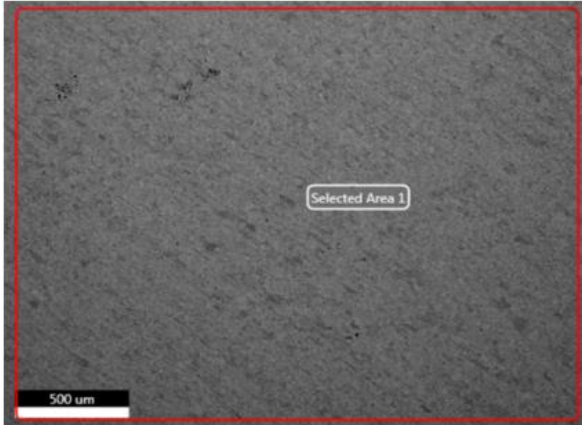
eZAF Smart Quant Results

Element	Weight %	Atomic %	Net Int.	Error %	Kratio	Z	A	F
CK	3.08	12.00	97.00	9.51	0.0091	1.2970	0.2272	1.0000
NK	0.38	1.27	21.39	12.16	0.0014	1.2709	0.2809	1.0000
OK	2.08	6.08	285.38	7.13	0.0111	1.2478	0.4267	1.0000
AlK	0.24	0.41	34.61	11.22	0.0010	1.1202	0.3664	1.0019
SiK	0.33	0.55	66.06	8.35	0.0019	1.1465	0.4928	1.0032
MoL	1.09	0.53	121.13	4.45	0.0083	0.8794	0.8728	1.0019
CaK	0.41	0.48	75.28	4.17	0.0044	1.0904	0.9316	1.0407
CrK	21.35	19.23	2849.54	1.85	0.2244	0.9832	0.9911	1.0782
MnK	1.43	1.22	162.93	3.74	0.0144	0.9636	0.9923	1.0539
FeK	66.36	55.64	6292.17	1.83	0.6295	0.9802	0.9626	1.0055
NiK	3.25	2.59	227.84	3.55	0.0293	0.9928	0.9031	1.0070

Martin polished

Author: student
 Creation: 05/16/2019 2:01:55 PM
 Sample Name: Sample 2003 polished

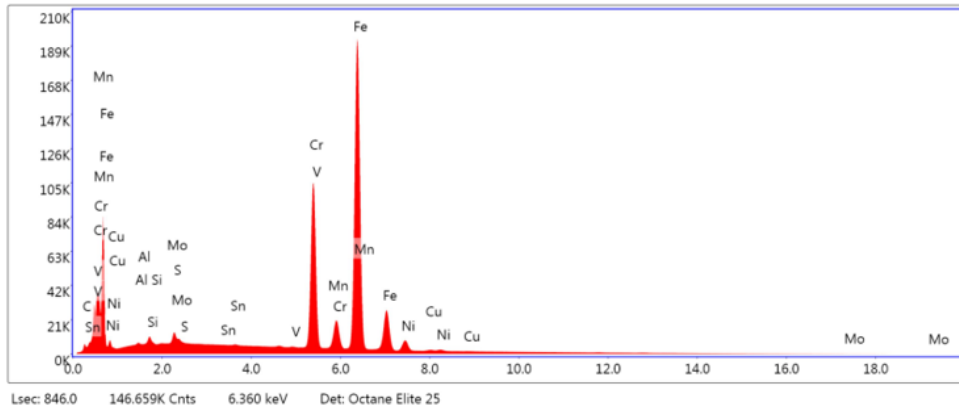
SS_2003_polished



Selected Area 1

kV: 20 Mag:140 Takeoff: 42 Live Time(s): 846 Amp Time(μs):7.68 Resolution:(eV)125.8

Selected Area 1 - Det 1



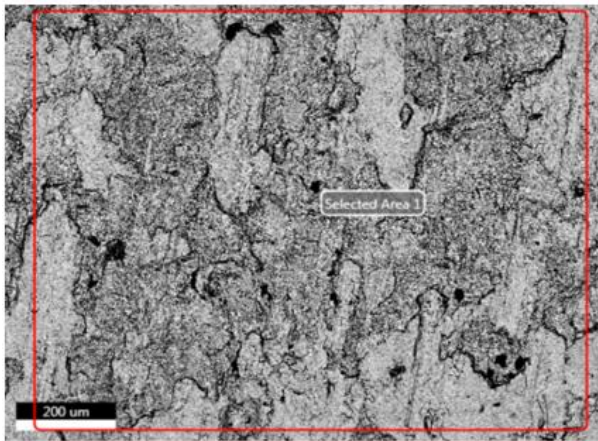
eZAF Smart Quant Results

Element	Weight %	Atomic %	Net Int.	Error %	Kratio	Z	A	F
CK	0.24	1.09	7.84	15.90	0.0007	1.3198	0.2254	1.0000
AlK	0.01	0.01	0.86	68.93	0.0000	1.1402	0.3778	1.0019
SiK	0.25	0.48	49.70	8.07	0.0015	1.1670	0.5053	1.0032
MoL	0.72	0.41	79.06	3.89	0.0056	0.8952	0.8703	1.0020
SK	0.25	0.42	53.76	9.33	0.0021	1.1460	0.7254	1.0086
SnL	0.12	0.06	10.17	17.50	0.0011	0.8439	1.0472	1.0120
VK	0.19	0.20	26.89	12.32	0.0020	0.9854	0.9832	1.1090
CrK	24.34	25.48	3130.04	1.80	0.2596	1.0014	0.9909	1.0748
MnK	1.80	1.78	197.25	3.13	0.0184	0.9816	0.9912	1.0502
FeK	68.59	66.85	6266.18	1.85	0.6608	0.9986	0.9599	1.0051
NiK	3.15	2.92	213.84	3.43	0.0290	1.0118	0.9044	1.0067
CuK	0.34	0.29	19.47	14.26	0.0031	0.9622	0.9236	1.0110

Martin Berntsen

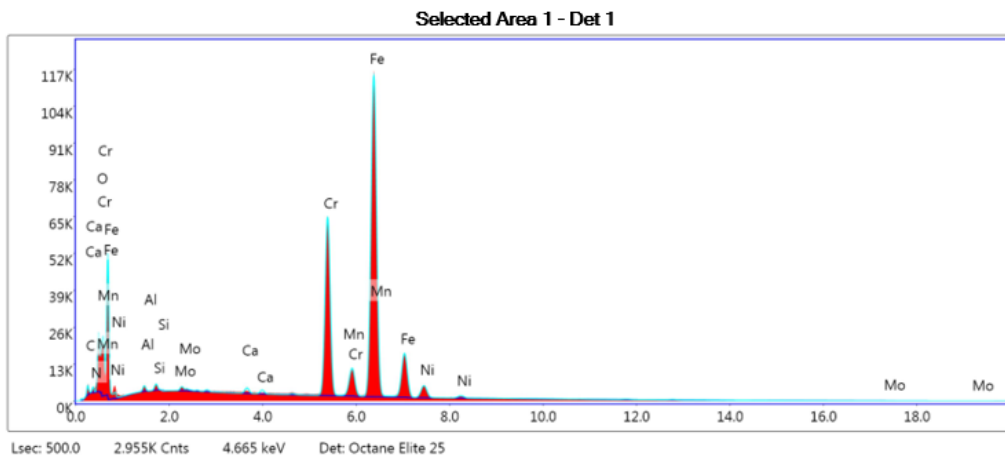
Author: student
 Creation: 03/12/2019 11:20:56 AM
 Sample Name: SS 2304

SS 2304



Selected Area 1

kV: 20 Mag:300 Takeoff: 36.4 Live Time(s): 500 Amp Time(μs):7.68 Resolution:(eV)125.8



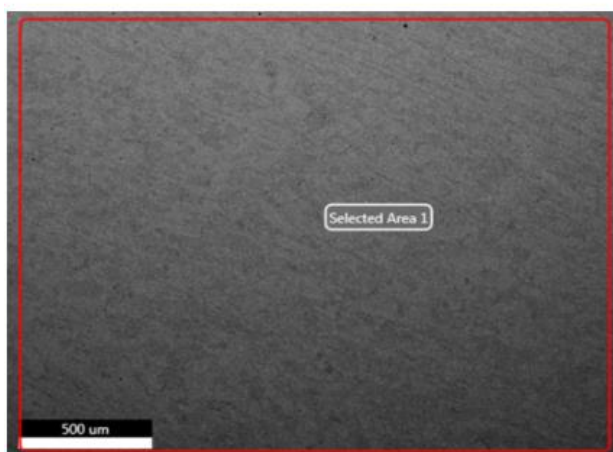
eZAF Smart Quant Results

Element	Weight %	Atomic %	Net Int.	Error %	Kratio	Z	A	F
C K	1.58	6.48	49.47	10.30	0.0046	1.3037	0.2236	1.0000
N K	0.43	1.52	26.12	11.14	0.0016	1.2775	0.2953	1.0000
O K	1.68	5.17	245.34	6.99	0.0094	1.2542	0.4445	1.0000
AlK	0.41	0.74	59.81	9.49	0.0016	1.1260	0.3549	1.0018
SiK	0.35	0.62	70.26	8.34	0.0020	1.1524	0.4796	1.0032
MoL	0.43	0.22	49.38	6.08	0.0033	0.8840	0.8645	1.0020
CaK	0.38	0.47	71.55	4.21	0.0040	1.0962	0.9304	1.0418
CrK	23.96	22.65	3303.83	1.82	0.2523	0.9884	0.9913	1.0747
MnK	1.30	1.16	152.61	4.08	0.0131	0.9688	0.9917	1.0511
FeK	65.84	57.94	6435.28	1.89	0.6244	0.9854	0.9570	1.0056
NiK	3.62	3.03	261.72	3.50	0.0327	0.9982	0.8984	1.0067

Martin polished

Author: student
 Creation: 05/16/2019 2:34:50 PM
 Sample Name: Sample 2304 polished

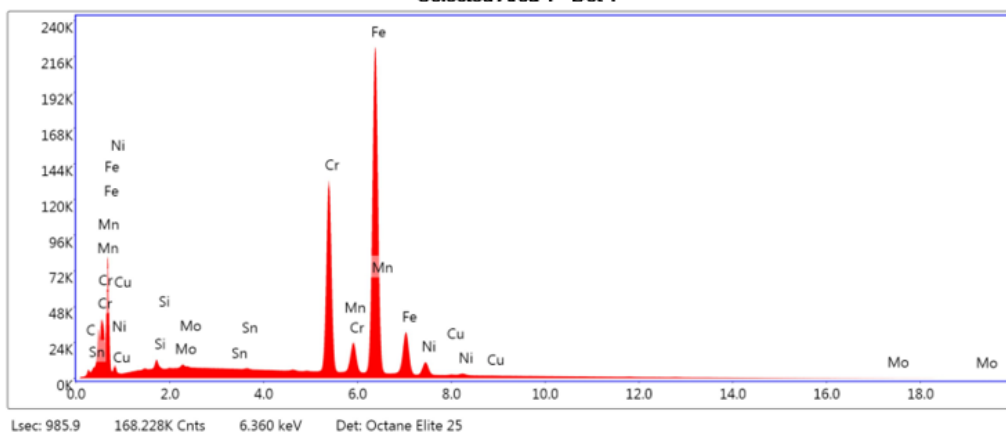
SS_2304_polished



Selected Area 1

kV: 20 Mag:156 Takeoff: 41.2 Live Time(s): 985.9 Amp Time(μs):7.68 Resolution:(eV)125.8

Selected Area 1 - Det 1



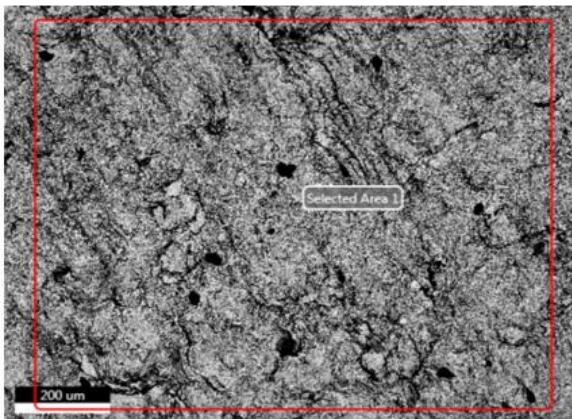
eZAF Smart Quant Results

Element	Weight %	Atomic %	Net Int.	Error %	Kratio	Z	A	F
C K	0.13	0.60	4.35	20.68	0.0004	1.3206	0.2273	1.0000
Si K	0.34	0.67	69.57	7.55	0.0020	1.1677	0.5002	1.0032
Mo L	0.34	0.19	38.27	4.46	0.0027	0.8958	0.8674	1.0021
Sn L	0.50	0.23	43.34	3.20	0.0045	0.8445	1.0499	1.0121
Cr K	26.08	27.43	3432.87	1.78	0.2775	1.0021	0.9906	1.0719
Mn K	1.88	1.87	211.42	2.81	0.0192	0.9823	0.9908	1.0480
Fe K	66.63	65.22	6230.63	1.88	0.6405	0.9993	0.9565	1.0058
Ni K	3.79	3.53	263.42	3.13	0.0349	1.0125	0.9034	1.0066
Cu K	0.30	0.26	17.52	15.86	0.0027	0.9628	0.9227	1.0110

Martin Berntsen

Author: student
 Creation: 03/12/2019 9:37:12 AM
 Sample Name: SS 2205

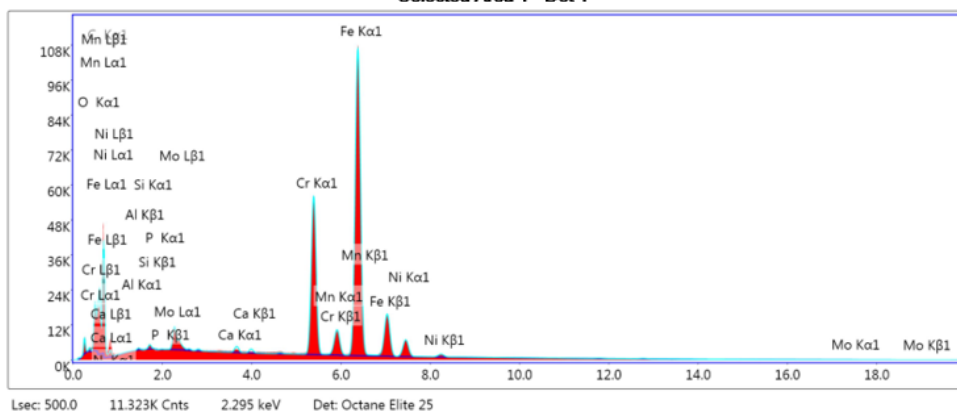
SS 2205



Selected Area 1

kV: 20 Mag:299 Takeoff: 38.1 Live Time(s): 500 Amp Time(µs):7.68 Resolution:(eV)125.8

Selected Area 1 - Det 1



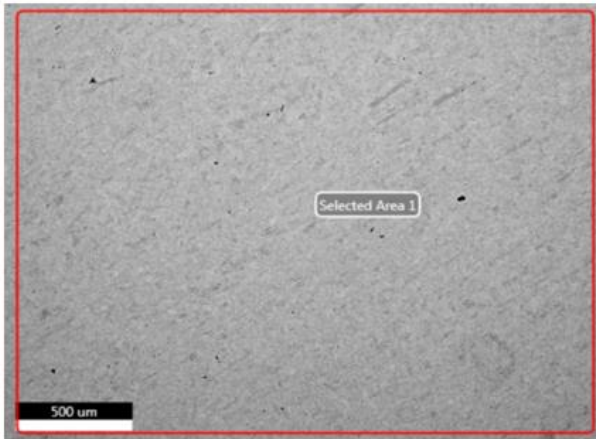
eZAF Smart Quant Results

Element	Weight %	Atomic %	Net Int.	Error %	Kratio	Z	A	F
CK	2.58	10.39	79.53	9.61	0.0075	1.3027	0.2239	1.0000
NK	0.32	1.10	17.46	12.42	0.0011	1.2766	0.2760	1.0000
OK	1.63	4.94	215.23	7.35	0.0085	1.2534	0.4131	1.0000
AlK	0.15	0.27	21.69	12.91	0.0006	1.1254	0.3672	1.0019
SiK	0.24	0.42	47.54	9.27	0.0014	1.1518	0.4937	1.0033
PK	0.00	0.00	0.00	99.99	0.0000	1.1078	0.6131	1.0056
MoL	2.49	1.26	274.55	3.63	0.0192	0.8835	0.8722	1.0019
CaK	0.43	0.52	76.06	4.22	0.0045	1.0957	0.9258	1.0387
CrK	21.79	20.29	2852.28	1.86	0.2290	0.9881	0.9887	1.0758
MnK	1.29	1.14	144.46	4.12	0.0130	0.9685	0.9902	1.0535
FeK	64.01	55.50	5985.24	1.87	0.6106	0.9852	0.9607	1.0079
NiK	5.07	4.18	351.43	3.23	0.0461	0.9980	0.9052	1.0073

Martin polished

Author: student
 Creation: 05/16/2019 1:30:34 PM
 Sample Name: Sample 2205 polished

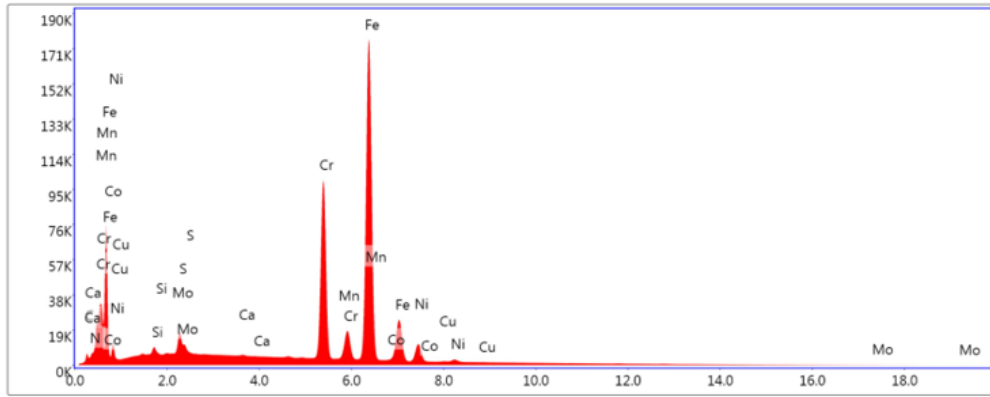
SS_2205_polished



Selected Area 1

kV: 20 Mag:140 Takeoff: 41.1 Live Time(s): 783.6 Amp Time(μs):7.68 Resolution:(eV)125.8

Selected Area 1 - Det 1



Lsec: 783.6 5.659K Cnts 3.680 keV Det: Octane Elite 25

eZAF Smart Quant Results

Element	Weight %	Atomic %	Net Int.	Error %	Kratio	Z	A	F
C K	0.37	1.68	11.99	13.96	0.0011	1.3186	0.2213	1.0000
N K	0.09	0.34	5.64	24.22	0.0004	1.2921	0.3105	1.0000
Si K	0.22	0.43	45.17	8.54	0.0013	1.1660	0.5014	1.0032
Mo L	1.50	0.85	167.35	3.09	0.0117	0.8945	0.8691	1.0019
S K	0.39	0.67	87.04	6.83	0.0033	1.1450	0.7225	1.0086
Ca K	0.11	0.15	20.10	8.74	0.0012	1.1094	0.9293	1.0403
Cr K	24.44	25.45	3196.61	1.82	0.2599	1.0006	0.9896	1.0738
Mn K	1.43	1.41	159.53	3.62	0.0146	0.9809	0.9904	1.0512
Fe K	66.10	64.10	6163.06	1.87	0.6370	0.9978	0.9587	1.0074
Co K	0.13	0.12	10.74	32.79	0.0013	0.9765	0.9582	1.0066
Ni K	5.07	4.68	351.39	3.07	0.0468	1.0110	0.9055	1.0067
Cu K	0.13	0.11	7.50	30.29	0.0012	0.9615	0.9242	1.0112

Appendix E: Open Circuit Potentials

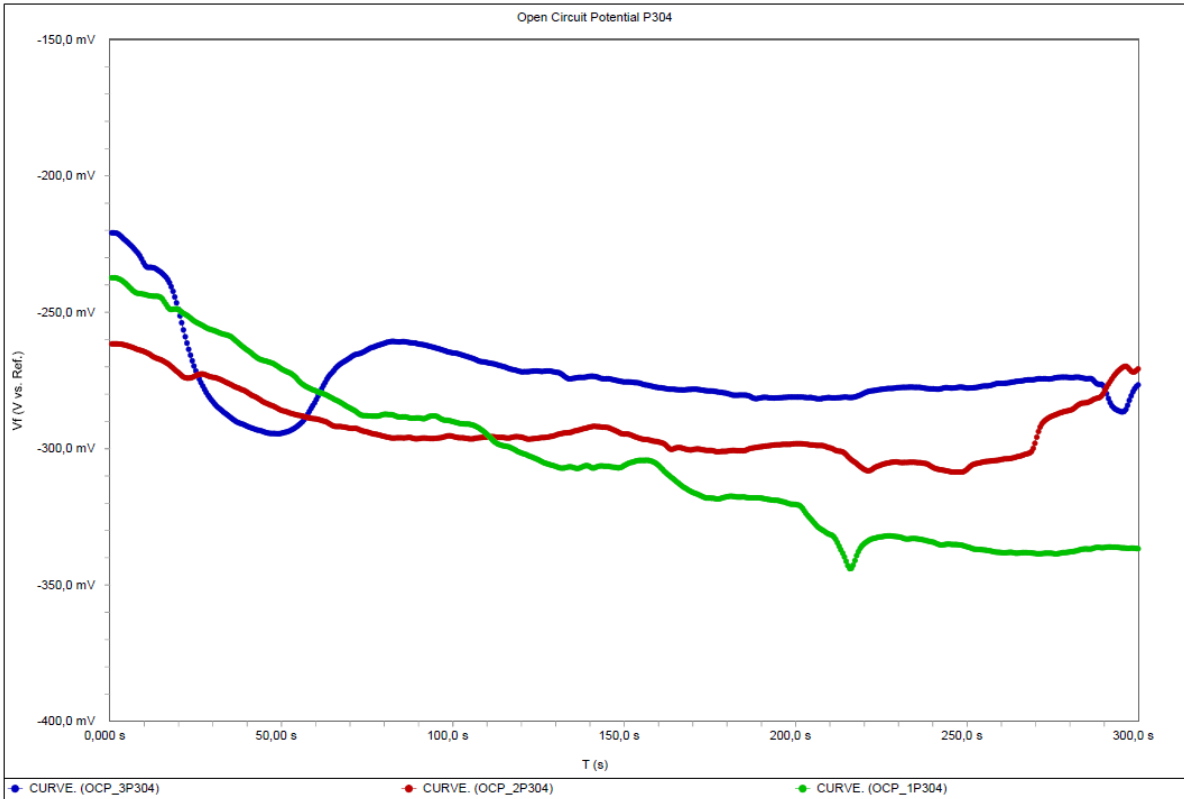


Figure 1: OCP ordinary P304

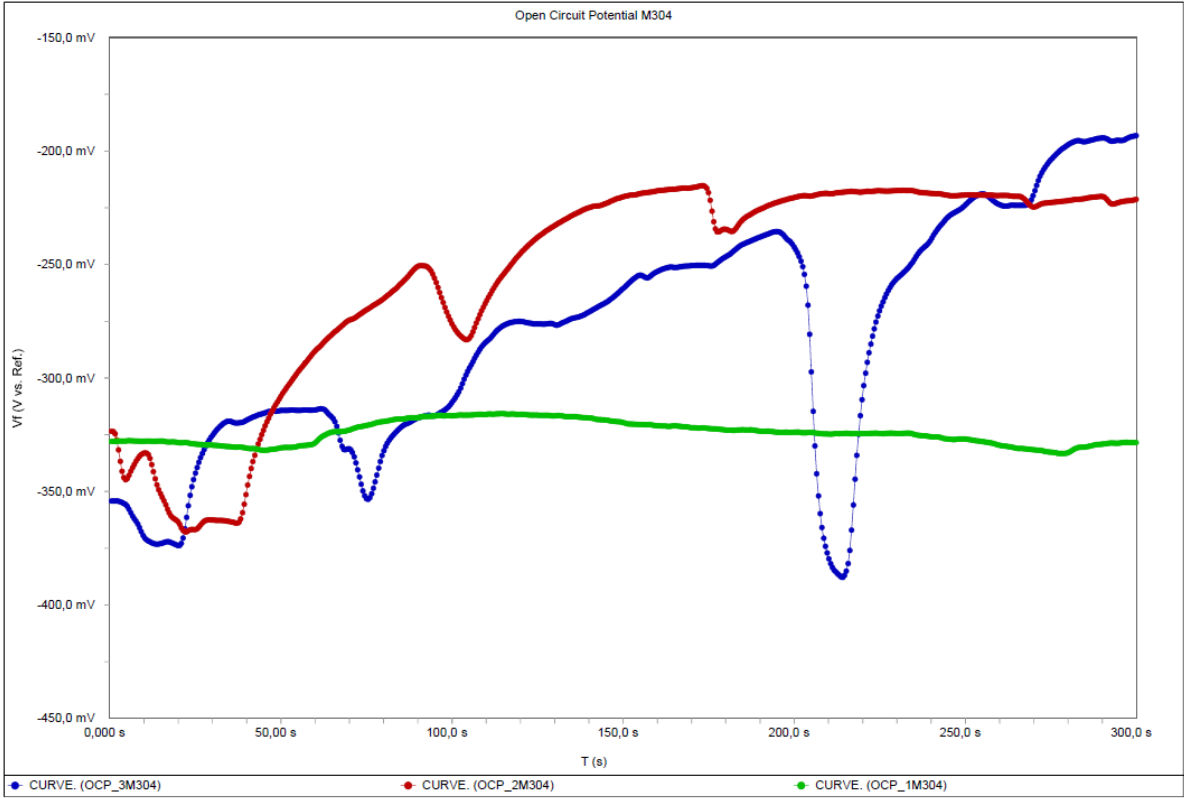


Figure 2: OCP modified M304



Figure 3: OCP ordinary P316L

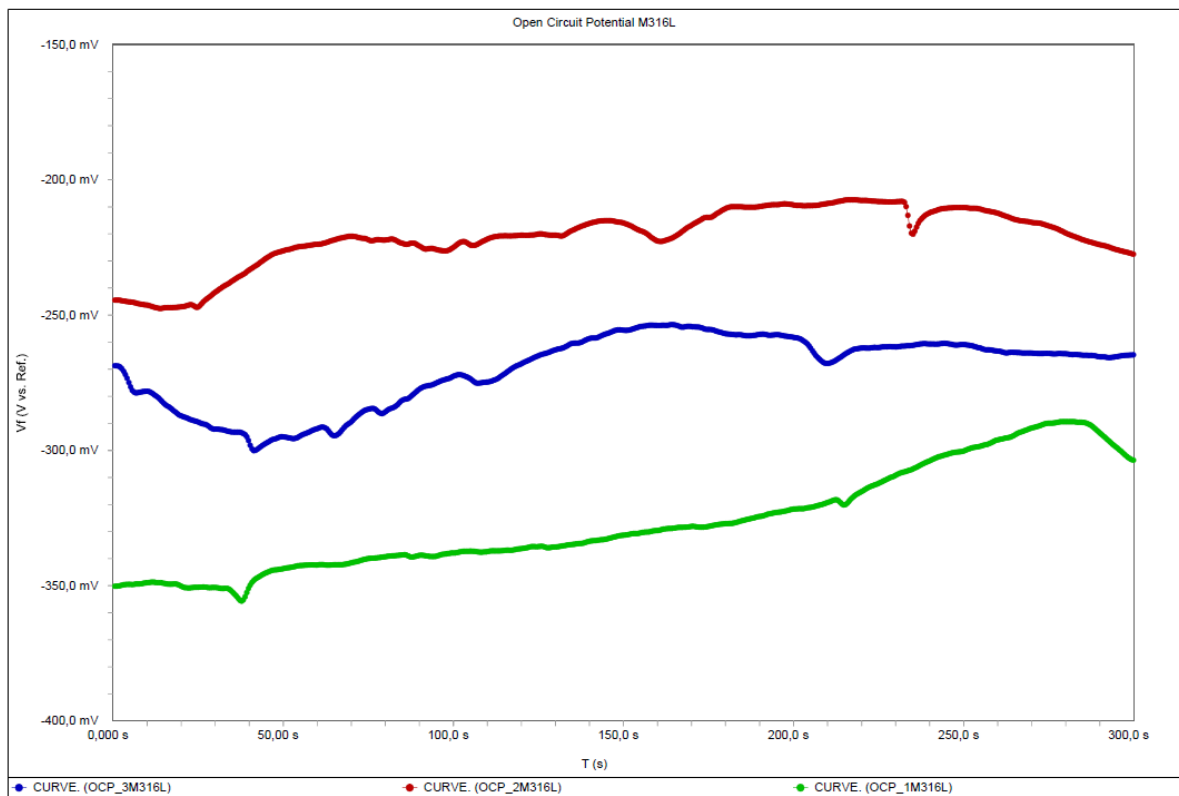


Figure 4: OCP modified M316L

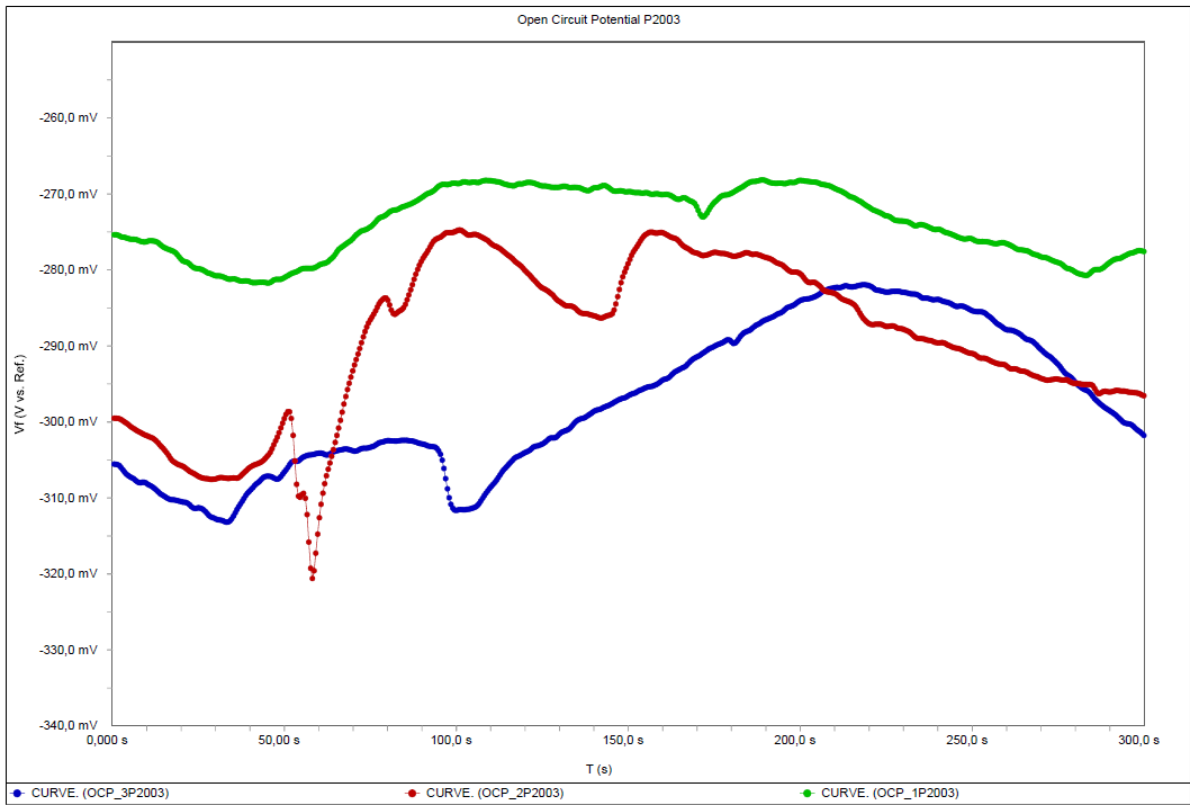


Figure 5: OCP ordinary P2003

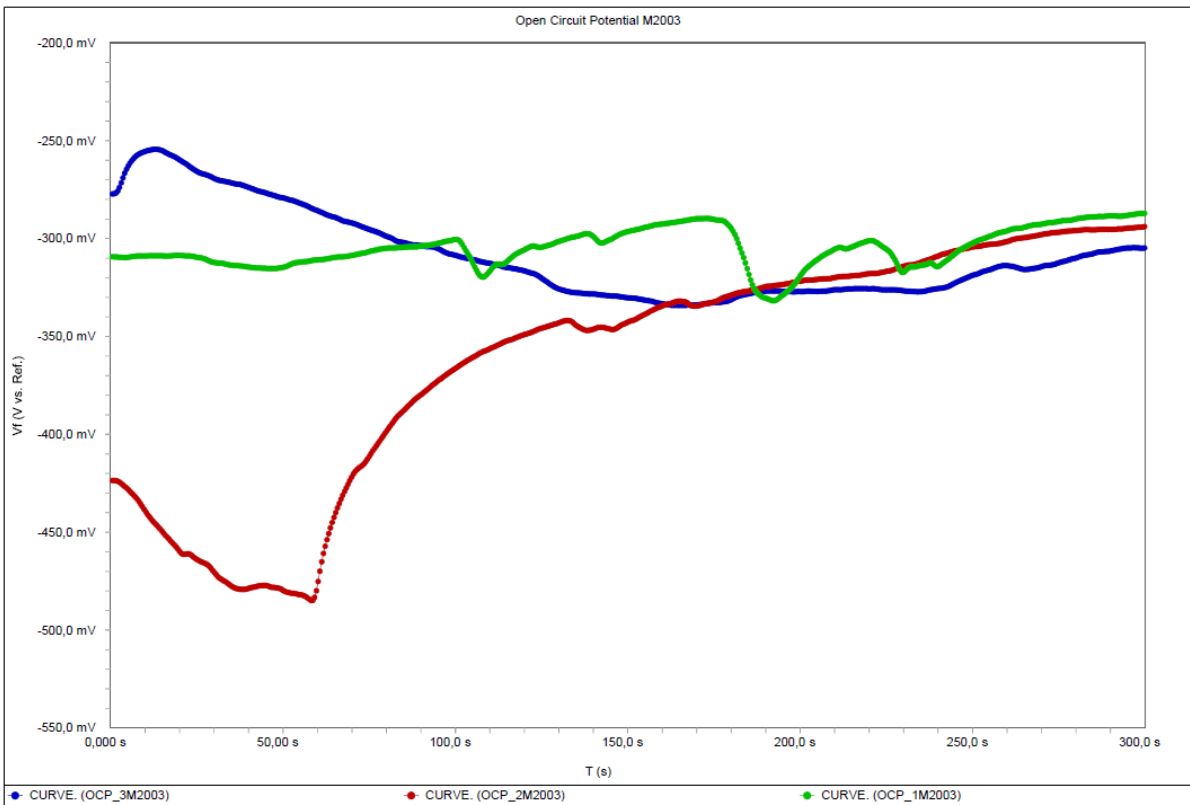


Figure 6: OCP modified M2003



Figure 7: OCP ordinary P2304



Figure 8: OCP modified M2304

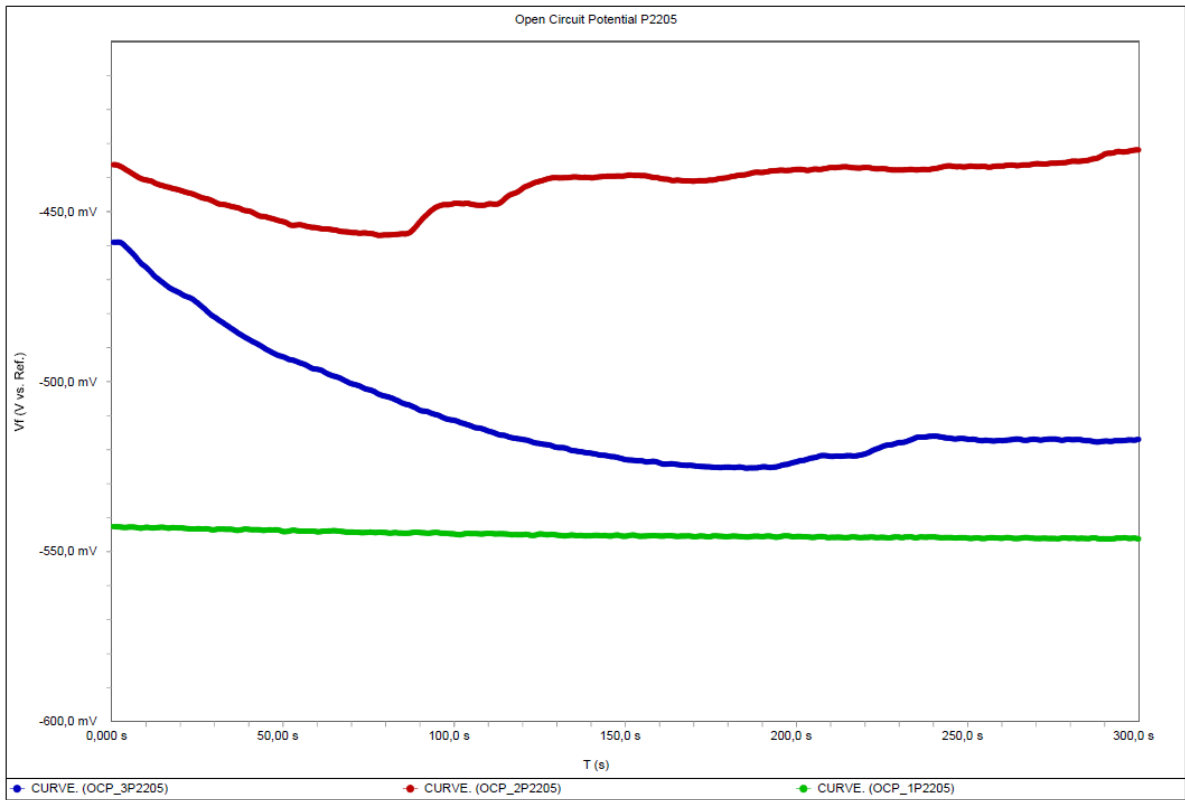


Figure 9: OCP ordinary P2205

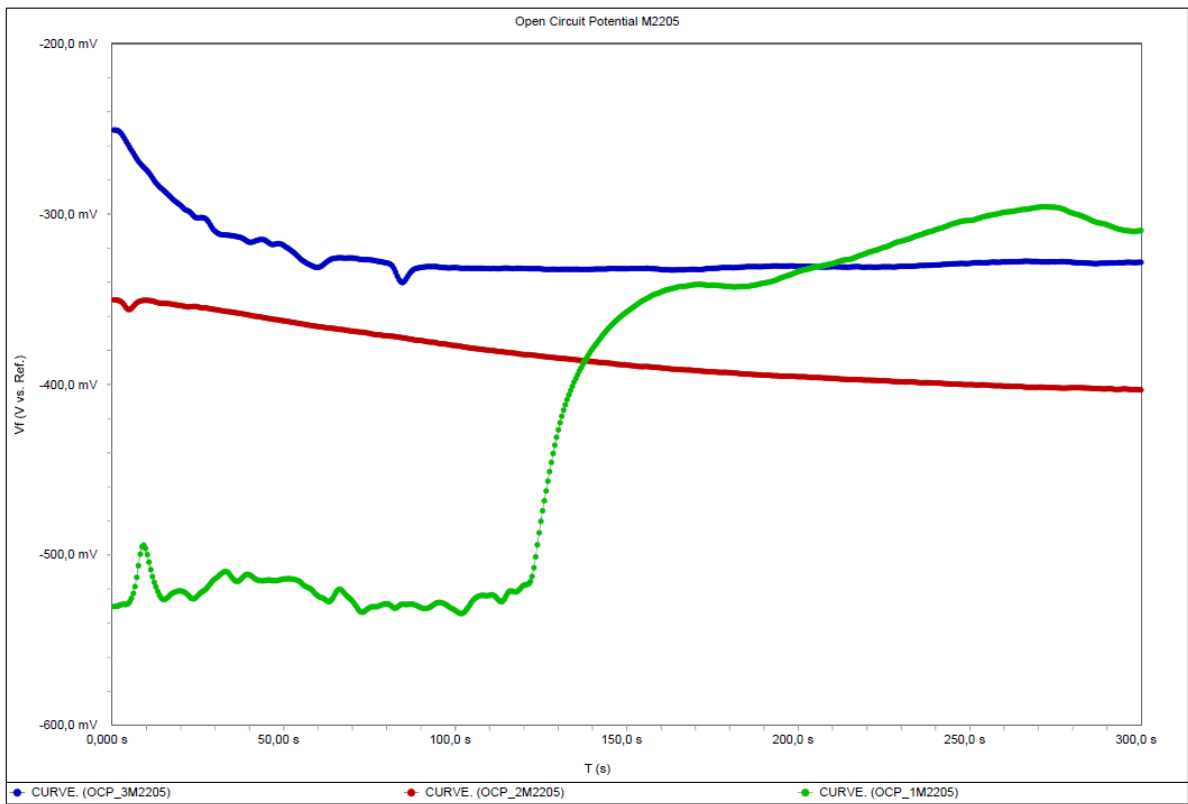


Figure 10: OCP modified M2205

Appendix F: Surface Images of The Materials

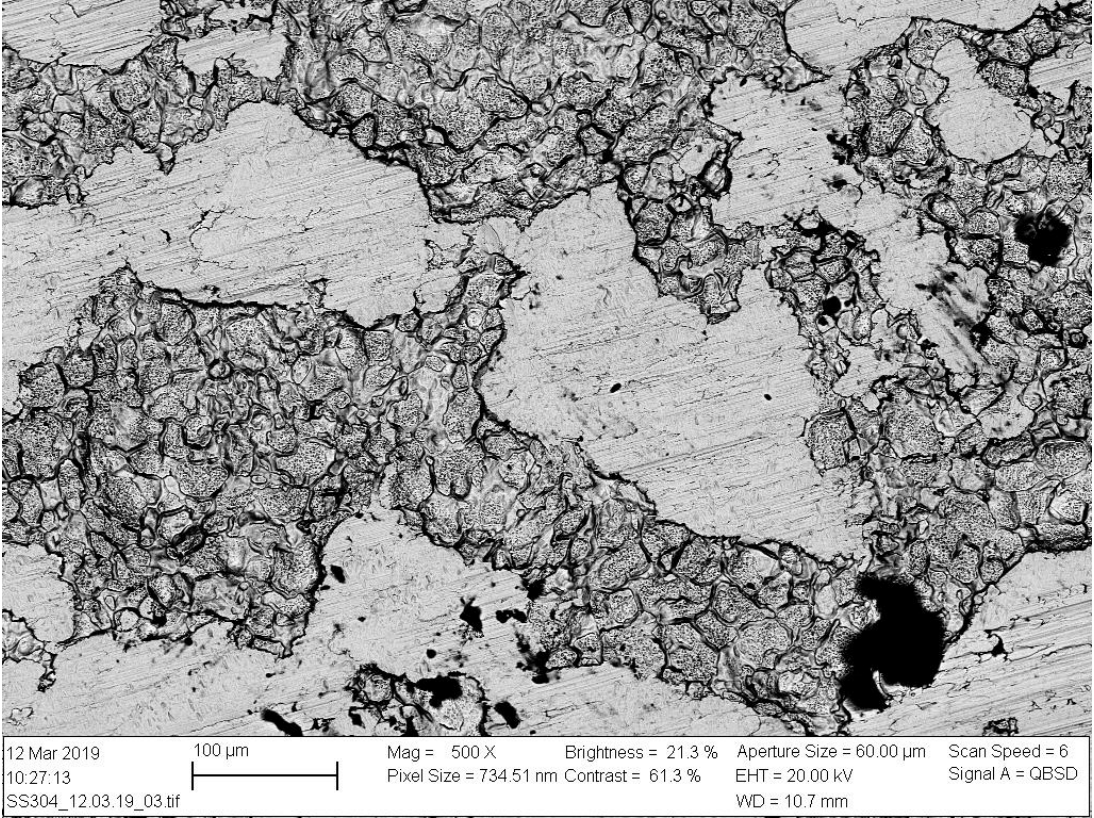


Figure 1: Surface image at 100 μm of sample 304

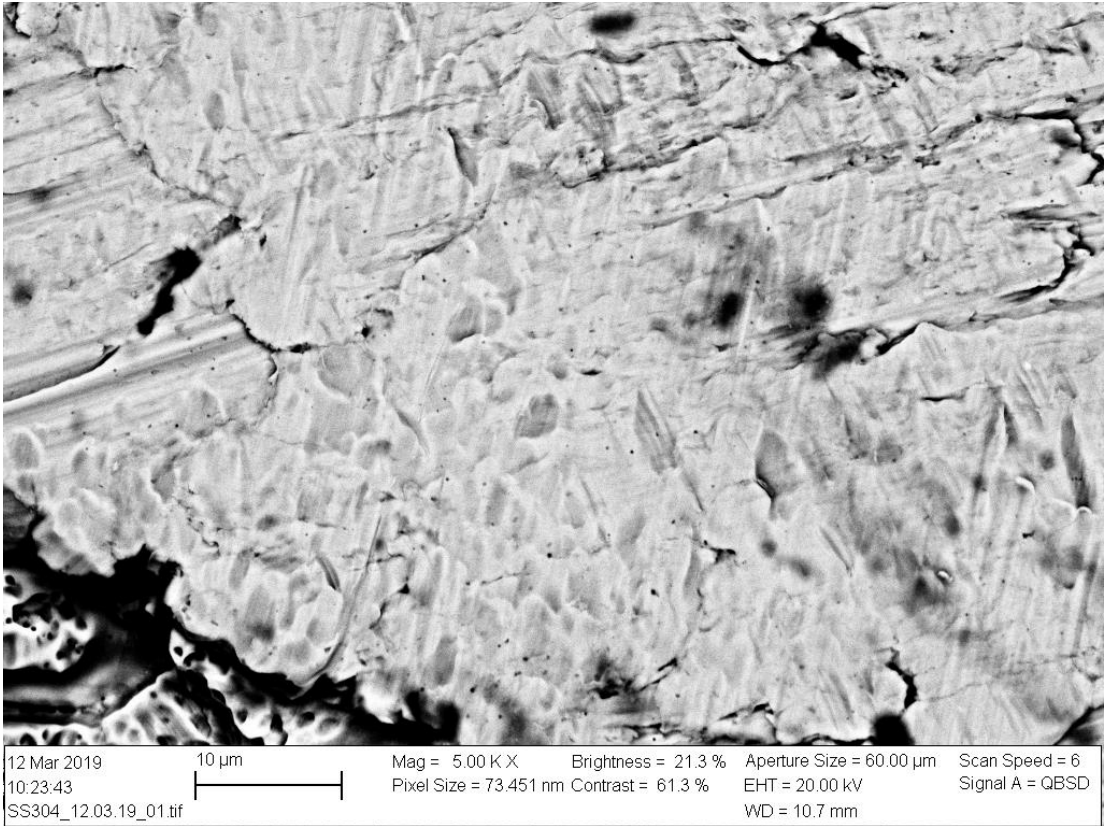


Figure 2: Surface image at 10 μm of sample 304

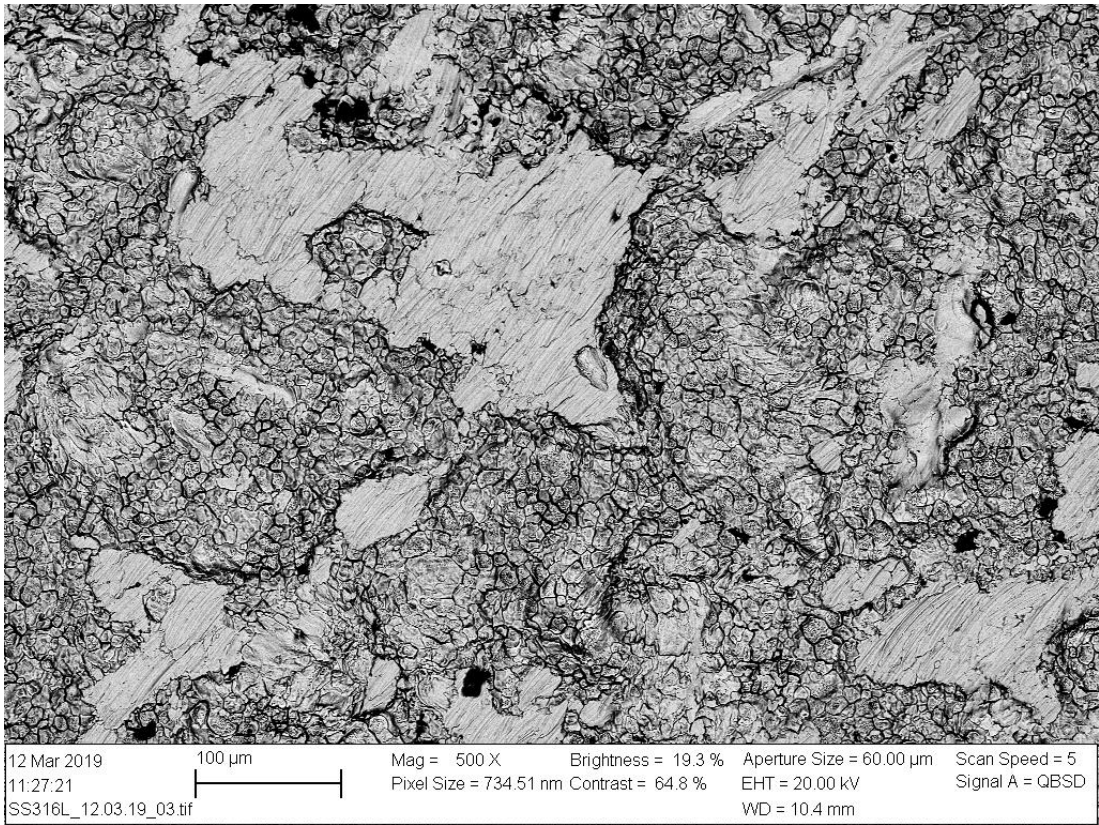


Figure 3: Surface image at 100 μm of sample 316L

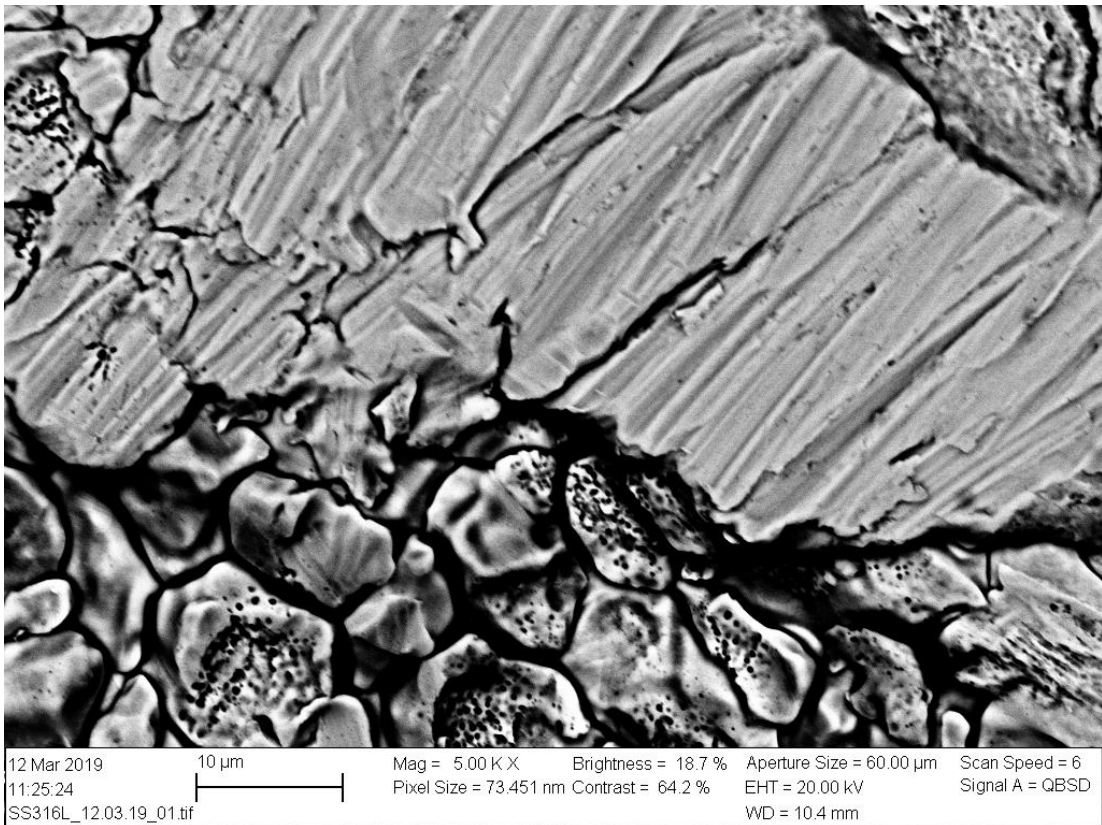


Figure 4: Surface image at 10 μm of sample 316L

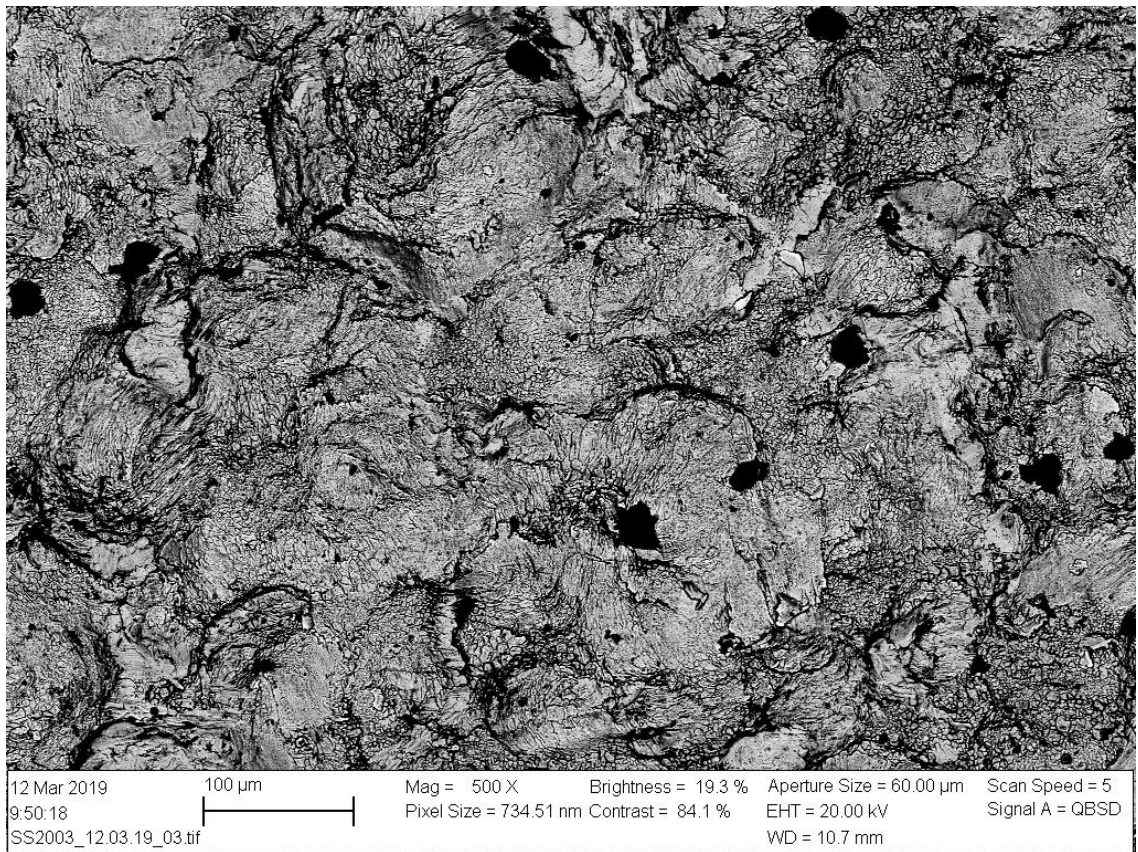


Figure 5: Surface image at 100 μm of sample 2003

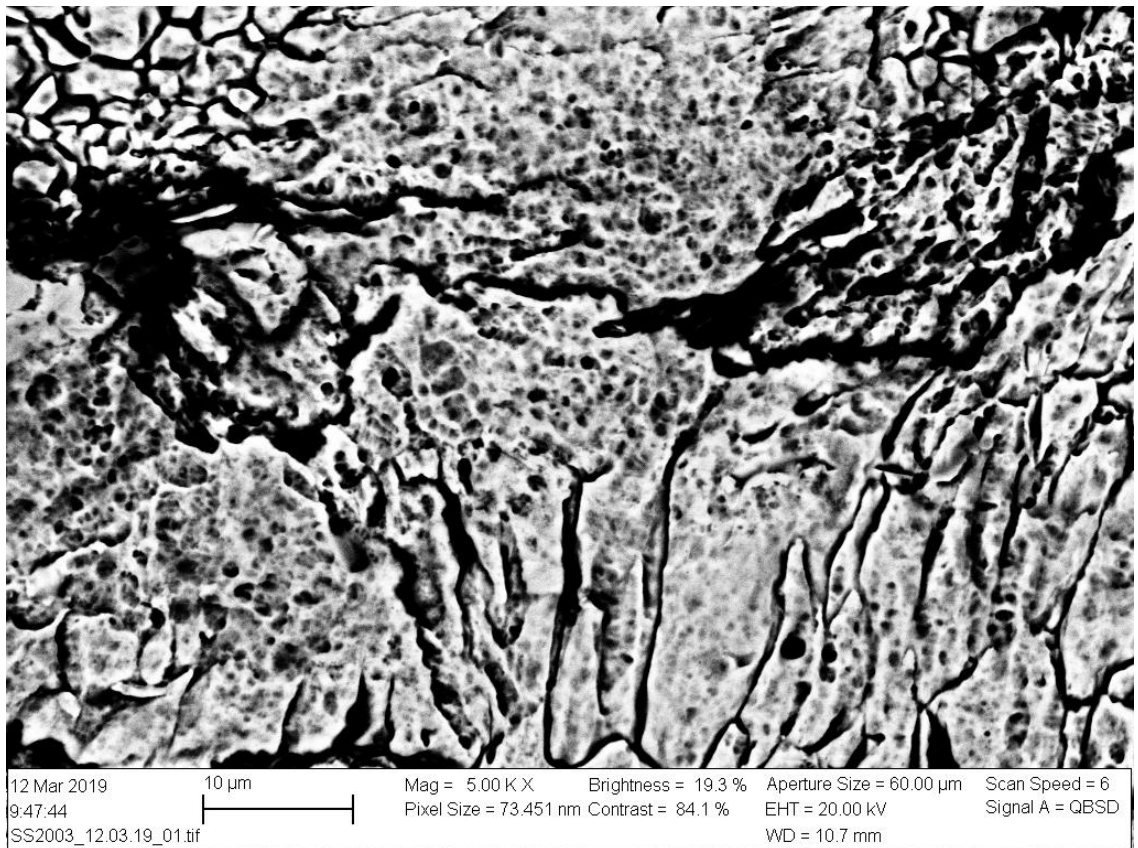


Figure 6: Surface image at 10 μm of sample 2003

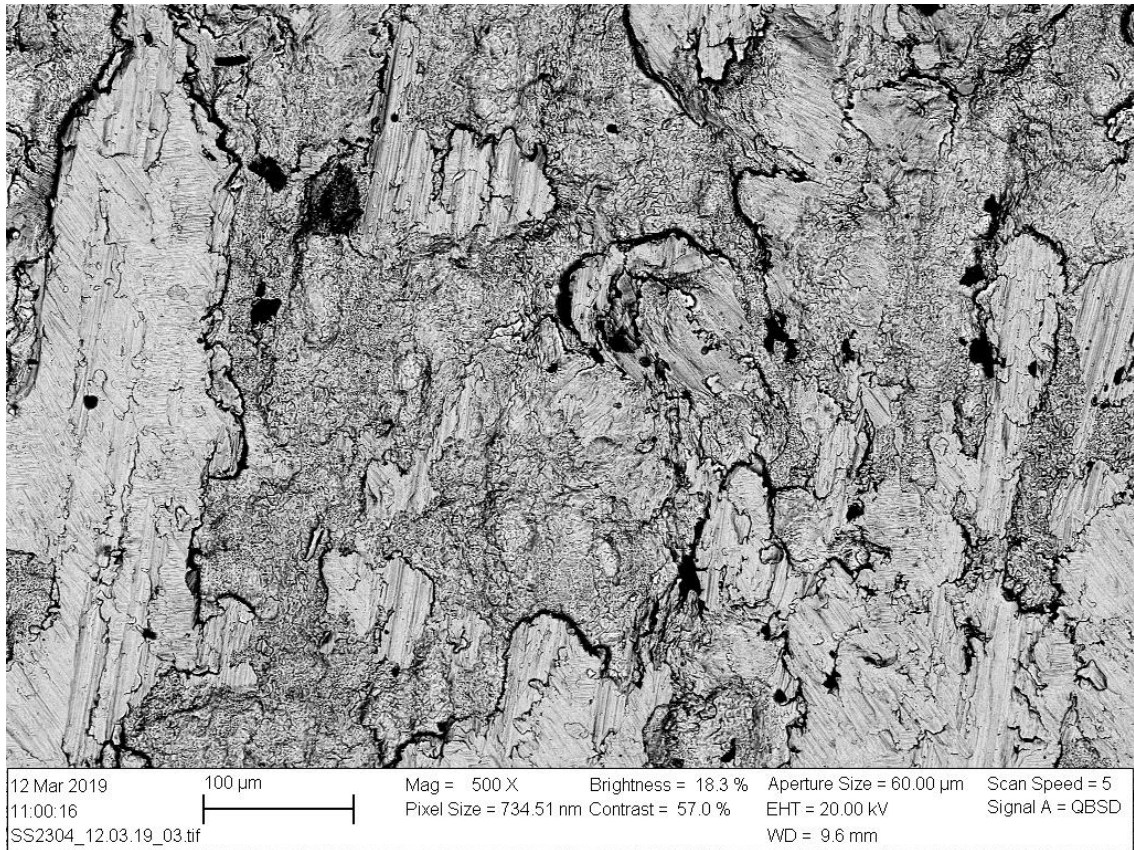


Figure 7: Surface image at 100 μm of sample 2304

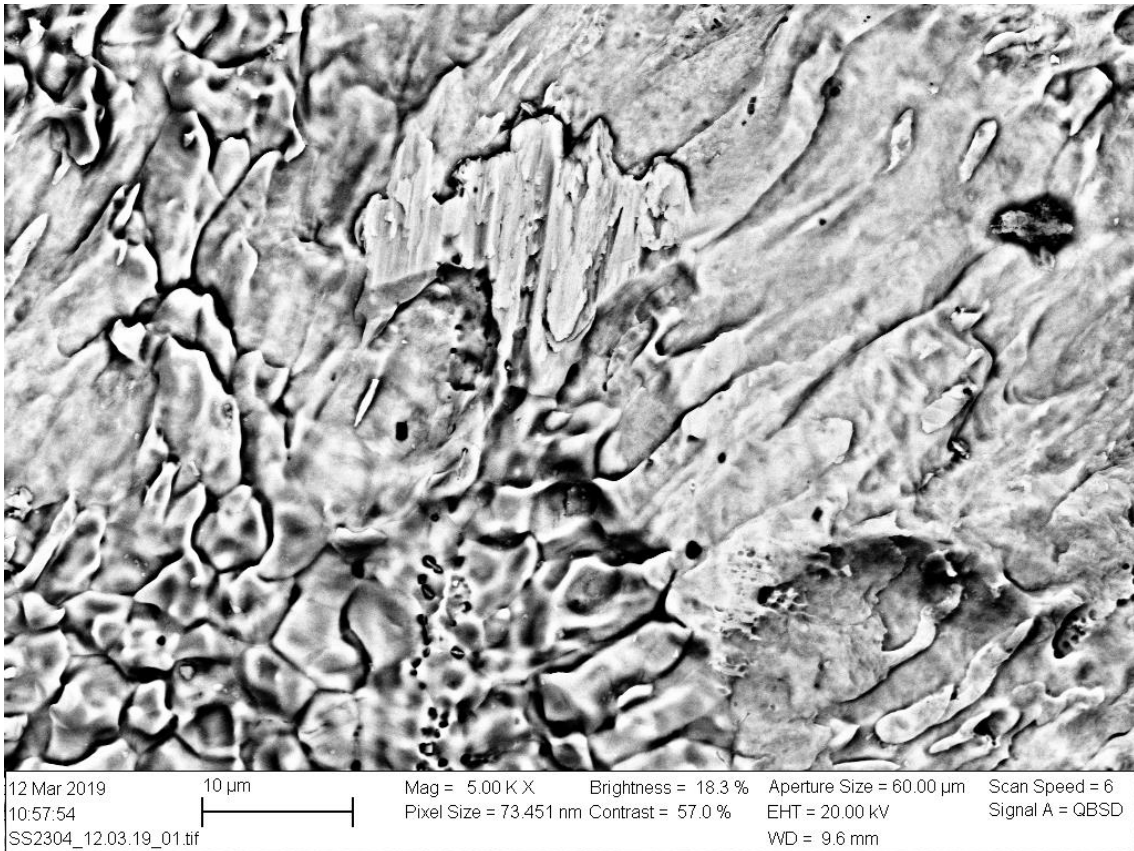


Figure 8: Surface image at 10 μm of sample 2304

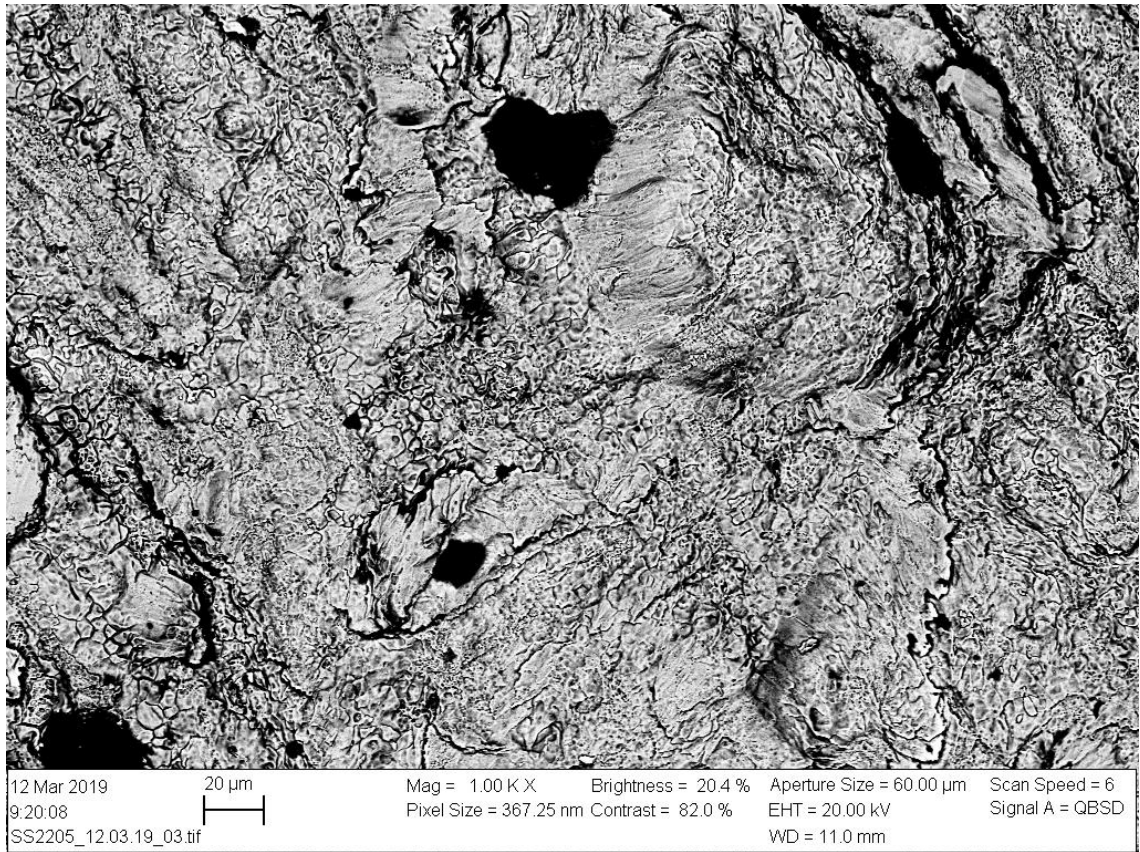


Figure 9: Surface image at 20 μm of sample 2205

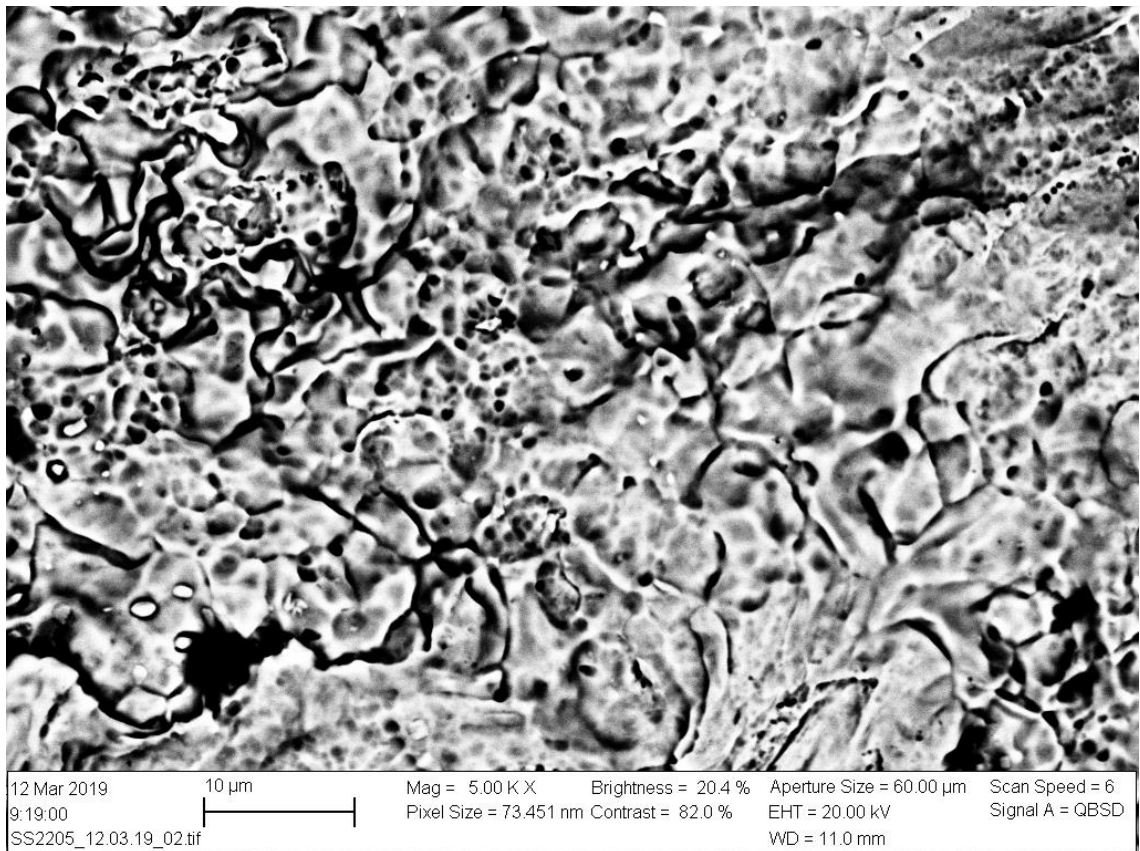


Figure 10: Surface image at 10 μm of sample 2205